

Deciphering the metamorphic framework of ophiolite
alteration and devolatilization at Linnajarvi, N-Norway

Master of Science Thesis

Halfdan Arstein



Department of Earth Science

University of Bergen

December 2021

Abstract

Kvitfjell ultramafic body is one of around 20 ultramafic bodies found in the Linnajavri area of Northern Norway. These ultramafic fragments are situated within the Kôli Nappe of the Upper Allochthon in the Caledonian tectonostratigraphy. At Kvifjell ultramafic body, secondary metamorphic olivine is observed, formed by a reaction of magnesite and antigorite which releases CO₂-bearing fluids. The metasediments adjacent to Kvifjell ultramafic body suggest that this decarbonation occurred at shallower depths than previously recorded. Peak PT conditions for Kvifjell ultramafic body, thus peak PT conditions at which decarbonation initiated, are derived from the metasediments surrounding Kvifjell ultramafic body which is presumed to have gone through the same metamorphic path as the ultramafic body itself. The PT estimate is acquired by conventional thermobarometry, trace element thermometry, image analyses and thermodynamic modelling based on the whole rock chemistry of the adjacent metasediment.

PT estimate from garnet-biotite and garnet-biotite-aluminosilicate-quartz geothermobarometry suggest that peak PT conditions are at a temperature of 593°C ±8°C and a pressure of 7.03 kbar ±0.17 kbar. This PT estimate is further supported by pseudosection modelling, observed and modelled mineral abundances, and peak PT estimate from the Ti-in-biotite thermometer coupled with the garnet-biotite-aluminosilicate-quartz barometer.

These findings reveal that the decarbonation at Kvifjell ultramafic body occurred at shallower depths than previously recorded. Transferring the temperature estimate from Kvifjell ultramafic body to subduction zones implies that the decarbonation processes may initiate at an earlier stage than previously assumed and that carbonates can become unstable before reaching sub-arc depths.

Acknowledgments

First and foremost, I would like to thank my supervisor Andreas Beinlich for guiding me through the past two and a half years and letting me work on such an interesting project. I am very grateful for all the help and thank you for always being available for questions and answering emails both day and night.

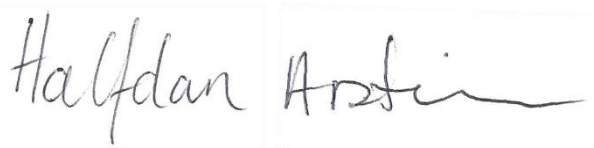
I would like to thank The Institute of Geoscience Research (TIGeR) at Curtin University, Australia for funding the field work, thin sections, and bulk rock analysis. Thank you to Tania Hildago at Commonwealth Scientific and Industrial Research Organisation for thin section scans. I am thankful to Eric Hellebrand at Utrecht University for conducting Electron microprobe analysis, and Oliver Plümper at Utrecht University for funding them.

Furthermore, I would like to thank Leif-Erik Rydland Perdersen and Siv Hjorth Dundas for helping me with the LA-ICP-MS during trace element analysis, and Irene Heggstad for help with the SEM. Thank you to Andreas L. Viken for making thin sections and removing carbon on them when needed.

I would like to thank Jamie D. Taylor and Trond Fjellet for feedback on the thesis. Thanks to Matz S. Slotnes and Vebjørn J. Selstad for a great time at “San Andreas”.

Finally, I would like to thank my girlfriend Lotte and my family for their support and motivation during the course of this project.

Bergen, 01.12.2021

A handwritten signature in black ink, reading "Halfdan Arstein", is placed within a light gray rectangular box.

Halfdan Arstein

TABLE OF CONTENTS

Chapter 1: Introduction	1
Chapter 2: Geological setting	3
2.1 The Caledonides	3
2.2 The Linnajavri area	4
Chapter 3: Methods	7
3.1 Field work and sampling	7
3.2 Analytical methods.....	10
Optical microscopy	10
Raman	10
Scanning electron microscope	10
Electron micro probe	10
LA-ICP-MS	11
Whole rock chemical analysis	12
3.3 Numerical methods.....	12
Conventional geothermobarometry	12
Trace element thermometry	14
Thermodynamic modelling	14
3.4 Image analyses	15
Chapter 4: Results	16
4.1 Bulk rock	16
4.2 Petrology	18
Amphibolite	18
Garnet-mica schist	23
Metagreywacke	27
4.3 Mineral chemistry.....	31
4.4 Thermobarometry	35
GB-GBAQ thermobarometry	35
Ti in biotite thermometry	37
Zr in rutile thermometry	39
4.5 Modelling and contours.....	40
4.6 Image analyses	44
Chapter 5: Discussion.....	47
5.1 Thermobarometry, modelling and peak metamorphic conditions	47
Garnet-biotite garnet-biotite-aluminosilicate-quartz thermobarometry	47
Ti-in-biotite thermometry	47

Zr in rutile thermometry	48
Contour lines and image analysis.....	50
Peak PT conditions.....	52
5.2 Linnajarvi PT estimate in the context of regional PT estimates.....	52
5.3 Limitations.....	55
5.4 Decarbonation	55
Chapter 6: Conclusion	58
Chapter 7: Future work.....	59
References:.....	60
Appendixes.....	64
Appendix 1 – Perple_X build file.....	65
Appendix 2 – EDS analysis.....	67
Appendix 3 – Bulk rock chemical composition	69
Appendix 4 – EMP analysis	70
Appendix 5 – EMPA areas.....	100
Appendix 6 – LA-ICP-MS analysis	112

CHAPTER 1: INTRODUCTION

In the Linnajavri area of N-Norway, around 20 ultramafic bodies belonging to a dismembered ophiolite complex are exposed within the metasedimentary country rocks of the Upper Allochthon of the Caledonian tectonostratigraphy, distributed over an area of $\sim 70 \text{ km}^2$ (Lindahl and Nilsson, 2008). These ultramafic bodies have been altered by CO₂-bearing reactive fluid to secondary soapstone (magnesite and talc) and listvenite (magnesite and quartz) (Beinlich et al., 2012, Tominaga et al., 2017, Beinlich et al., 2020). Precise estimates for the pressure and temperature conditions during the ultramafic rock alteration are scarce due to the lack of suitable equilibria. For the metasedimentary country rocks, PT conditions were approximated to upper greenschist to lower amphibolite facies based on hand specimens in the field by Beinlich et al. (2012) and Lindahl and Nilsson (2008). Due to the local structure of the Caledonian nappes overlaying the Baltica basement, a general increase in burial depth, and therefore pressure and temperature conditions from east to west can be inferred.

Earlier field investigations in 2010 and 2011 focused on the eastern part of the Linnjavri area. Ultramafic outcrops in the western area of Linnjavri (e.g., Kvifjell) were investigated in 2013 and 2019. So far, most of the post-fieldwork analytical research on samples from the Linnjavri area has focused on the samples collected from Kvifjell ultramafic body (Strobl et al., 2021). In contrast to all ultramafic bodies in the eastern part of Linnjavri that are either completely serpentinised, or altered to soapstone and listvenite, both Kvifjell and Njaskavàrri contain metamorphic secondary olivine and fluid escape structures (A. Beinlich, personal communication, Strobl, 2021, Strobl et al., 2021). The secondary olivine, which is present as isolated crystals in a matrix of magnesite and antigorite, pseudomorphically replaces the magnesite, and thereby preserving the magnesite cleavage in the olivine (A. Beinlich, personal communication). Preliminary microtextural observations by Strobl (2021) confirm that the olivine is formed by a reaction of magnesite with antigorite, which releases CO₂-bearing fluids. The Linnjavri area is a unique site that allows investigation of the uptake and release of carbon in rocks, and the development of devolatilization fluid transport networks in a relatively small area. The metasediments surrounding Kvifjell ultramafic body suggest that the decarbonation process, in which secondary olivine is formed, occurred at a shallow depth, which is a contrast to the previously estimated carbonate stability field.

The subduction of oceanic lithosphere into the mantle is the most important global geochemical cycle, where material from Earth's surface, most importantly CO₂, is delivered to the deep mantle (Bebout, 1995, Stewart and Ague, 2020). Global estimates on the influx of CO₂ into the mantle are greater than the outflux released by arc magmatism (Bebout, 1995, Kerrick and Connolly, 2001). The imbalance between the influx and outflux of CO₂ raises the question of whether the carbon gets carried deep into the mantle or is released before reaching the depth where arc magmas are generated (Kerrick and Connolly, 2001). Kerrick and Connolly (1998) estimated that carbonate would remain stable and that decarbonation would not start before reaching sub-arc depths (80-140 km). This results in that most of the subducted carbon is transported into the mantle (Kerrick and Connolly, 1998). Results from Kerrick and Connolly (1998) shows that the maximum CO₂ loss along the hottest PT path of a subduction zone is ~1.5 wt.%, while there is substantial dehydration. In their thermodynamic modelling, Kerrick and Connolly (1998) used CaCO₃ bearing rocks. The study of Pickard and Needs (2015) shows that CaCO₃ is more stable than MgCO₃ at pressures over 100 GPa. Stewart and Ague (2020) state that ~40% to ~65% of the carbon in the subducted lithosphere gets released by decarbonation at forearc depths. This contradicts the transport of most CO₂ into the deep mantle and rather suggests a depletion of the carbon content in the mantle throughout Earth's history (Stewart and Ague, 2020). Due to the large differences in measurements of diffuse outgassing of carbon at shallow depths, there is still little known about the global estimates (Kelemen and Manning, 2015).

This thesis aims at making an estimate for the PT at peak metamorphic conditions for Kvitfjell ultramafic body. Since ultramafic rocks are unsuitable for constraining PT, the PT estimate will be made from the metasediments surrounding Kvitfjell ultramafic body which is presumed to have gone through the same metamorphic path as the ultramafic body itself. The PT estimate from the metasediments should therefore be applicable for the conditions of which secondary olivine is formed, and hence CO₂ fluid release. The PT estimate will be made through conventional geothermobarometry and trace element thermometry on samples from the metasediments adjacent to the ophiolite fragment. The approach for obtaining the PT estimate will also include thermodynamic modelling based on the whole rock chemistry of the adjacent metasediments.

CHAPTER 2: GEOLOGICAL SETTING

2.1 The Caledonides

The formation of the Scandinavian Caledonides started in the Neoproterozoic when Baltica rifted off Laurentia, thus opening the Iapetus Ocean (Corfu et al., 2007). In Silurian to Early Devonian, oblique plate convergence resulted in the subduction of Baltica beneath Laurentia (Roberts, 2003). This collision was accompanied by extensive thrusting of sedimentary nappes onto the Baltica active continental margin. These nappes are divided into the Lower, Middle, Upper and Uppermost Allochthon based on their position in the Caledonian tectonostratigraphy, and overlay the Baltica Precambrian crystalline basement Parautochthon and Autochthon (Roberts and Gee, 1985).

The Lower Allochthon mainly consists of sediments from the Latest Proterozoic to Early Palaeozoic age (Roberts and Gee, 1985). Fossen and Hurich (2005) report that these sediments have been transported tens of kilometres. A major part of the Lower Allochthon and Parautochthon is composed of phyllites that formed by metamorphism of Fennoscandian and Timanian sediments (Slama and Pedersen, 2015).

Sheets of strongly deformed crystalline Precambrian rocks and thick Late Proterozoic sandstones sequences dominate the Middle Allochthon and are locally intruded by mafic dikes (Roberts and Gee, 1985). Their metamorphic grade reaches mainly greenschist facies, except for occurrences in Troms, Finnmark, and the westernmost areas that have reached amphibolite facies (Roberts and Gee, 1985).

The Upper Allochthon is the most heterogeneous nappe, and contains both island-arc and ophiolite sequences (Roberts and Gee, 1985). These rocks were first thought to have formed close to the continental margin of Baltica (Brekke et al., 1984). However, Pedersen et al. (1992) reported that granitic intrusions in the ophiolites are contaminated by crustal material containing Archean zircons. Since equivalent source rocks are absent from southern Norway but present in the Laurentian province, Pedersen et al. (1992) concluded that the ophiolite sequences were already accreted to the Laurentian margin prior to thrusting onto Baltica during the Caledonian orogeny.

Most of the bedrock exposed in Nordland and southern Troms is part of the Uppermost Allochthon, comprising gneisses, schists, sandstones and marbles (Roberts and Gee, 1985). Roberts et al. (2007) suggest that these rocks were derived from the eastern margin of Laurentia.

2.2 The Linnajavri area

This M.Sc. thesis focuses on metasediments surrounding the Kvifjell ultramafic body, in the Linnajavri area of Northern Norway (Fig 2.1). The Linnajavri area is situated in the Hamarøy municipality, Nordland county, between the Swedish boarder in the east and the lake Forsvatnet, formerly known as Linnajävri, to the west. The Kvifjell ultramafic body is one of ~20 individual ultramafic bodies scattered in an area of 70 km² (Lindahl and Nilsson, 2008). The exposed area of the ultramafic bodies ranges between several 100 m² and a couple km² (Beinlich et al., 2020). The local rocks in the Linnajavri area belong to the Middle and Upper Allochthonous nappes of the Caledonian tectonostratigraphy (Rehnström and Corfu, 2004).

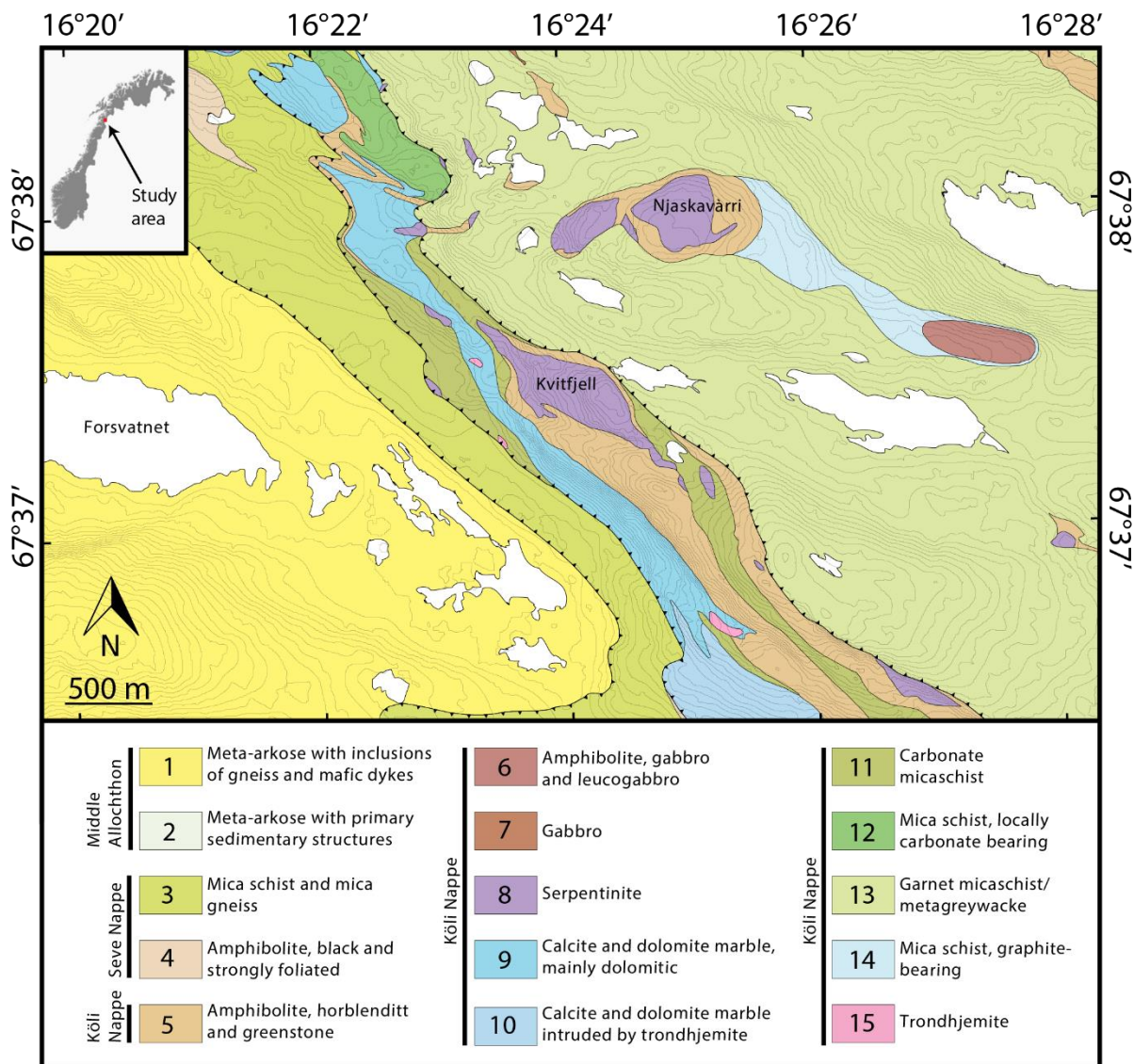


Figure 2.1 Geological map of the Linnajavri area. The first thrust from the west represents the boundary between Middle Allochthon and Seve Nappe (Upper Allochthon). The second thrust represents the boundary between Seve and Köli Nappe. The third thrust represents the boundary between the Ridoalgičohkka Nappe and Čohkul Nappe, both local nappes within the Köli Nappe. Redrawn from Lindahl and Nilsson (2008).

The stratigraphically lowermost rocks in the Linnajavri area belong to the Middle Allochthon (Beinlich et al., 2012). They comprise strongly foliated granitic gneisses in the lower parts, and quartzites and meta-arkose in the upper parts, some preserving soft-sedimentary structures (Lindahl and Nilsson, 2008). These rocks are underlying and separated from the Seve nappe of the Upper Allochthon by prominent thrusts (Lindahl and Nilsson, 2008).

The rocks of the Seve nappe form the lowermost part of the Upper Allochthon and consist of mica schists, mica gneisses and amphibolites (unit 3 and 4 in Fig. 2.1) (Lindahl and Nilsson, 2008).

The Köl Nappe constitutes the upper part of the Upper Allochthon, and is overlying the Seve Nappe in the Linnajavri area (Stephens et al., 1985). Previous studies have divided the Köl Nappe into several sub-units (e.g. Stephens et al., 1985, Brattli and Prestvik, 1987b, Crowley and Spear, 1987, Lindahl and Nilsson, 2008). In the 1:50,000-scale bedrock map, Brattli and Prestvik (1987a) divided the Köl Nappe rocks in the Linnajavri area into Middle and Lower Nappe and Cokkulvarre Nappe. They place most of the rocks in the area into the Middle and Lower Nappe. Lindahl and Nilsson (2008) support the conclusion of Brattli and Prestvik (1987a), but they divided the rocks in the area into three local nappes instead of two.

Lindahl and Nilsson (2008) named the majority Middle and Lower Nappe from Brattli and Prestvik (1987a) the Ridoalaggičohkka Nappe. They describe the base of this nappe as composed of calcite and dolomite marble (Fig. 2.1), containing intrusions of trondhjemite. According to Lindahl and Nilsson (2008), a layer of carbonate bearing mica schist is situated in between the marbles and the ophiolitic fragments. They describe that this layer has a thickness of more than 1 km at the greatest.

The second local nappe described by Lindahl and Nilsson (2008), within the Köl Nappe, is the Čohkul Nappe. They observe that the main rocks in this nappe are garnet-mica schist, metagreywacke, and graphite-bearing mica schist, which can be seen in the north-eastern part of Figure 2.1. As in the Ridoalaggičohkka Nappe, ophiolite fragments are also present in the Čohkul Nappe. The Čohkul Nappe has an angular unconformity contact to the underlying Ridoalaggičohkka Nappe (Lindahl and Nilsson, 2008), and is situated in the central part of a large synclinal structure.

The uppermost part of Köl Nappe is described as the Stipok Nappe (Lindahl and Nilsson, 2008). The Stipok Nappe consists of carbonate bearing mica schist, overlayed by calcite and

dolomite marble (Lindahl and Nilsson, 2008). Sundblad (1986) interpreted these rocks as being a repetition of the lower part of the Ridoalggijohkka nappe.

The majority of the ophiolite sequences in Norway are allocated in the Koli nappe (Bucher-Nurminen, 1991), and the ophiolites in the Linnajavri area are no exception, where the ophiolite fragments are all located in the Ridoalggijohkka and Čohkul Nappes (Lindahl and Nilsson, 2008). The Kvifjell ultramafic body is situated above the carbonate-bearing mica schist in the Ridoalggijohkka Nappe (Lindahl and Nilsson, 2008). The synclinal structure, which the Čohkul Nappe is in the middle of, goes over in an anticlinal structure to the south and southwest of Kvifjell ultramafic body (Brattli and Prestvik, 1987a). Kvifjell ultramafic body is situated on the limb, in the middle of the synclinal and anticlinal structures (Brattli and Prestvik, 1987a). Lindahl and Nilsson (2008) describe the ultramafic fragments as being parts of tectonic mélange zones. The mélange zones are characterised as alteration zones, crushing zones and areas where a large number of exotic blocks or fragments are present (Lindahl and Nilsson, 2008).

CHAPTER 3: METHODS

3.1 Field work and sampling

The field work in the Linnajavri area (Hamarøy municipality, Nordland) was carried out by A. Beinlich, O. Plümper and M. Ohl in July 2019. A total of 22 samples were collected from Kvitfjell ultramafic body and surrounding metasedimentary country rocks (Fig 3.1). In this thesis I investigate a subset of five samples that are representative for metasediments adjacent to the Kvitfjell ultramafic body (samples: Lin_12-19, Lin_13-19, Lin_14-19, Lin_15-19, and Lin_16-19) (Fig 3.2a-g). Thin sections had been made from all samples by the start of this study. These are called Lin_12a-19, Lin_12b-19, Lin_13-19, Lin_14-19, Lin_15-19, and Lin_16-19. Two duplicate thin sections were made from the samples of Lin_14-19 and Lin_15-19 during this project. These are referred to as Lin_14b-19 and Lin_15b-19.

Table 3.1 Rock names given in the field, units they belong to from the geological map and coordinates for all samples used in this study.

Sample ID	Field rock name	Unit	Coordinates
Lin_12-19	Schist	5	67° 37.467' N 16° 24.458' E
Lin_13-19	Schist	5	67° 37.474' N 16° 24.458' E
Lin_14-19	Garnet schist	11	67° 37.484' N 16° 24.477' E
Lin_15-19	Garnet schist	11	67° 37.491' N 16° 24.468' E
Lin_16-19	Metagreywacke	13	67° 37.673' N 16° 24.339' E

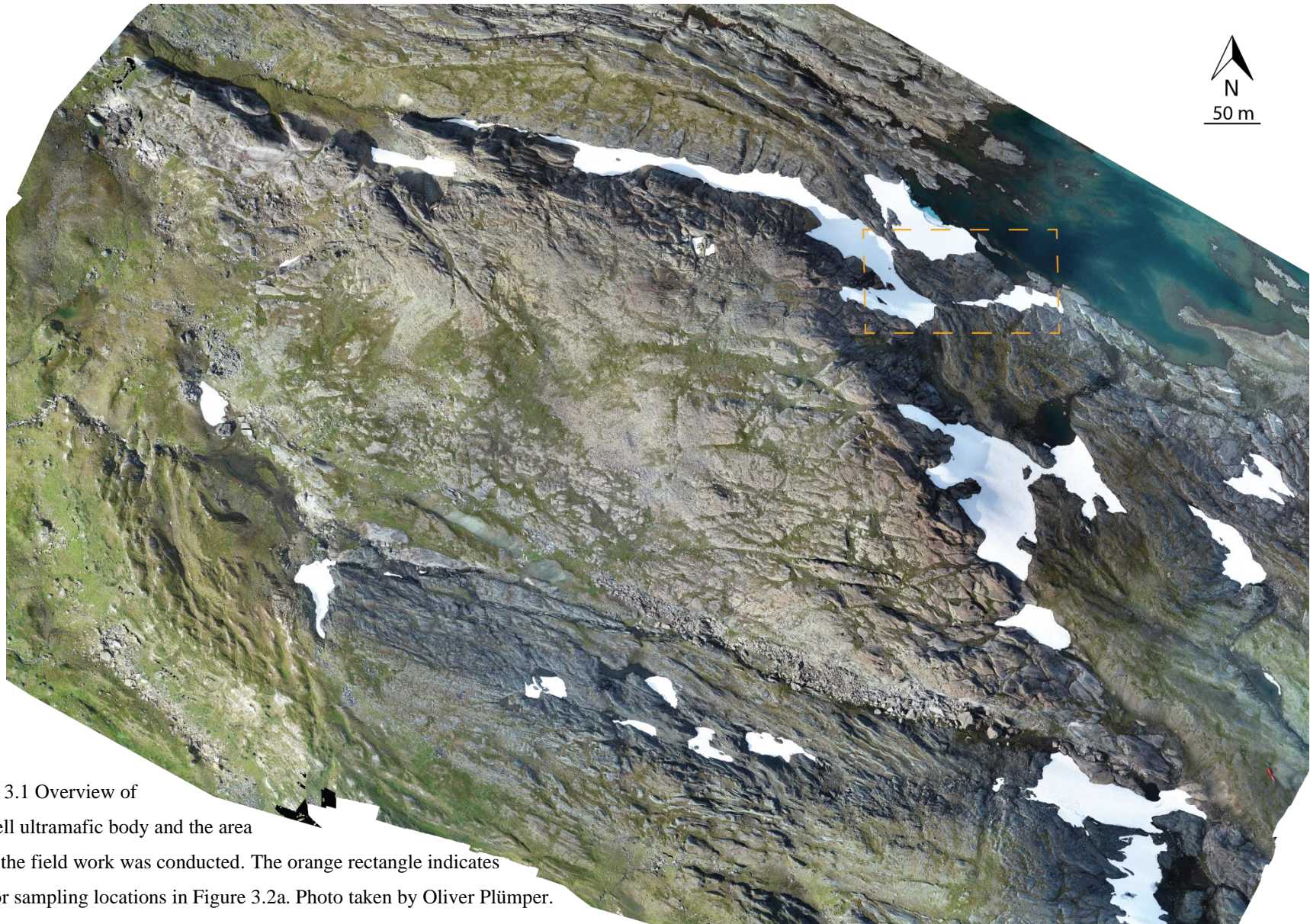


Figure 3.1 Overview of Kvitfjell ultramafic body and the area where the field work was conducted. The orange rectangle indicates area for sampling locations in Figure 3.2a. Photo taken by Oliver Plümper.

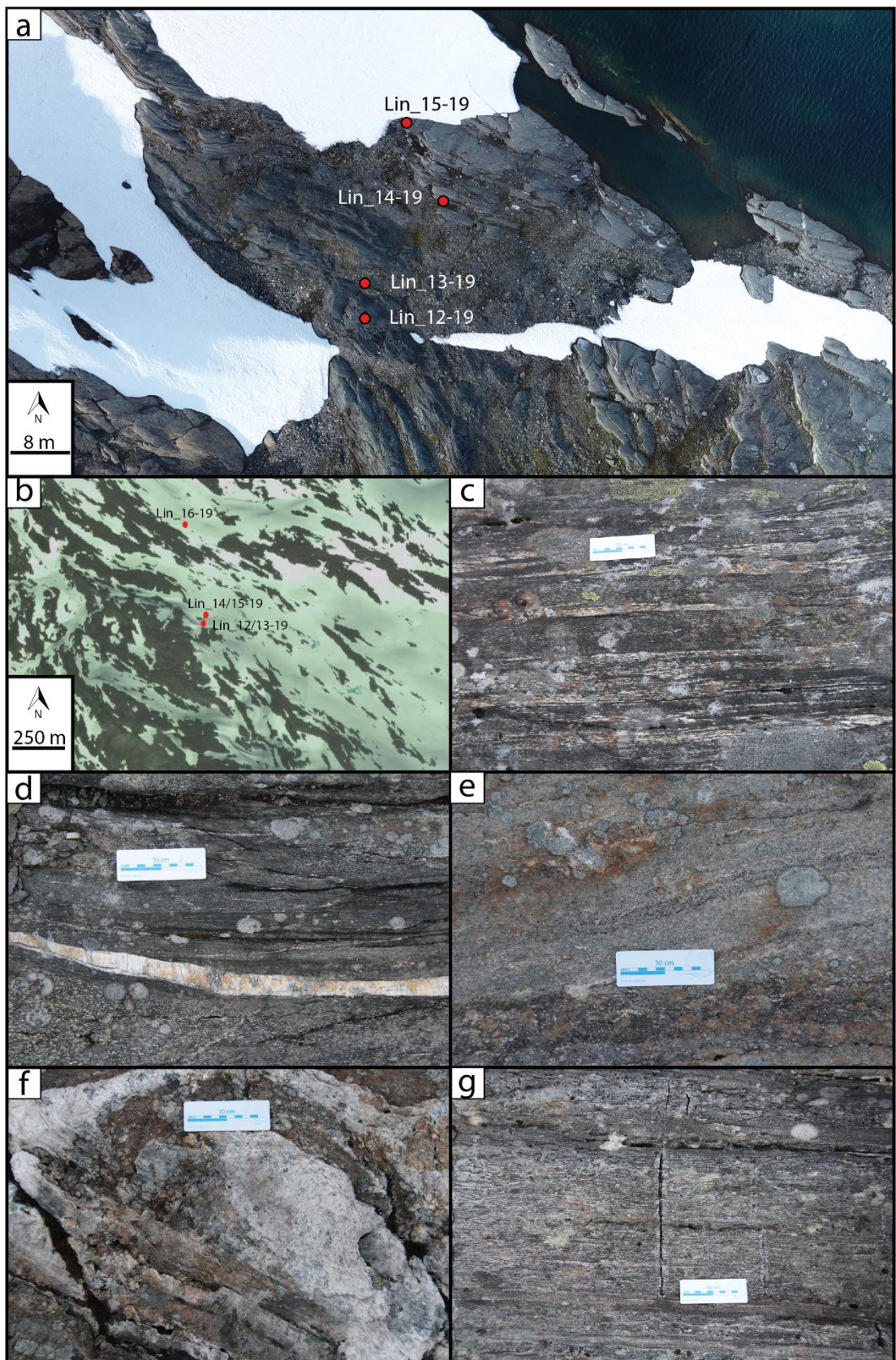


Figure 3.2 Sampling localities and sampling outcrops. (a) Sampling locations for the schist and garnet schist (b) sampling location of the metagreywacke compared to the schist and garnet schist. Satellite image © Google Earth 2021. (c) Outcrop for Lin_12-19 (d) outcrop for Lin_13-19 (e) outcrop for Lin_14-19 (f) outcrop for Lin_15-19 (g) outcrop for Lin_16-19. Photos taken by Oliver Plümper.

3.2 Analytical methods

Optical microscopy

All the eight thin sections were first studied using a Nikon Eclipse E200 polarizing microscope to identify target areas for subsequent investigations, and to characterize the mineral content and reaction textures. The different minerals present in the thin sections were identified by their optical properties such as colour, birefringence, relief, cleavage, crystal habit and interference figure. After an overview was established, all samples were studied in more detail using a Nikon Eclipse LV100POL microscope in both transmitted and reflected light. The software NIS-Elements BR 5.11.01 was used to take photomicrographs.

Raman

Single Raman spectroscopic measurements were done using a Horiba Jobin Yvon Labram-HR system, located at the University of Bergen. Measurements were done with a 50x objective and a 488 nm Ar-ion laser through a D0.3 density filter (50% laser power) with an 1800 g/mm grating. For mineral identification the obtained Raman spectra were matched with RRUFF reference spectra using the software CrystalSleuth (Laetsch and Downs, 2006).

Scanning electron microscope

Backscattered Electron (BSE) imaging and in situ semi-quantitative chemical analyses by Energy Dispersive Spectroscopy (EDS) were conducted using a Zeiss Supra 55VP Scanning Electron Microscope (SEM) located at the University of Bergen. The three thin sections Lin_14-19, Lin_15-19, and Lin_16-19 were coated with carbon before entering the SEM. Analyses were done with a working distance of 8.5 mm, acceleration voltage of 15 kV and an aperture diameter of 60 µm. All the different minerals present in the thin sections were analysed to confirm the assumptions from the optical microscopy. The element analyses were done with EDS, and the software Pathfinder from ThermoFisher Scientific. After all the minerals had been identified, the SEM was set to make BSE mosaics of all the three thin sections using Zeiss Atlas 3.0. All 1469 mosaic tiles made by the SEM were stitched together with Microsoft Image Composite Editor.

Electron micro probe

A BSE map showing where to do the analyses was needed before analyses with a microprobe could be done. Adobe Illustrator was then used to mark all the spots on the BSE mosaic that were going to be analysed (Appendix – 5). The BSE map and the three thin sections, Lin_14-

19, Lin_15-19 and Lin_16-19, were sent to the Department of Earth Science at the University of Utrecht for EMP analyses.

Quantitative compositional analyses were acquired on an electron microprobe (Jeol JXA-8530F) equipped with 5 tunable wavelength dispersive spectrometers. The operating conditions were 40° take off angle, a beam energy of 15 keV and a beam diameter of 5 μm . The beam current was set to 15 nA for the garnets, and 10 nA for all other mineral phases. Elements were acquired using analyzing crystals LIFH for Ti K α 1, Fe K α 1, Mn K α 1, PETH for Si K α 1, Cl K α 1, PETL for Ca K α 1, K K α 1, Cr K α 1, TAPH for Mg K α 1, Al K α 1, Na K α 1 and LDE1 for F K α 1. The standards were a combination of both in-house and internationally certified standards. Jadeite for Na K α 1, KTiPO₅ for Ti K α 1 and K K α 1, fluorite for F K α 1, tephroite for Mn K α 1, scapolite USNM R6600-1 for Cl K α 1, GOR-132G for Mg K α 1, KL-2G for Fe K α 1, Si K α 1, Al K α 1, Ca K α 1, and chromite NMNH 117075 for Cr K α 1. Both on and off-peak counting time was 60 s for Fe, and 28 s for all other elements. Off Peak correction method was Exponential for Ti K α 1 and Fe K α 1, and Linear for all other elements. Unknown and standard intensities were corrected for deadtime. Standard intensities were corrected for standard drift over time. Interference corrections were applied to F for interference by Fe (Donovan et al., 1992). Oxygen was calculated by cation stoichiometry and included in the matrix correction. For micas, an ideal H:O of 1:6 was specified and included in the matrix correction (Donovan et al., 2011). The matrix correction method was ZAF or Phi-Rho-Z calculations and the mass absorption coefficients dataset was LINEMU Henke (LBL, 1985) <10KeV/CITZMU> 10KeV. The ZAF or Phi-Rho-Z algorithm utilized was Armstrong/Love Scott (Armstrong, 1988).

LA-ICP-MS

Both Lin_14b-19 and Lin_15b-19 were first ground along the sides to be able to fit in the mount of the LA-ICP-MS. In situ trace element analysis of rutile was performed using laser ablation inductively coupled plasma mass spectrometer (LA-ICP-MS). Prior to laser ablation both thin sections were cleaned with 99.9% ethanol to remove potential surface contaminants. The analysis was carried out using a Laser Resonetics 193 nm ArF excimer laser ablation system (REOSolution M-50 LR) laser connected to a Nu ATTOM high resolution single collector ICP-MS. The laser was fired with a spot size of 26 μm , a frequency of 5 Hz, and fluence of 2.5 J/cm². Using the standard in-house method for trace element in rutile, analysing the following masses ²⁹Si, ⁴³Ca, ⁴⁷Ti, ⁴⁹Ti, ⁵¹V, ⁵²Cr, ⁵³Cr, ⁵⁶Fe, ⁵⁷Fe, ⁹⁰Zr, ⁹¹Zr, ⁹³Nb, ⁹⁵Mo, ⁹⁸Mo, ¹¹⁷Sn, ¹¹⁸Sn, ¹²¹Sb, ¹⁷⁸Hf, ¹⁸⁰Hf, ¹⁸¹Ta, ¹⁸²W and ¹⁸³W was performed using link scan mode.

The analysis was conducted with standard-sample bracketing to monitor analytical performance and correct for instrument drift during the analysis run. Rutile R632 (Axelsson et al., 2018) was used as primary standard, while NIST612 (GEOREM preferred values 09.07.2018), and NIST610 (GEOREM preferred values 09.07.2018) was used as secondary standard. Processing of raw data was performed in Iolite 4 (v. 4.4.5 (Paton et al., 2011)) using the trace element data reduction scheme (Longerich et al., 1996) to correct for down hole fractionation, instrumental mass bias compensation, element fractionation, and gas blanks correction. Ti47 was used as an internal standard.

Only ^{90}Zr is used from this data to calculate temperature estimates with the Zr in rutile thermometer by Kohn (2020). Standard performance for ^{90}Zr (4340.82 ppm) is within 0.25% of the reference value of ^{90}Zr in R623 (4330 ppm). The method for calculating temperature estimates is described further below.

Whole rock chemical analysis

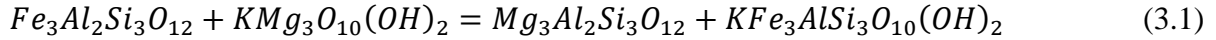
Whole rock chemical analysis was carried out by Bureau Veritas Minerals Pty Ltd, Perth, Australia. Code in brackets represent the service done by Bureau Veritas in their Minerals Service Guide. The sample preparation contained sorting and drying (PR001), crushing (PR103) and pulverising (PR301), while the analysis consisted of X-Ray Fluorescence Spectrometry (XRF) analysis (XF103), fused bead LA-ICP-MS (LA100) and LA-ICP-MS element determination (LA101). All five samples were crushed and pulverized in a vibrating disc pulveriser. SiO_2 , Al_2O_3 , Fe_2O_3 , CaO , MgO , MnO , TiO_2 , V_2O_5 , SO_3 , P_2O_5 , K_2O , Na_2O , SrO , Cr_2O_3 , As, Co, Cu, Ni, Zn, and Cl contents were determined by XRF on oven dry samples. Loss on ignition results was determined by heating the oven dry sample material to 1000°C using a robotic thermogravimetric analyser. FeO was determined volumetrically, and carbon was determined by Total Combustion Analysis. The pulverized samples were cast using a 66:34 flux with 4% lithium nitrate added to form a glass bead. Fused beads were analysed by LA-ICP-MS for trace and rare earth elements concentration of Ag, As, Bi, Cd, Ce, Co, Cr, Cu, Dy, Er, Eu, Ga, Gd, Ge, Hf, Ho, La, Lu, Mo, Nb, Nd, and Ni.

3.3 Numerical methods

Conventional geothermobarometry

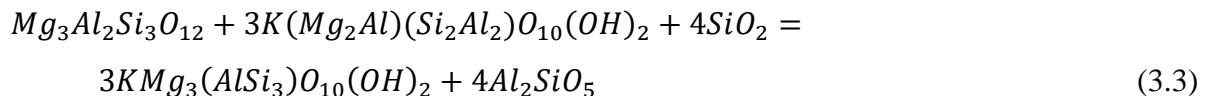
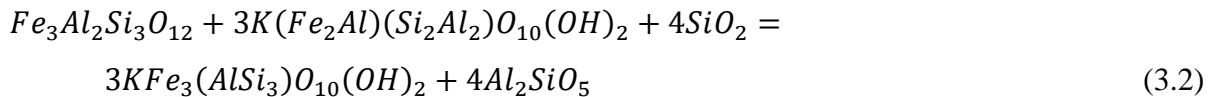
The conventional geothermobarometer used in this study is the garnet-biotite garnet-biotite-aluminosilicate-quartz (GB-GBAQ) geothermobarometer. This geothermobarometer couples the GB thermometer from Holdaway (2000) with the GBAQ barometer from Wu (2017).

The GB thermometer is based on the partitioning of Fe^{2+} and Mg^{2+} between garnet (almandine and pyrope) and biotite (annite and phlogopite) (Ferry and Spear, 1978) following:



The GB thermometer has been widely used and calibrated many times. The study of Wu and Cheng (2006) applied 26 calibrations of the GB thermometer to both experimental and natural metapelites. They concluded that the calibrations of Holdaway (2000) and Kleemann and Reinhardt (1994) were the best ones due to small errors in reproducing the experimental temperatures.

The GBAQ barometer is based on the two net-transfer reactions (Eq. 3.2) (Eq. 3.3) (Wu, 2017). These reactions involve Tschermak's substitution in the biotite solid solution which is sensitive to changes in pressure (Wu, 2017). The tschermak's substitution changes the total amount of Fe_{2+} and Mg atoms in the mineral formula (Miyashiro and Shido, 1985). Due to the activity models for both garnet and biotite in the GBAQ barometer are identical to those in the GB thermometer, both the barometer and the thermometer can be used simultaneously to acquire both pressure and temperature in the range of 450-950°C and 1-17 kbar (Wu, 2017). The PT estimates are acquired using an Excel spreadsheet provided by Wu (2017). The spreadsheet requires oxide weight percent data from both garnet and biotite. Once these are inserted into the spreadsheet, the PT conditions can be iteratively estimated. The GB thermometer has an absolute error of $\pm 25^\circ\text{C}$ while the GBAQ barometer has an error of 1.8 kbar.



In addition to the GB-GBAQ thermobarometer, this study will also make use of the Ti in biotite thermometer by Wu and Chen (2015). The thermometer is based on the amount of Ti incorporated in biotite crystals relative to the amounts of both Fe and Mg, in rutile and/or ilmenite bearing rocks (Wu and Chen, 2015) (Eq 3.4). Both Henry and Guidotti (2002) and Henry et al. (2005) previously calibrated the thermometer at pressure conditions of 3.3 kbar and 4-6 kbar, respectively. The thermometer by (Wu and Chen, 2015) is calibrated at a wider pressure range, 1-20 kbar, and has an error of $\pm 65^\circ\text{C}$.

$$\begin{aligned} \ln[T(\text{°C})] = & 6.313 + 0.224 \cdot \ln(X_{Ti}) - 0.288 \cdot \ln(X_{Fe}) \\ & - 0.449 \cdot \ln(X_{Mg}) + 0.15 \cdot P(\text{GPa}) \end{aligned} \quad (3.4)$$

To calculate the molar fractions for Ti, Fe and Mg, the weight percent oxide data from the microprobe analyses is first inserted into an excel spreadsheet by Li et al. (2020b) which calculates the chemical formula for the biotite crystals. The molar fractions are then calculated with the following equation by Wu and Chen (2015):

$$X_j = j/(Fe + Mg + Al^{IV} + Ti) \quad (3.5)$$

Trace element thermometry

The principle behind the Zr in rutile (ZrR) thermometer (Kohn, 2020) is that the amount of Zr that gets incorporated in rutile crystals is strongly temperature dependent (Troitzsch and Ellis, 2004). The thermometer is based on the net-transfer reaction from Kohn (2020):



Both a pressure estimate, which is acquired from the GBAQ barometer, and a Zr concentration, acquired from the LA-ICP-MS analysis, is needed in equation 3.7 (Kohn, 2020) to be able to calculate a temperature. The natural samples used in the calibration had a P-T range of 480-725°C and 3.5-31.5 kbar, and the final calculated temperature has an uncertainty of ±15°C (Kohn, 2020).

$$T(\text{°C}) = \frac{71360 + 0.378 \cdot P(\text{bars}) - 0.130 \cdot C(\text{ppm})}{130.66 - R \cdot \ln[C(\text{ppm})]} - 273.15 \quad (3.7)$$

Thermodynamic modelling

Determining PT-estimates through thermodynamic modelling was done with Perple_X (Connolly, 1990). A PT-pseudosection was made for Lin_14-19 in a KCNFMASHTi system. The input composition was based on the bulk rock data for Lin_14-19 and Lin_15-19. The composition was allowed to vary between the compositional values of Lin_14-19 and Lin_15-19, since both samples were from the same outcrop approximately 14 m apart. All input values were taken from the Lin_14-19 bulk rock data except FeO, H₂O and N₂O. CaO, MnO and P₂O₅ were excluded for simplification. The H₂O concentration was decreased from 0.93 wt.% to 0.85 wt.%, while the FeO and N₂O concentrations were taken from Lin_15-19. The input composition used can be seen in the build file (see Appendix - 1). The solution models used were Bi (W), Gt (W), Chl (W), Pl (JH), Mica (W), and St (W) (White et al., 2014, Jennings and Holland, 2015), together with the thermodynamic dataset by of Holland and Powell (1998) and

the CORK equation of state by Holland and Powell (1991). Minerals that had not been observed in the thin sections but appeared in the pseudosection were excluded during the modelling. Since the plagioclase solution model was already included, the albite endmember was excluded, together with the high temperature phases sanidine and osumilite.

Contour lines showing the volume percent for garnet, biotite, muscovite, kyanite, staurolite, plagioclase, quartz, rutile, and ilmenite were calculated with the “werami” executor in Perple_X (Connolly, 1990). The text files generated by Perple_X were plotted with the Matlab plotting script PERPLE_X_PLOT.

3.4 Image analyses

Image analysis was applied to estimate the volume percent of the different mineral phases in thin section, and to match microtextural observations with the outcome of the pseudosection modelling. This was done using the large-area BSE mosaic of Lin_14-19 and the image processing package Fiji in the ImageJ distribution (Schindelin et al., 2012). Due to the large file size, the large-area BSE mosaic was cut into nine tiles that were analysed separately, but all tiles were processed using an identical workflow. The tiles were first edited with the “Brightness/Contrast” function to make a sharper contrast between the different mineral phases. The tiles were then despeckled to remove pixels with significant color change. Outliers, both bright and dark, were then removed, followed by the “Sharpen” function. A shading gradient was detected in all tiles. The plug-in, *a posteriori* shading correction 514 v3 by Pinchon et al. (2005), was used to extract the background with the appropriate shading gradients. The background files were then subtracted from the tiles to remove the shading gradient. All tiles were thresholded to separate the greyscales (mineral phases) from each other. The thresholded images were then both eroded and dilated once before the “Close” function was used. The final step of the editing was to count the pixels in each of the thresholded images using the “Analyse particles” function using a small area cut-off of 10 pixels.

CHAPTER 4: RESULTS

4.1 Bulk rock

Five drill cores samples were analysed for their bulk rock geochemical composition. The resulting concentrations for rare earth elements (REE) (Fig 4.1a) and trace elements (Fig 4.1b) are presented in spider diagrams, normalized against Post Archean Australian Shale (PAAS). The normalized REE pattern for Lin_12a-19 and Lin_13-19 show that these samples are depleted in the light rare earth elements (LREE) La, Ce, Pr, Nd and Sm, and have a similar abundance of the heavy rare earth elements (HREE), Eu, Gd, Tb, Dy, Ho, Er, Tm, Yb, Lu, compared to PAAS. The pattern for Lin_12a-19 shows a depletion of up to ~17 times PAAS for La, and an increased concentration of the LREE up to Sm, which is depleted two times compared to PAAS. The abundance of LREE in Lin_13-19 is quite similar. Lin_13-19 has a depletion of 25 times PAAS for La, and a gradual increase in LREE. Lin_13-19 is depleted 1.5 times PAAS for Sm and has an HREE concentration very similar to PAAS. The three samples Lin_14-19, Lin_15-19 and Lin_16-19 all show normalized REE patterns which are very similar to PAAS.

Normalized trace element patterns for Lin_12a-19 and Lin_13-19 show that these samples are depleted in almost all high field strength elements (HFSE) and large-ion lithophile elements (LILE) except for Sr and Y. Concentration of Th in Lin_13-19 is 0, while it is depleted 500 times compared to PAAS for Lin_13-19. Both samples are slightly enriched in Sr, while they have a normal concentration of Y, compared to PAAS. Lin_12a-19 is slightly enriched in Sc, V and Co, and slightly depleted in V and Ni compared to PAAS, while Lin_13-19 is slightly enriched in all the elements, Sc, V, Cr, Co, and Ni compared to PAAS. The three samples Lin_14-19, Lin_15-19 and Lin_16-19 all show normalized trace element patterns which are very similar to PAAS. The REE and trace element patterns for these three samples show that they are perfectly normal sediments.

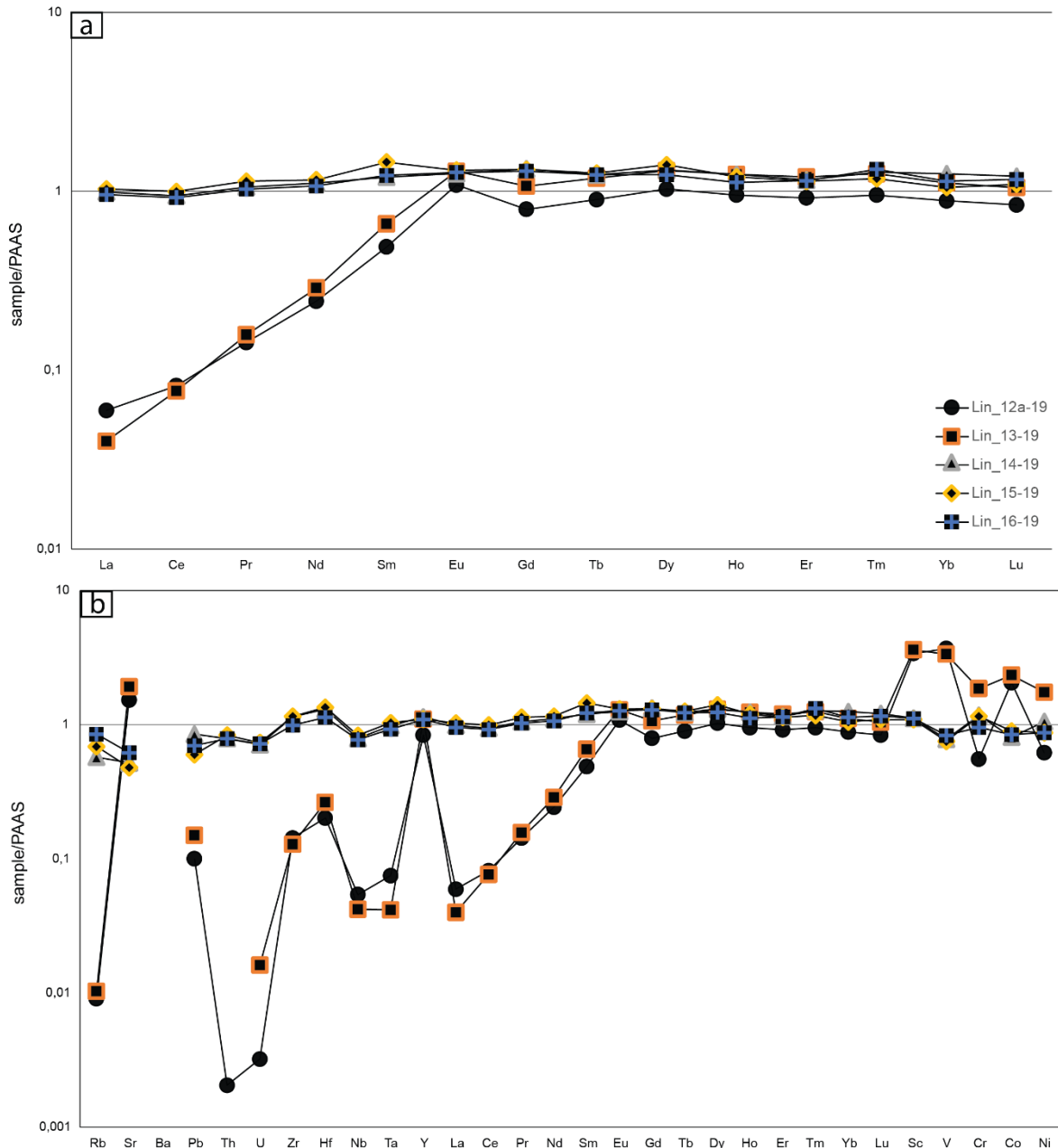


Figure 4.1 a) PAAS-normalized REE pattern for all rock samples. b) PAAS-normalized trace element pattern for all rock samples. Concentration of Ba was not measured. Normalisation values are taken from Taylor and McLennan (1985).

4.2 Petrology

All three rock types which were sampled (Table 3.1) were studied in a microscope. Based on petrological observations, the schist and garnet schist are renamed and from here on referred to as amphibolite and garnet-mica schist respectively. The three rock types described in this subchapter are amphibolite, garnet-mica schist, and metagreywacke.

Amphibolite

The amphibolite is characterized by a nematoblastic texture with alternating layers of foliated subidioblastic to xenoblastic actinolite crystals (Fig 4.4a) and layers of quartz and plagioclase. Accessory phases include epidote, rutile, opaque, and calcite. Epidote occurs as aggregates and is for the most part associated with the actinolite layers (Fig 4.2f Fig 4.3e-f and Fig 4.4b). Rutile and opaque are often found in direct contact and occur as clusters throughout the actinolite layers (Fig 4.2e and Fig 4.4c). Calcite is present both in the actinolite dominated layers (Fig 4.2d and Fig 4.4d) and the quartz and plagioclase layers. The actinolite contains inclusions of both rutile, opaque, epidote, quartz, and plagioclase. The calcite contains inclusions of actinolite, rutile, and opaque. Lin_12a-19, Lin_12b-19 and Lin_13-19 all have similar mineral assemblages but different mineral modes (Table 4.1). Lin_12a-19 consists of one actinolite layer where pockets of quartz and plagioclase, and the accessory phases, occur between the actinolite that is aligned with the rock foliations (Fig 4.2a). The top part of the Lin_12b-19 drill core consists of a layer of quartz and plagioclase, with minor amounts of actinolite and the accessory phases (Fig4.2b). Further down, the assemblage transitions into a layer which predominantly consists of actinolite together with small amounts of quartz, plagioclase, and the accessory phases (Fig 4.2c), and alternates with quartz, plagioclase rich layers. The deepest part of the sample that is captured in the thin section consists of an assemblage resembling sample Lin_12a-19, where quartz and plagioclase are dominant relative to the overlaying actinolite layers. Lin_13-19 is dominated by a layer almost exclusively consisting of actinolite, which covers two thirds of the thin section (Fig 4.3a-b). Minor amounts of quartz, plagioclase, rutile, opaque, and calcite are found within the actinolite layer, together with epidote (Fig 4.3e-f). The last third of the thin section consists of a quartz vein, which has a sharp boundary towards the actinolite layer (Fig 4.3c), with minor amounts of actinolite, rutile, opaque, epidote, and calcite (Fig 4.3d).

Table 4.1 Overview of size, mode and crystal shape of all mineral phases present in Lin_12-19, Lin_12b-19 and Lin_13-19.

Mineral	Size	Lin_12a-19	Lin_12b-19	Lin_13-19	Shape
		mode (%)	mode (%)	mode (%)	
Act	Up to 2625 µm	~72	~62	~55	subidioblastic
Qz	Up to 1075 µm	~17	~24	~33	subidioblastic
Pl	Up to 375 µm	~8	~11	~3	subidioblastic
Ep	Up to 250 µm	~2	~1	~4	xenoblastic
Opq	Up to 1000 µm	~1	~1	~1	xenoblastic
Rt	Up to 250 µm	~1	~1	~2	xenoblastic/ subidioblastic
Cal	Up to 1075 µm	>1	>1	>1	xenoblastic

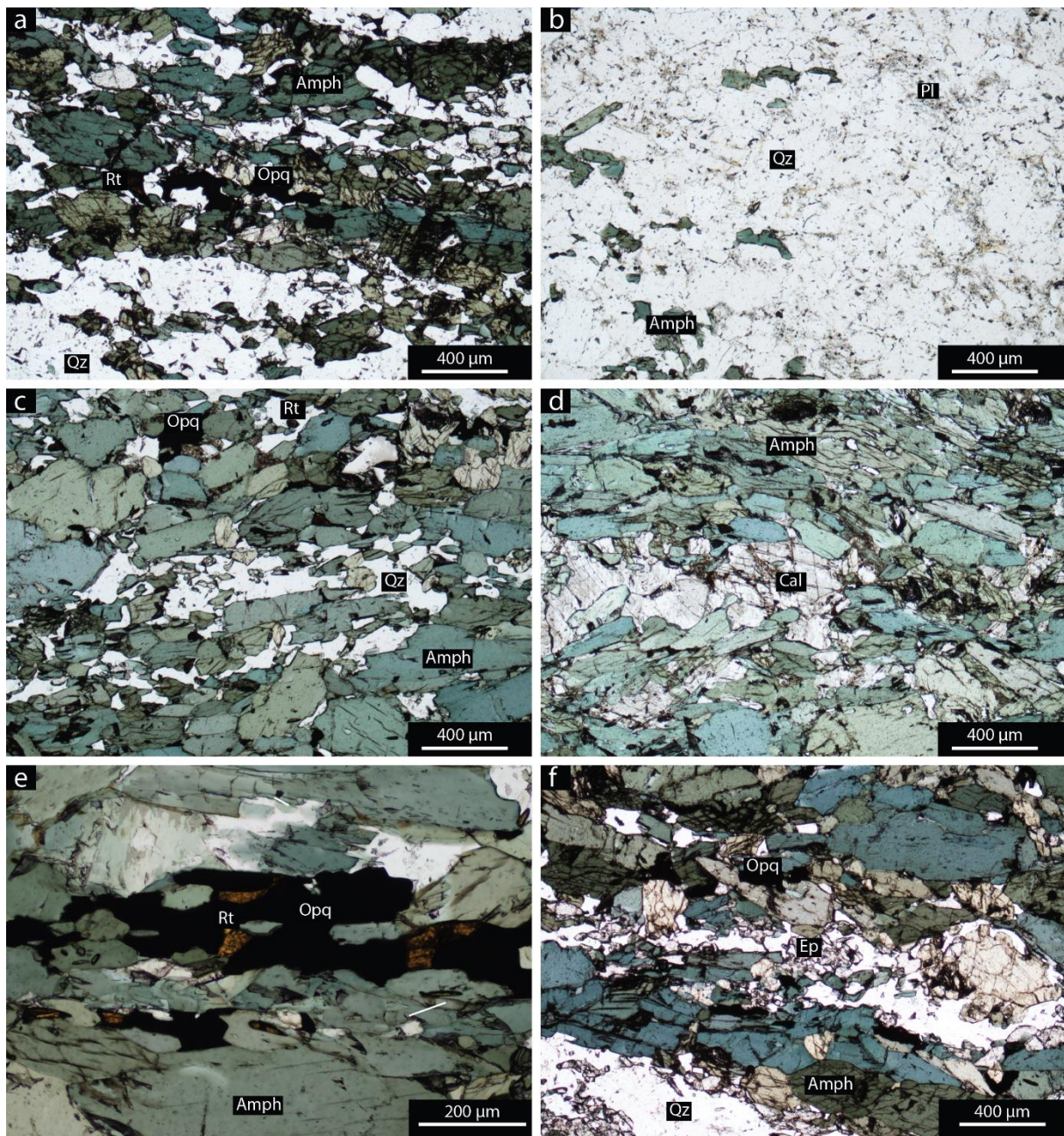


Figure 4.2 Photomicrographs of Lin_12a-19 and Lin_12b-19. a) Representative mineral assemblage in Lin_12a-19. b) Representative photomicrograph of the quartz and plagioclase layer in Lin_12b-19. c) Photomicrograph of the actinolite dominated layer in Lin_12b-19. d) Carbonate in Lin_12b-19. e) Coexisting rutile and opaque in Lin_12b-19. f)

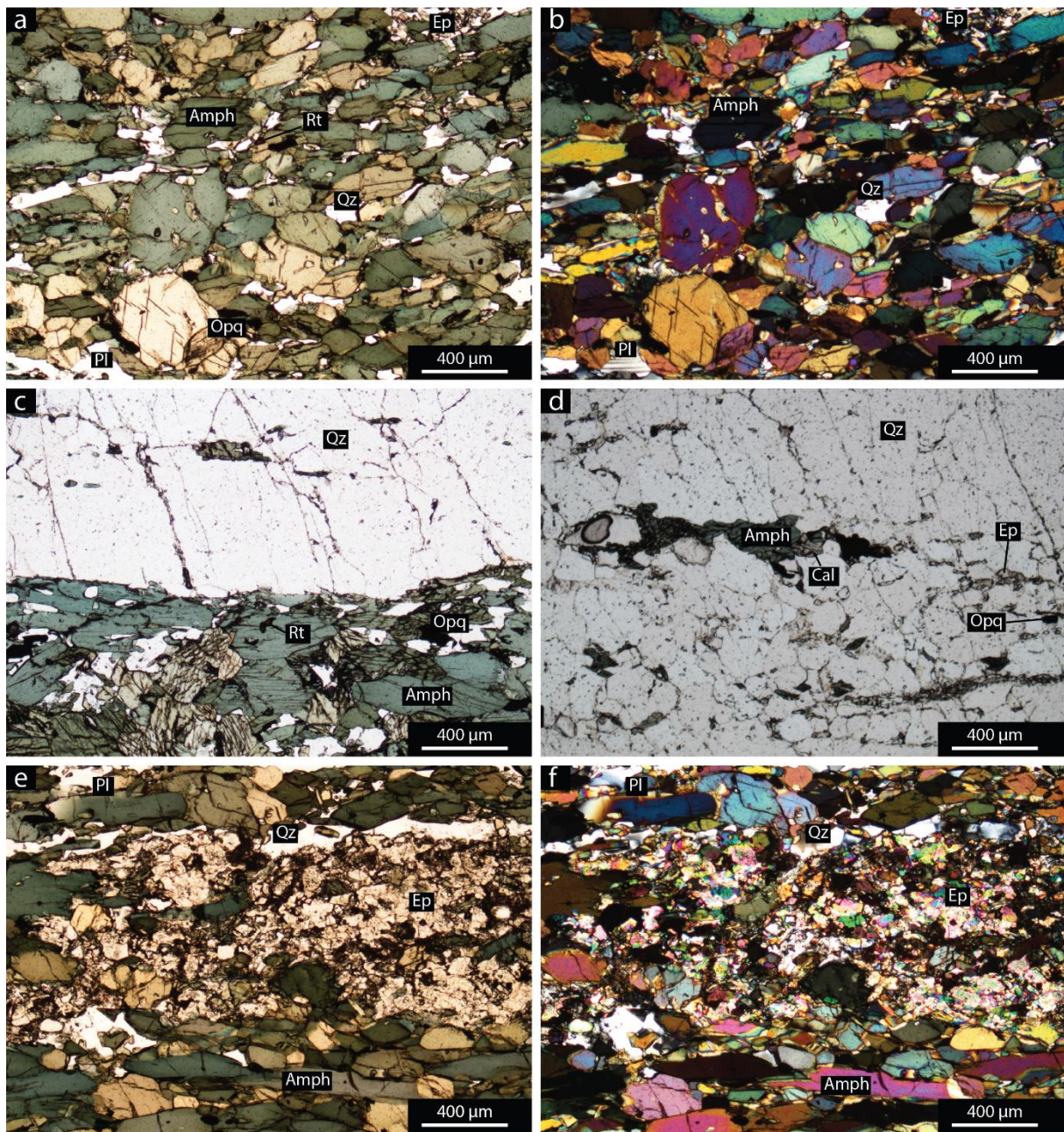


Figure 4.3 Photomicrographs of Lin_13-19. a) and b) representative mineral assemblage, consisting mainly of actinolite, with small amounts of quartz, plagioclase, rutile, opaque, and epidote (plane light (a) and crossed polars (b)). c) contact between the quartz vein and the actinolite. d) Inclusions of actinolite, calcite, epidote, and opaque in quartz vein. e) and f) cluster of epidotes in the actinolite (plane light (e) and crossed polars (f)).

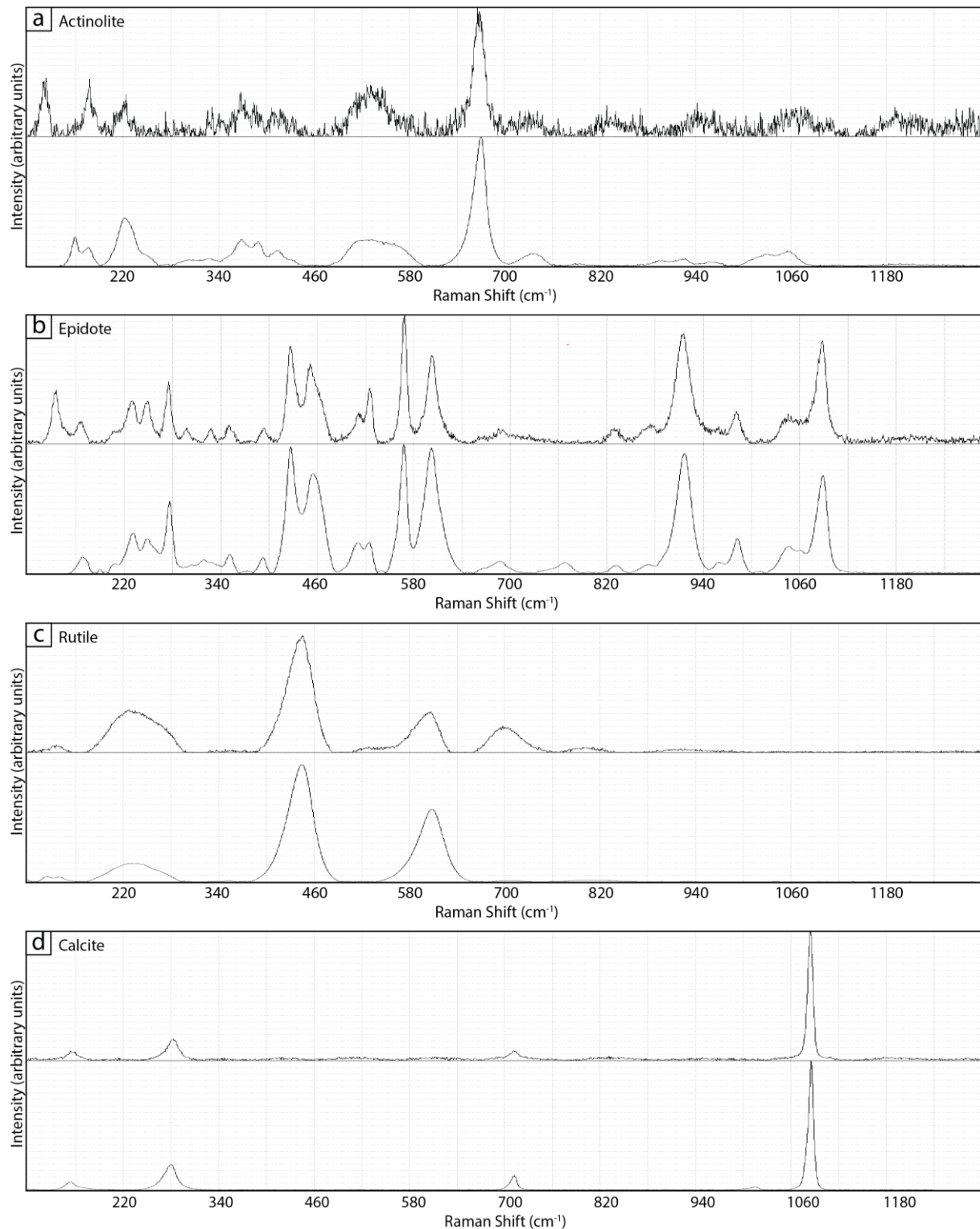


Figure 4.4 Raman spectra of minerals from the amphibolite (upper) compared with RRUFF reference spectra (lower) from CrystalSleuth (Laetsch and Downs, 2006). a) Raman spectra from actinolite compared with actinolite 532 nm (R050336). b) Raman spectra from the epidote seen in Figure 4.3e-f compared with epidote 532 nm (R050202). c) Raman spectra from rutile compared with rutile 532 nm (R050336). d) Raman spectra from calcite compared with calcite 532 nm (R040170).

Garnet-mica schist

Four thin sections, Lin_14-19, Lin_14b-19, Lin_15-19 and Lin_15b-19 were prepared from the same garnet-mica schist. Thin sections containing the letter b are duplicate sections. Samples Lin_14-19 and Lin_15-19 were sampled from the same outcrop but with different distances from the contact to the Kvitfjell ultramafic body. An overview of the mineralogy is shown in Table 4.3. The thin sections are characterised by porphyroblasts of subidioblastic to xenoblastic garnet (Fig 4.5a-b), in a matrix of quartz, biotite, plagioclase, muscovite, and chlorite (Fig 4.5c). Minor phases include kyanite, staurolite, tourmaline, and carbonates (Fig 4.5f and 4.6a-c), while the accessory phases are rutile, ilmenite, and zircon (Fig 4.5e and Fig 4.6b). All sheet silicates are foliated parallel to each other, giving the thin section a lepidoporphroblastic texture. Garnet contains inclusions of quartz, plagioclase, biotite, rutile, and ilmenite. Biotite is partly replaced by chlorite (Fig 4.5d) and contains zircon with pleochroic haloes (Fig 4.5e), as well as inclusions of rutile, ilmenite, quartz, and tourmaline. Zircon also occurs in the matrix, along the grain boundaries of biotite (Fig 4.5e and Fig 4.7c). White mica contains inclusions of both rutile and ilmenite. Kyanite contains inclusions of rutile, ilmenite, biotite, white mica, quartz, and tourmaline (Fig 4.5f and Fig 4.7a). Staurolite contains inclusions of quartz, rutile, and tourmaline (Fig 4.6a). Tourmaline crystals are zoned (Fig 4.6b). Rutile (Fig 4.7b) and ilmenite (see Appendix 2) occur both as separate crystals (Fig 4.5c) and in clusters (Fig 4.6b) throughout all thin sections.

Table 4.2 Overview of size, mode and crystal shape of all mineral phases present in Lin_14-19, Lin_14b-19, Lin_15-19 and Lin_15b-19.

Mineral	Size	Mode (%)	Shape
Qz	Up to 675 µm	46-50	xenoblastic
Bt	Up to 1750µm	15-20	xenoblastic/subidioblastic
Pl	Up to 600 µm	20-22	xenoblastic
Grt	1500 µm to 3125µm	5-7	subidioblastic/xenoblastic
Ms	Up to 425 µm	~1	xenoblastic
Chl	Up to 625µm	~1	xenoblastic
Ky	Up to 2550 µm	~1	subidioblastic/xenoblastic
St	Up to 450 µm	<1	subidioblastic
Tur	75µm to 225 µm	<1	idioblastic
Rt	Up to 250 µm	<1	subidioblastic/xenoblastic
Ilm	Up to 375 µm	<1	xenoblastic
Cal	1625µm	<1	xenoblastic
Zrn	Up to 100 µm	<1	idioblastic

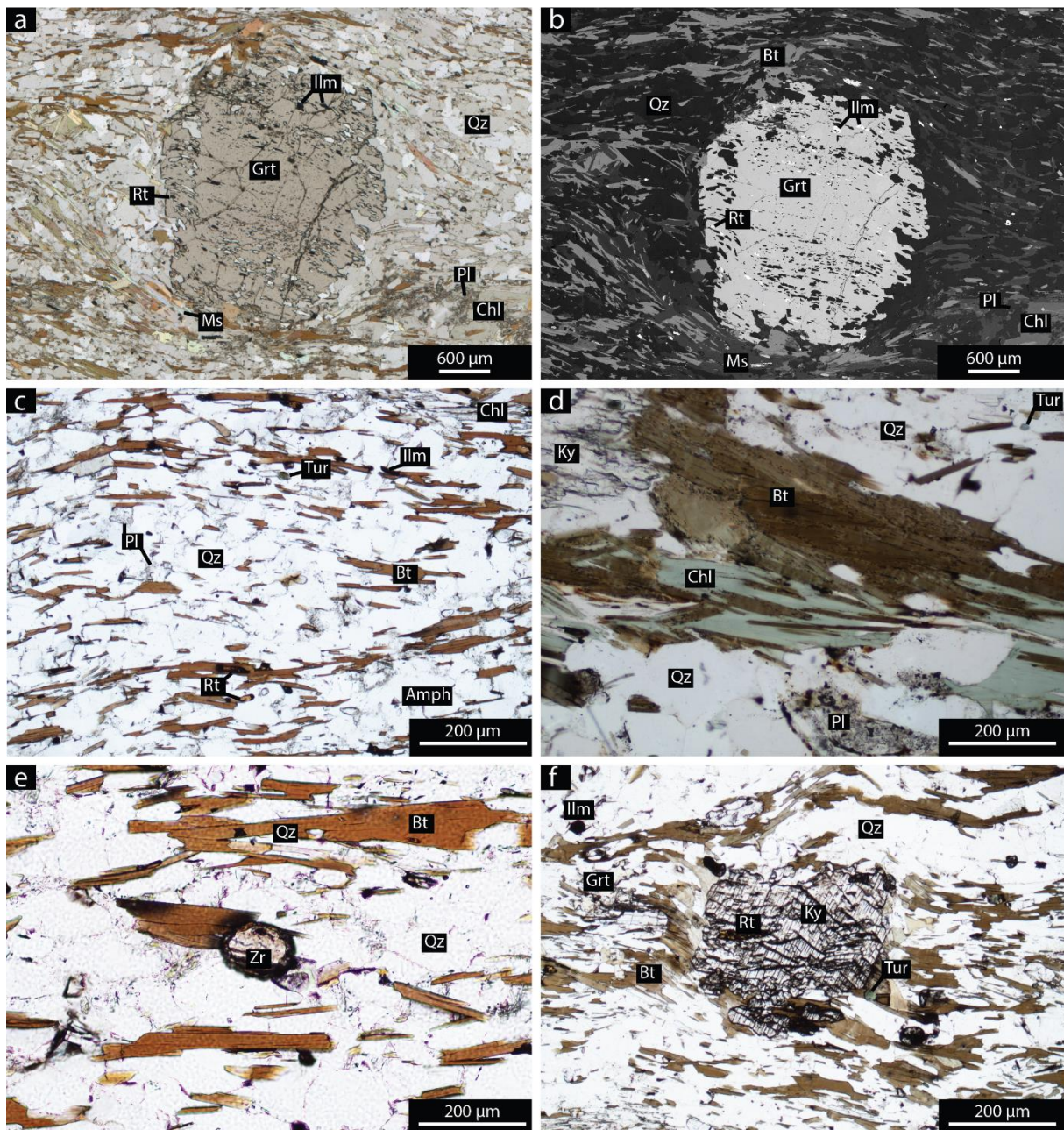


Figure 4.5 Photomicrographs of the garnet-mica schist. a) and b) Subidioblastic garnet with inclusions of quartz, rutile, and ilmenite (photomicrograph (a), and BSE image (b)). c) Representative mineral assemblage of the matrix with foliated biotite in Lin_14b-19. Pleochroic haloes around zircon inclusions in biotite can be seen at the top of the photomicrograph. d) Chloritization of biotite in Lin_15b-19. e) Zircon crystal in the matrix in Lin_14-19. f) Kyanite with rutile inclusion in Lin_15b-19.

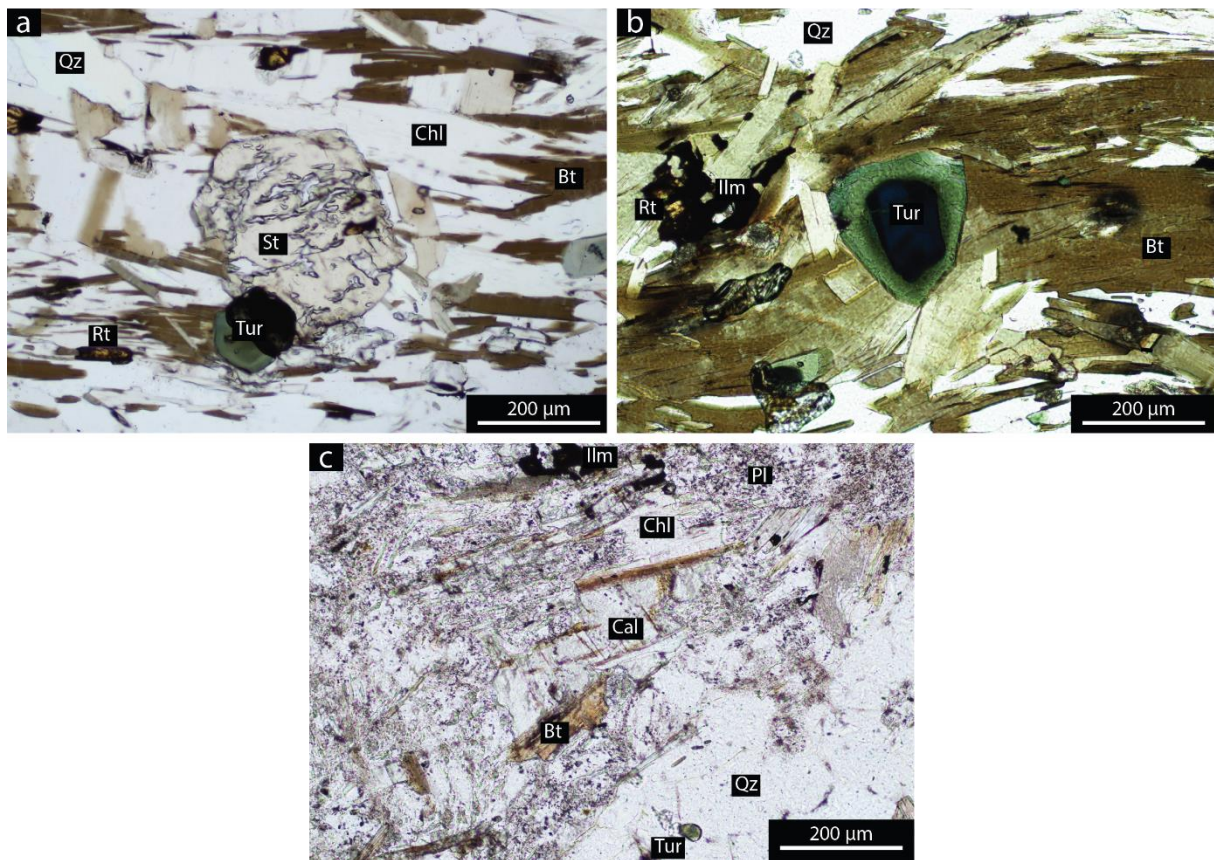


Figure 4.6 Photomicrographs of the garnet-mica schist. a) Subidioblastic staurolite with quartz and rutile inclusions in Lin15b-19. b) Zoned tourmaline in Lin_15b-19 with clusters of rutile and limenite. c) Calcite crystal in the matrix of Lin_14-19.

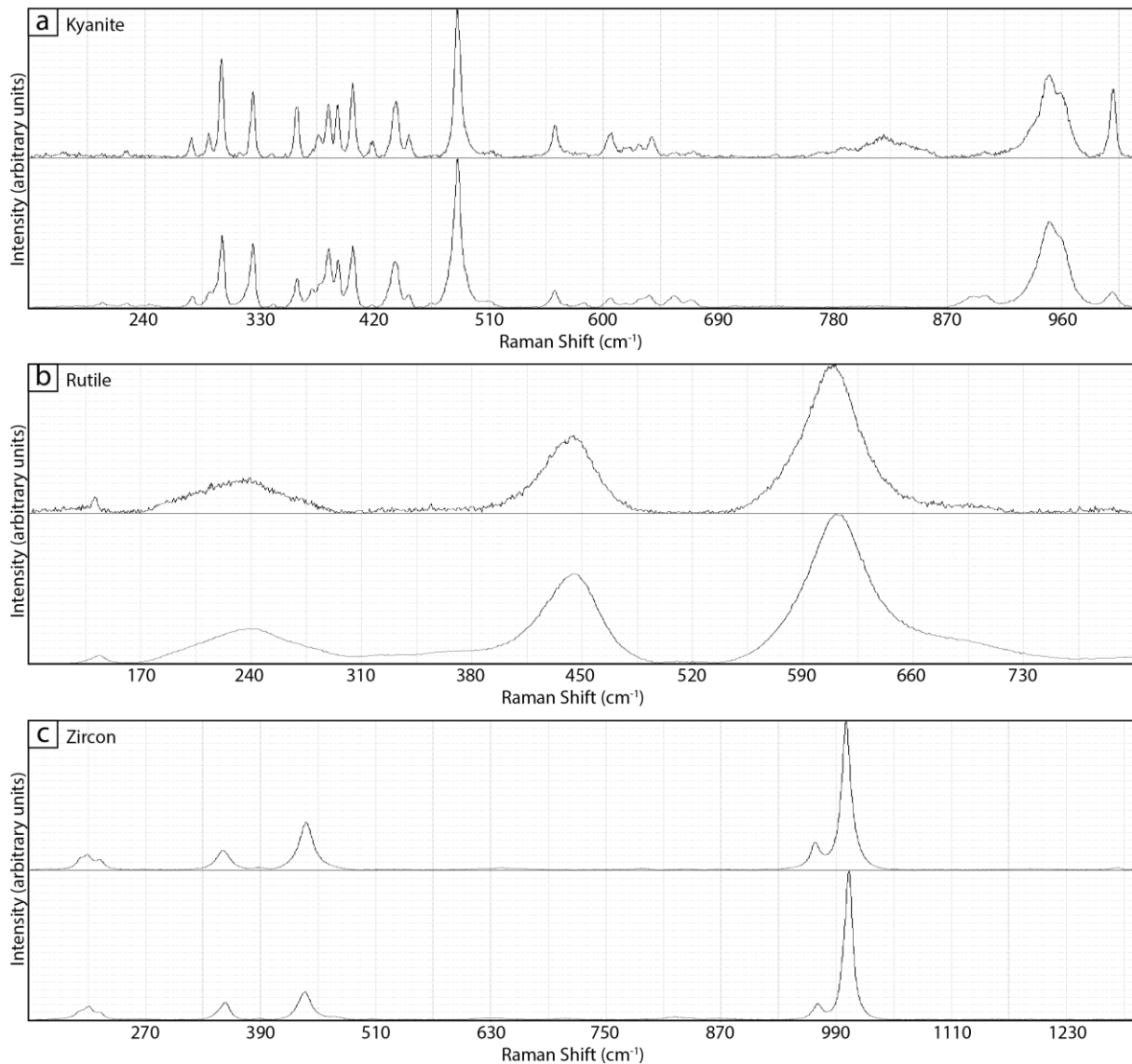


Figure 4.7 Raman spectra of minerals in the garnet-mica schist (upper) compared with RRUFF reference spectra (lower) from CrystalSleuth (Laetsch and Downs, 2006). a) Raman spectra from kyanite compared with kyanite 532 nm (R040119). b) Raman spectra from rutile compared with rutile 514 nm (R050034). c) Raman spectra from the zircon seen in Figure 4.5e compared with zircon 532 nm (R050034).

Metagreywacke

The metagreywacke contains porphyroblasts of xenoblastic garnet (Fig 8.6a) and tschermakite (Fig 4.8b) in a matrix of muscovite, biotite, chlorite, quartz, and plagioclase (Fig 4.8c). The accessory minerals are comprised of tourmaline, dolomite (Fig 4.9c), epidote (Fig 4.9a), rutile (Fig 4.9b), and opaque. All sheet silicates are foliated parallel to each other, giving the thin section a lepto-porphyroblastic texture. The anhedral garnet porphyroblasts contain inclusions of quartz, epidote, and opaque, while the tschermakite porphyroblasts contain inclusions of quartz, epidote, opaque, and biotite. Biotite crystals are sometimes partly replaced by chlorite (Fig 4.8c) and contain zircon surrounded by pleochroic haloes (Fig 4.8e), as well as inclusions

of rutile, opaque, quartz, and tourmaline. Muscovite contains inclusions of quartz, tourmaline, rutile, and opaque. Xenoblastic aggregates and idioblastic crystals of epidote are predominantly concentrated within, and in the area around the tschermakite porphyroblasts (Fig 4.8b) with only small amounts in the matrix (Fig 4.8f). The epidote contains inclusions of quartz and opaque. Idioblastic tourmaline crystals in the matrix are zoned (Fig 4.8f).

Table 4.3 Overview of size, mode and crystal shape of all mineral phases present in Lin_16-19.

Mineral	Size	Mode (%)	Shape
Qz	Up to 1425 µm	~32	xenoblastic/subidioblastic
Bt	Up to 1755 µm	~38	xenoblastic/subidioblastic
Pl	Up to 750 µm	~16	xenoblastic/subidioblastic
Grt	1250-2750 µm	~1	xenoblastic
Ts	Up to 2000 µm	~1	xenoblastic
Ms	Up to 2125 µm	~3	xenoblastic
Chl	Up to 375 µm	<1	xenoblastic
Tur	Up to 200 µm	<1	idioblastic
Ep	Up to 275 µm	~4	idioblastic/xenoblastic
Rt	Up to 100 µm	<1	xenoblastic
Opq	Up to 750 µm	~2	xenoblastic/idioblastic
Dol	Up to 2375 µm	~2	subidioblastic

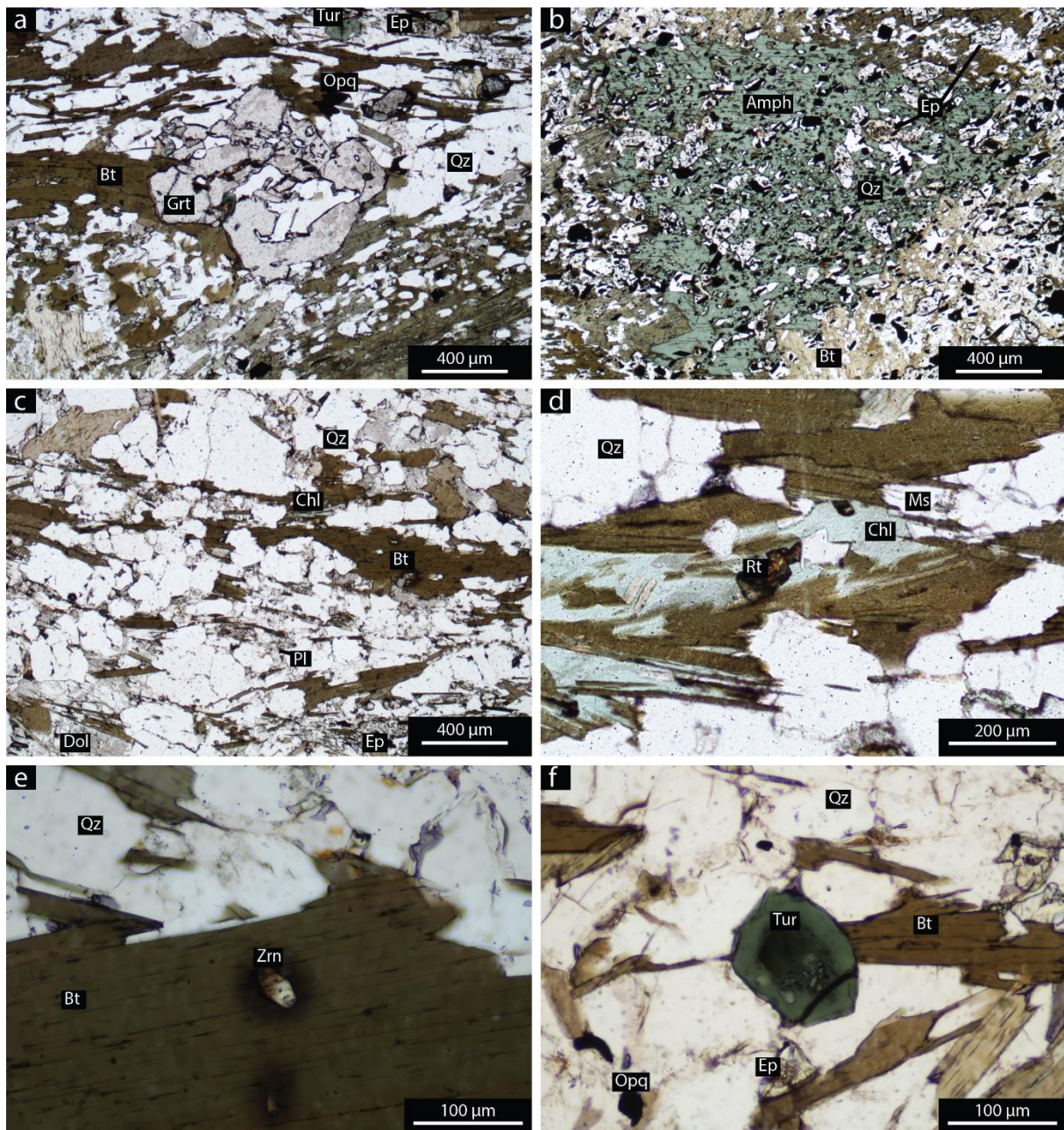


Figure 4.8 Photomicrographs of the metagreywacke. a) Porphyroblast of xenoblastic garnet with inclusions of tourmaline, quartz, and ilmenite. b) Porphyroblast of xenoblastic amphibole with inclusions of epidote, quartz, ilmenite, and biotite. c) Representative mineral assemblage in the matrix. d) Chloritization of biotite with quartz and rutile inclusion. e) Zircon crystal surrounded by pleochroic halo within a biotite crystal. f) Zoned tourmaline with fine-grained xenoblastic epidote.

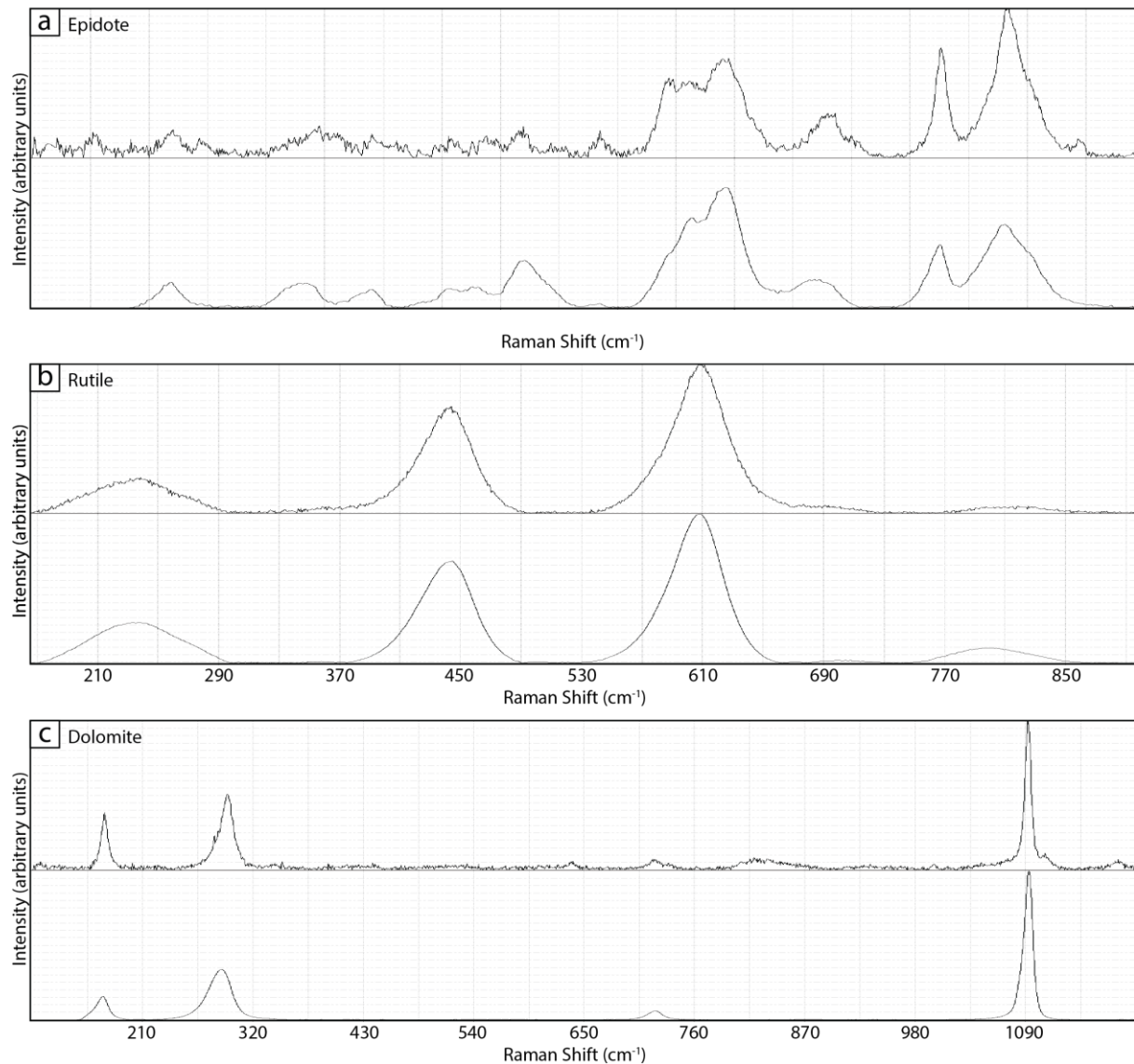


Figure 4.9 Raman spectra of minerals in the garnet mica schist (upper) compared with RRUFF reference spectra (lower) from CrystalSleuth (Laetsch and Downs, 2006). a) Raman spectra from epidote compared with epidote 532 nm (R070205). b) Raman spectra from rutile compared with rutile 532 nm (R050417). c) Raman spectra from dolomite compared with dolomite 532 nm (R050129).

4.3 Mineral chemistry

Garnet

Subidioblastic garnet in the garnet mica schist (samples Lin_14-19 and Lin_15-19) shows varying degrees of zoning (Fig 4.10a and b). The amount of almandine in the cores varies between ~63 and ~71%, grossular ~17 to ~23%, pyrope ~7 to ~14% and spessartine ~0.3 to ~7%. The average core composition of garnet in the garnet-mica schist is $\text{Alm}_{68}\text{Grs}_{19}\text{Prp}_{10}\text{Sps}_3$. The amount of almandine on the rim varies between ~65 and ~71%, grossular ~14 to ~20%, pyrope ~10 to ~16% while the amount of spessartine varies between ~0.1 and ~4%. The average rim composition for the garnets in the garnet mica schists is $\text{Alm}_{68}\text{Grs}_{17}\text{Prp}_{13}\text{Sps}_1$.

Subidioblastic garnet in the metagreywacke (samples Lin_16-19) shows slight zoning. The amount of almandine in the cores is approximately ~61-62%. The content of grossular ranges between ~12 and ~14%, pyrope ~14 to ~15% and a spessartine content of ~9 to ~11%. The rims vary slightly more in composition. The content of almandine ranges from ~57 to ~63%, grossular ~13 to ~15%, pyrope ~13 to ~15% and spessartine ~9 to ~16%. Garnet in the metagreywacke has an average core composition of $\text{Alm}_{62}\text{Grs}_{13}\text{Prp}_{14}\text{Sps}_{11}$, and an average rim composition of $\text{Alm}_{60}\text{Grs}_{14}\text{Prp}_{14}\text{Sps}_{13}$.

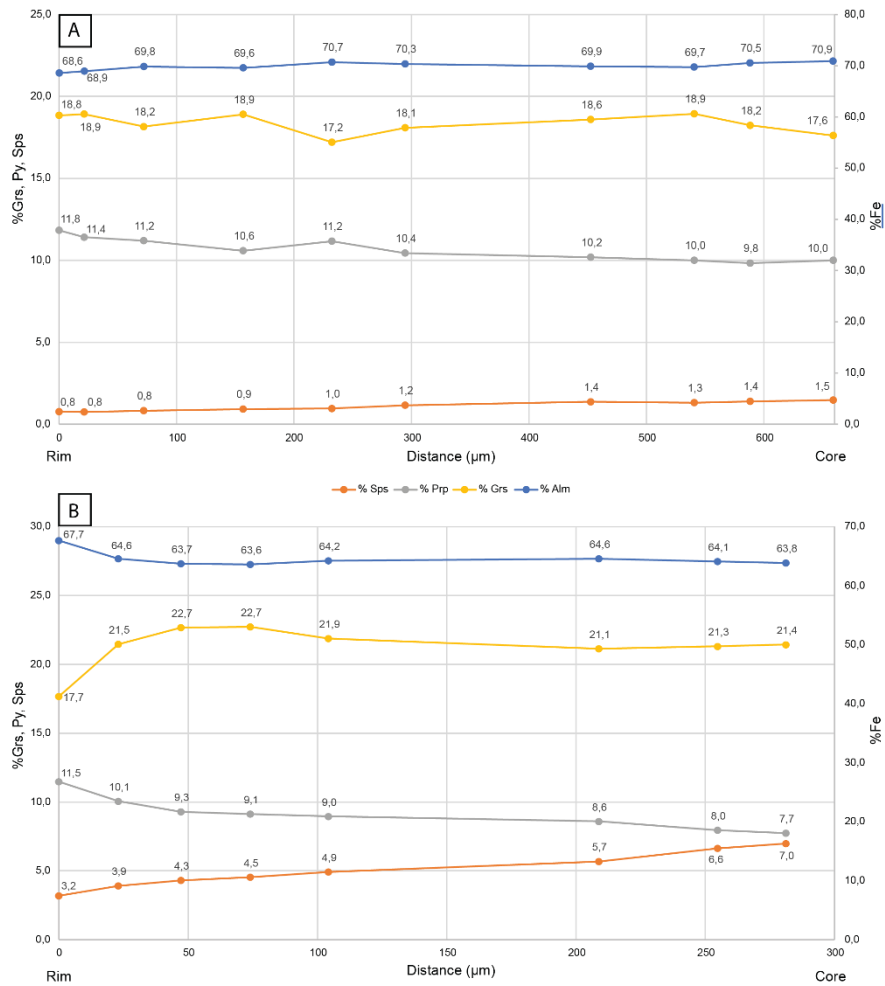


Figure 4.10 Chemical composition profiles from rim to core (i.e., half grains) of garnet in Lin_14-19 and Lin_15-19. a) Representative composition of garnet in Lin_14-19 (Appendix 5, Lin_14-19/Site 1/Area 4). b) Representative composition of a garnet from Lin_15-19 (Appendix 5, Lin_15-19/Site 3/Area 3).

Biotite

Subidioblastic foliated biotite in the garnet mica schists and metagreywacke has a chemical composition between phlogopite, “eastonite”, annite and siderophyllite (Fig 4.11). Biotite in the garnet mica schists has more Al and Fe than biotite in the metagreywacke, and therefore has a composition that is closer to the “eastonite” endmember. Biotite in the metagraywacke has less Al and Fe, i.e., closer to phlogopite. X_{Ti} in biotite from both the garnet mica schist and metagreywacke range between 0.03 and 0.05.

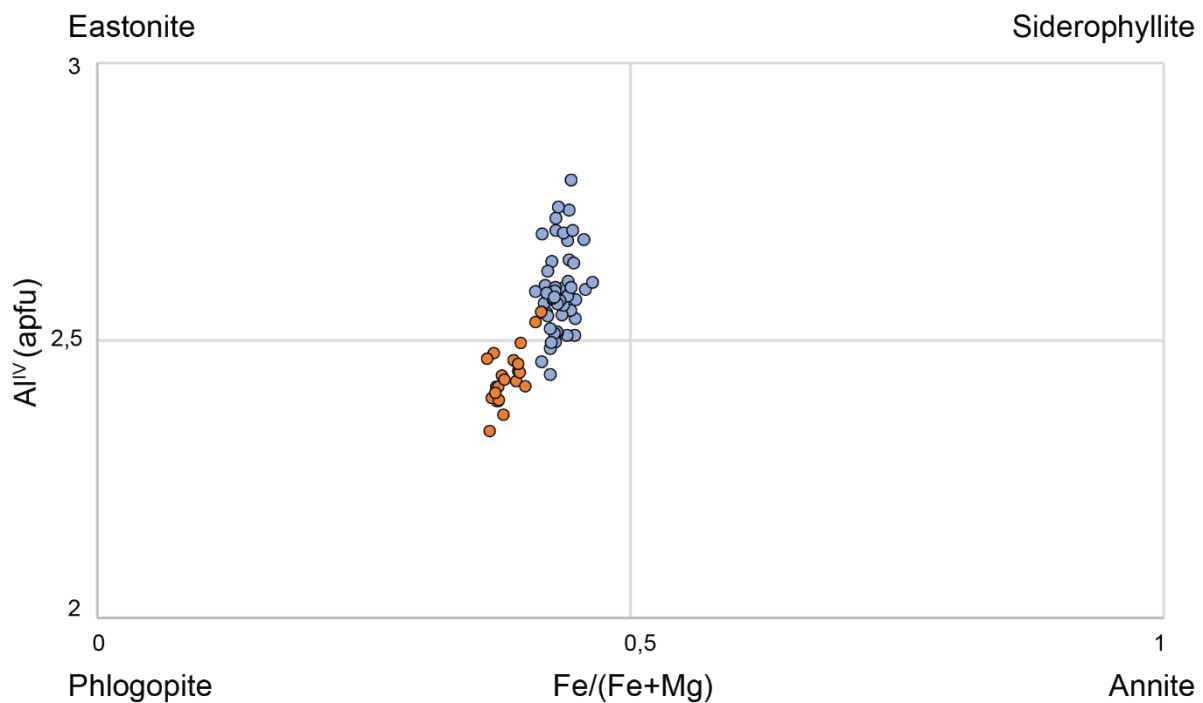


Figure 4.11 Showing the classification of biotite in Lin_14-19 and Lin_15-19 (blue, n=52) and Lin_16-19 (orange, n=22). The chemical formulae for biotite were calculated using the results from the EMP and the Microsoft Excel spreadsheet from Li et al. (2020b). The diagram follows Deer et al. (1992).

White mica

White mica in both the garnet mica schist and the metagreywacke has a chemical composition which corresponds to muscovite (Fig 4.12). In the metagreywacke, white mica has slightly more Mg and Fe²⁺ than white mica in the garnet mica schist. White mica in the garnet mica schist has an average of 1.74 K atoms per formula unit (apfu) based on 24 oxygens, and 0.19 Na apfu. Hence, white mica has a composition of 90% muscovite and 10% paragonite. White mica in the metagreywacke has an average of 1.89 K apfu and 0.12 Na apfu, and hence is classified as 94% muscovite and 6% paragonite.

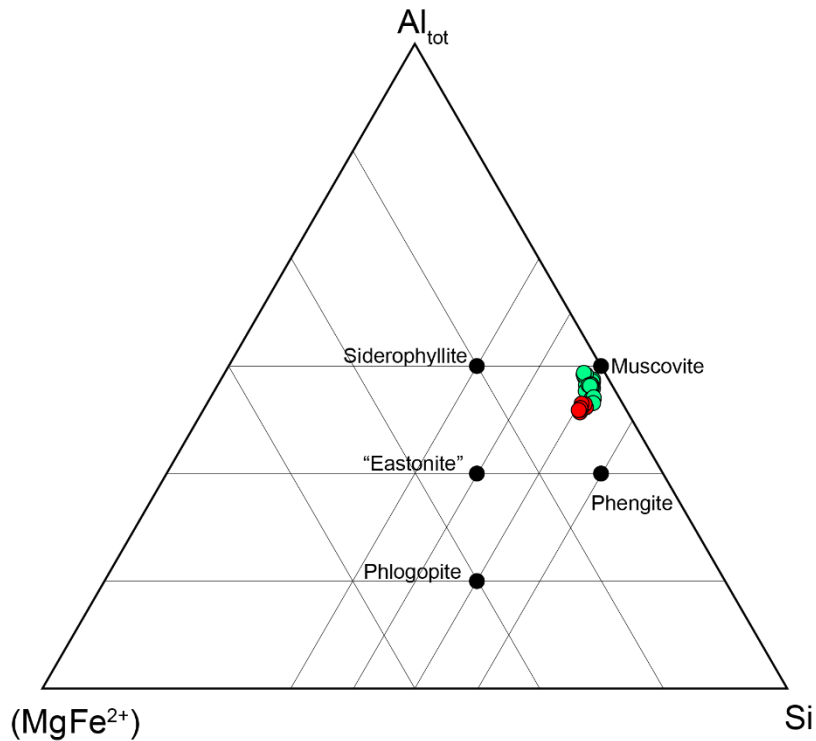


Figure 4.12 Ternary plot of the chemical composition of white mica present in the three thin sections Lin_14-19, Lin_15-19 (green, n=17) and Lin_16-19 (red, n=8). Siderophyllite: $\text{Al}_{\text{tot}}=6$, $\text{MgFe}^{2+}=4$, $\text{Si}=4$. “Eastonite”: $\text{Al}_{\text{tot}}=4$, $\text{MgFe}^{2+}=5$, $\text{Si}=5$. Phlogopite: $\text{Al}_{\text{tot}}=2$, $\text{MgFe}^{2+}=6$, $\text{Si}=6$. Muscovite: $\text{Al}_{\text{tot}}=6$, $\text{MgFe}^{2+}=0$, $\text{Si}=6$. Phengite: $\text{Al}_{\text{tot}}=4$, $\text{MgFe}^{2+}=1$, $\text{Si}=7$. The diagram follows Deer et al. (1992)

Plagioclase

Plagioclase compositions in all three thin sections are mostly albite rich (Fig 4.13), while the potassic feldspar content is on average 0.4%. The plagioclase in the garnet mica schist has an average composition of 70% albite and 30% anorthite, while it is 64% albite and 36% anorthite in the metagreywacke.

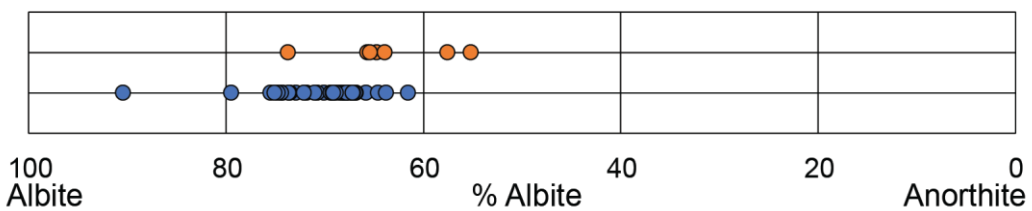


Figure 4.13 Plot of the plagioclase composition of Lin_14-19 and Lin_15-19 (blue, n=43) and Lin_16-19 (orange, n=7).

Amphibole

Amphibole in sample Lin_16-19 is classified as sodium-rich tschermakite (Fig 4.14). The chemical formulae for the amphibole were calculated using the Microsoft Excel spreadsheet from Li et al. (2020a) and the results from the EMP analysis.

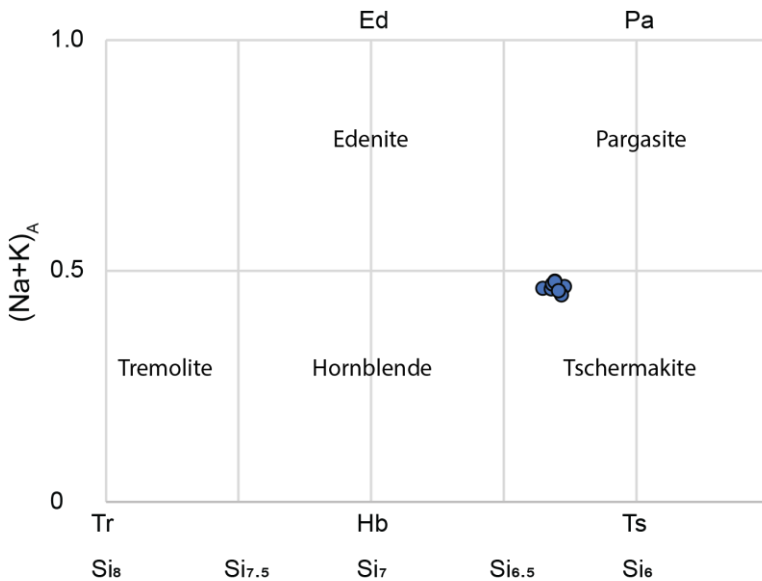


Figure 4.14 Classification of the amphiboles in Lin_16-19 (n=10). The diagram follows Deer et al. (1992).

4.4 Thermobarometry

GB-GBAQ thermobarometry

A total of 343 spots analyses were conducted with the Electron Microprobe at the University of Utrecht (see Appendix – 4). These analyses were collected from garnet, biotite, plagioclase, muscovite, and amphibole.

Calculations of pressure (P) and temperature (T) from the GB-GBAQ thermobarometer is done using the Microsoft Excel spreadsheet from Wu (2017), where the GBAQ barometer is coupled with the GB thermometer by Holdaway (2000). Only garnet and biotite that were in direct contact, and therefore assumed to be equilibrated, were used PT calculations. The ferric iron content in biotite was calculated by using a Microsoft Excel spreadsheet from Li et al. (2020b). The ferric iron content in garnet was estimated to be zero. When the chemical formula for garnet is calculated from the microprobe data, it results an Al value of more than two per 12 oxygens. This means that all Al in the chemical formula is placed in the octahedral site of the garnet. When the octahedral site is filled with Al, there is no more room for Fe^{3+} , and the Fe^{3+} is therefore assumed to be 0.

Pressure and temperature were calculated for 7 pairs of garnet and biotite in direct contact in Lin_14-19 and Lin_15-19 (Fig 4.15a). The results show that the calculated pressure ranges between 6.68 kbar and 7.33 kbar, while the temperature ranges between 575°C and 608°C. To check whether chemical equilibrium has occurred on a thin section scale, PT calculations were also made for non-touching garnet and biotite (Fig 4.15b).

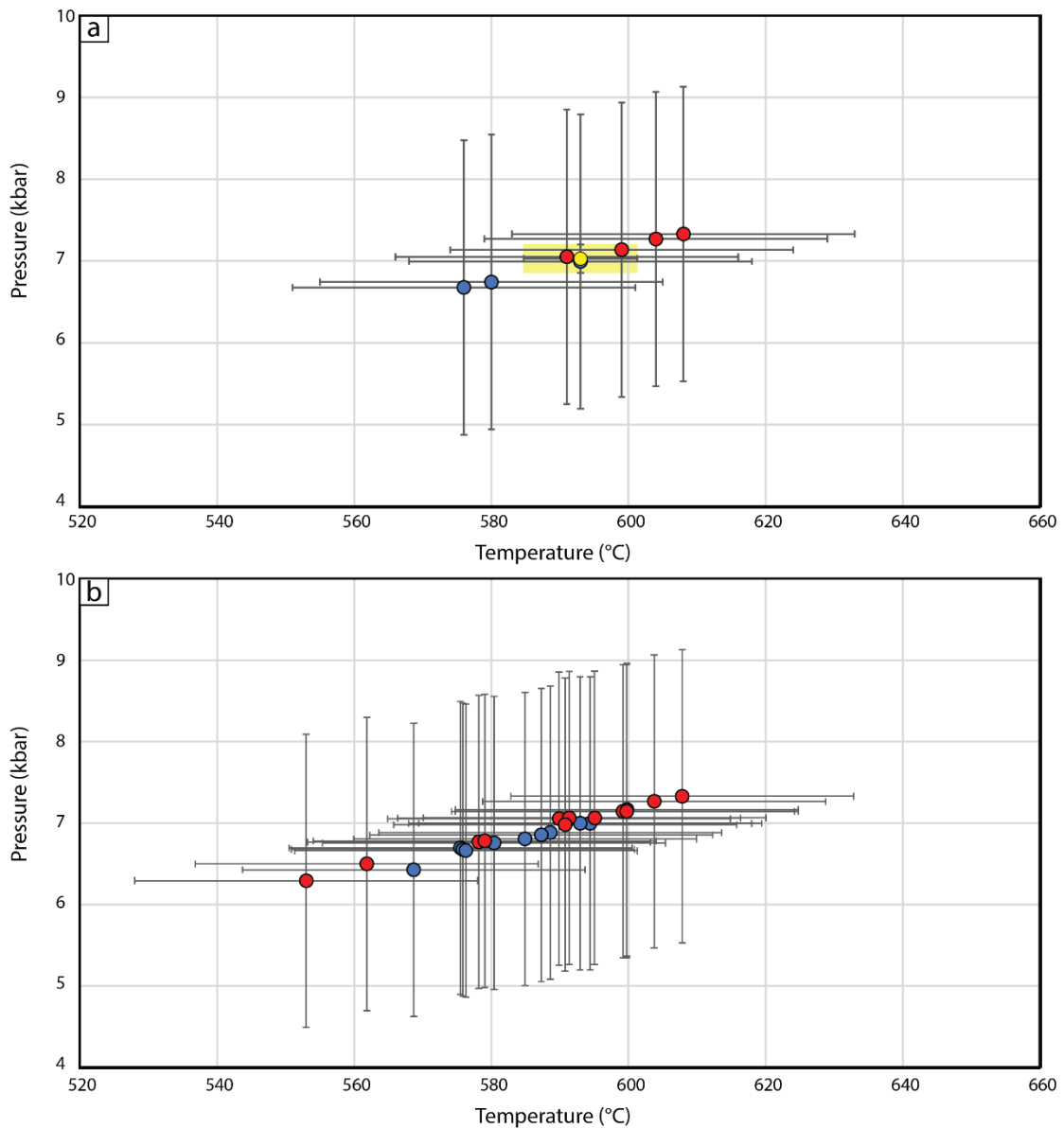


Figure 4.15 Calculated pressure and temperature from the GB-GBAQ geothermobarometer for Lin_14-19 (blue) and Lin_15-19 (red). Uncertainty in pressure is 1.8 kbar, which is inherited from the calculation (Wu, 2017). Uncertainty in temperature is 25°C, inherited from the calculation (Holdaway, 2000). a) The yellow rectangle represents the average of the data population and is located at a pressure of $7.03 \text{ kbar} \pm 0.17 \text{ kbar}$ ($2\sigma_{\text{mean}}$) and a temperature of $593^\circ\text{C} \pm 8^\circ\text{C}$ ($2\sigma_{\text{mean}}$). b) PT data from non-touching garnet and biotite.

The PT estimate based on sample Lin_16-19 is higher than that derived from samples Lin_14-19 and Lin_15-19 (Fig 4.16). The estimated pressure ranges between 7.48 and 7.93 kbar, while the temperature ranges between 598°C and 619°C. The average of the data population has a temperature of $602^{\circ}\text{C} \pm 6^{\circ}\text{C}$ ($2\sigma_{\text{mean}}$) and a pressure of $7.63 \text{ kbar} \pm 0.13 \text{ kbar}$ ($2\sigma_{\text{mean}}$).

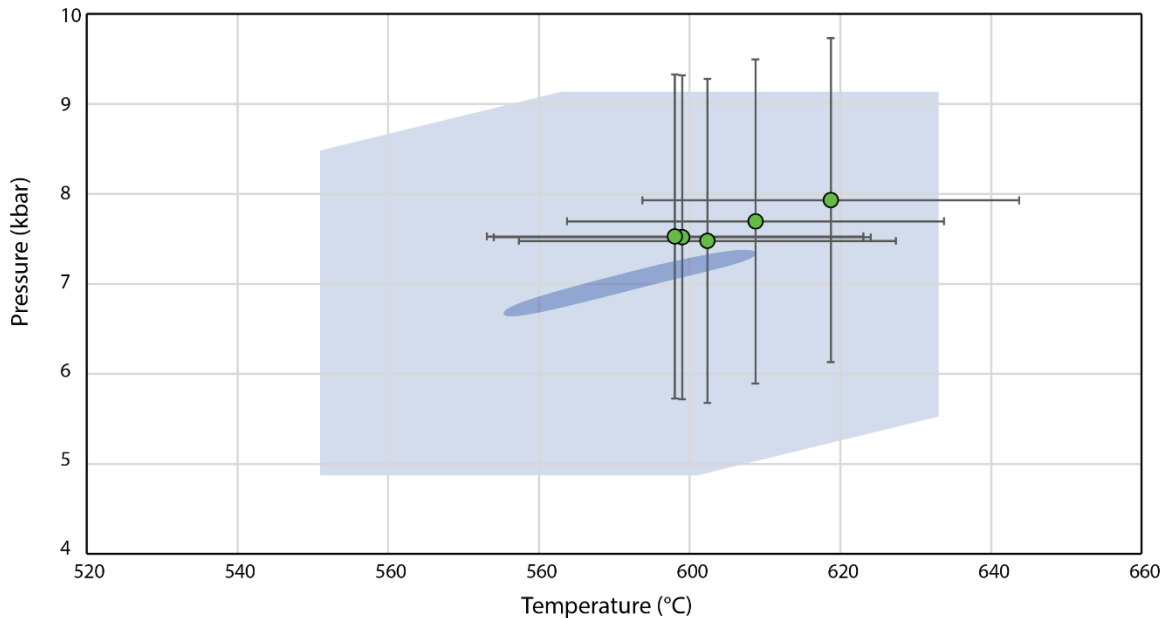


Figure 4.16 Calculated pressure and temperature from the GB-GBAQ geothermobarometer for Lin_16-19. The calculation is based on the composition of garnet and biotite that are in direct contact with each other. Blue ellipsoid and light blue field represent the data population for Lin_14-19 and Lin_15-19 and their uncertainty.

Ti in biotite thermometry

A total of 52 biotite crystals in Lin_14-19 and Lin_15-19 were analysed with the EMP and were used for Ti-in-biotite thermometry (Wu and Chen, 2015). The average, minimum Ti in biotite and maximum Ti in biotite thermometric slopes were plotted with a barometric slope from the GBAQ barometer (Wu, 2017) (Fig 4.17). The barometric slopes for all seven data points in Figure 4.15a were extracted and averaged to couple the Ti-in-biotite thermometer with the GBAQ barometer. The P-T field generated by the crossing barometric and thermometric slopes range in temperatures between 479°C and 632°C , and pressures between 2.63 kbar and 9.74 kbar. As previously stated, there is a 1.8 kbar uncertainty in the pressure estimate (Wu, 2017), while the temperature estimate has an uncertainty of 65°C (Wu and Chen, 2015).

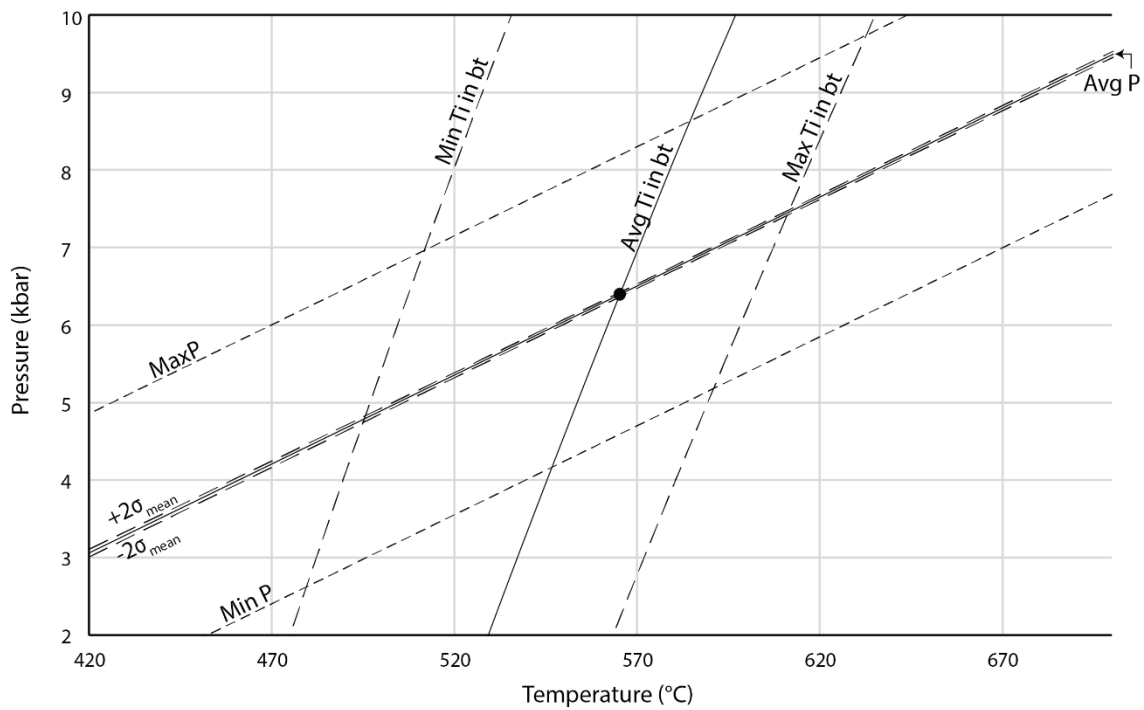


Figure 4.17 P-T data from the Ti in biotite thermometer coupled with the GBAQ barometer. Interception between the barometric and thermometric slopes is marked by a black circle and is located at a pressure of $6.40 \text{ kbar} \pm 0.09 \text{ kbar}$ ($2\sigma_{\text{mean}}$) and a temperature of $565^\circ\text{C} \pm 37^\circ\text{C}$ (2σ).

Zr in rutile thermometry

A total of 52 rutile crystals were analysed by LA-ICP-MS, while only 11 rutile crystals had a concentration of zirconium which corresponded when both external standards were used (Table 4.4).

Table 4.4 Concentration of Zr and two standard error from the 11 rutile crystals used for the Zr in rutile thermometer.

Sample	Zr (ppm)	2SE(ppm)
A1-S1	145	3
A1-S2	143	4
A5-S1	143	10
A5-S2	151	4
A5-S3	146	5
A5-S4	148	5
A5-S5	144	4
A6-S1	126	5
A8-S2	148	5
A9-S2	137	6
A9-S3	152	5
Average	144	4

The average highest and lowest concentrations of Zr is inserted to Eq 3.7 by Kohn (2020). The equation constructs three thermometric slopes which are plotted with the same barometric slopes as in Figure 4.17 (Fig 4.18). The ZiR thermometer in combination with the GBAQ barometer defines a T range of 531°C to 564°C at a pressure range between 3.82 kbar and 8.17 kbar. The uncertainty from the calculation of the ZiR thermometer is $\pm 15^\circ\text{C}$ (Kohn, 2020).

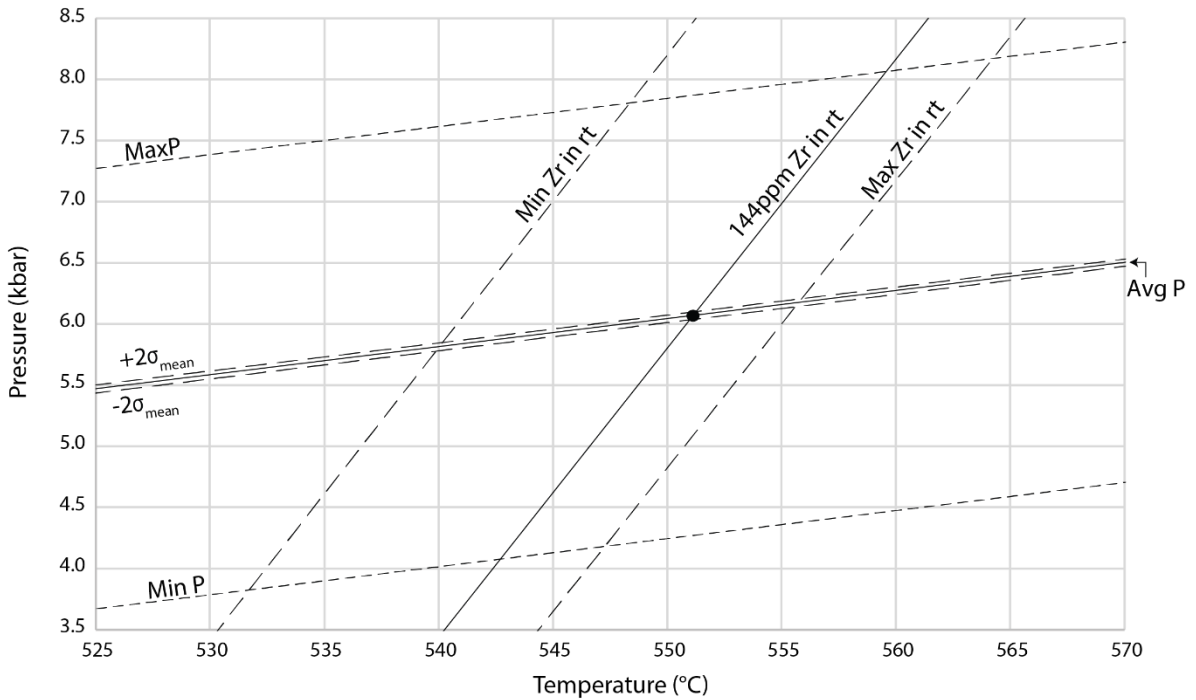


Figure 4.18 P-T data from the Zr in rutile thermometer coupled with the GBAQ barometer. Interception between the barometric and thermometric slopes is marked by a circle and is located at a pressure of $6.07 \text{ kbar} \pm 0.03 \text{ kbar}$ ($2\sigma_{\text{mean}}$) and a temperature of $551^\circ\text{C} \pm 8^\circ\text{C}$ ($2\sigma_{\text{mean}}$).

4.5 Modelling and contours

A PT pseudosection was calculated using the computer program Perple_X (Connolly, 1990) using the bulk rock composition of the garnet-mica schist (Fig 4.19a). Garnet, biotite, plagioclase, and quartz are stable over the entire PT range covered by the pseudosection. The peak metamorphic mineral assemblage of the garnet-mica schist consists of garnet, biotite, kyanite, staurolite, muscovite, plagioclase, quartz, and rutile (Table 4.2). This assemblage was reproduced in the pseudosection, and the respective field is outlined in orange.

In addition to the pseudosection, a set of contour plots was generated also using Perple_X (Connolly, 1990). The contour plots show the theoretical mineral abundance in volume % (vol.%) over the pseudosection PT range plots (Fig 4.19b-f, Fig 4.20a-d) and will be used in conjunction with the statistical analysis of large-area SEM BSE mosaics as a complementary constraint on the PT condition. Within the field outlined in orange (Fig 4.19a), the abundance of garnet is approximately 6 vol.% (Fig 4.19b), biotite ranges between 19 vol.% and 20 vol.% (Fig 4.19c), kyanite is $1.5\% \pm 0.5\%$ vol.% (Fig 4.19d), staurolite ranges between 0.1% and 0.5% vol.% (Fig 4.19e), and the muscovite content is approximately 1 vol.% (Fig 4.19f). The amount

of plagioclase present is around 25 vol.% (Fig 4.20a), that of quartz is 47 vol.% (Fig 4.20b), and rutile abundance is approximately 0.4 vol.% (Fig 4.20c), while ilmenite is not part of the assemblage (Fig 4.20d).

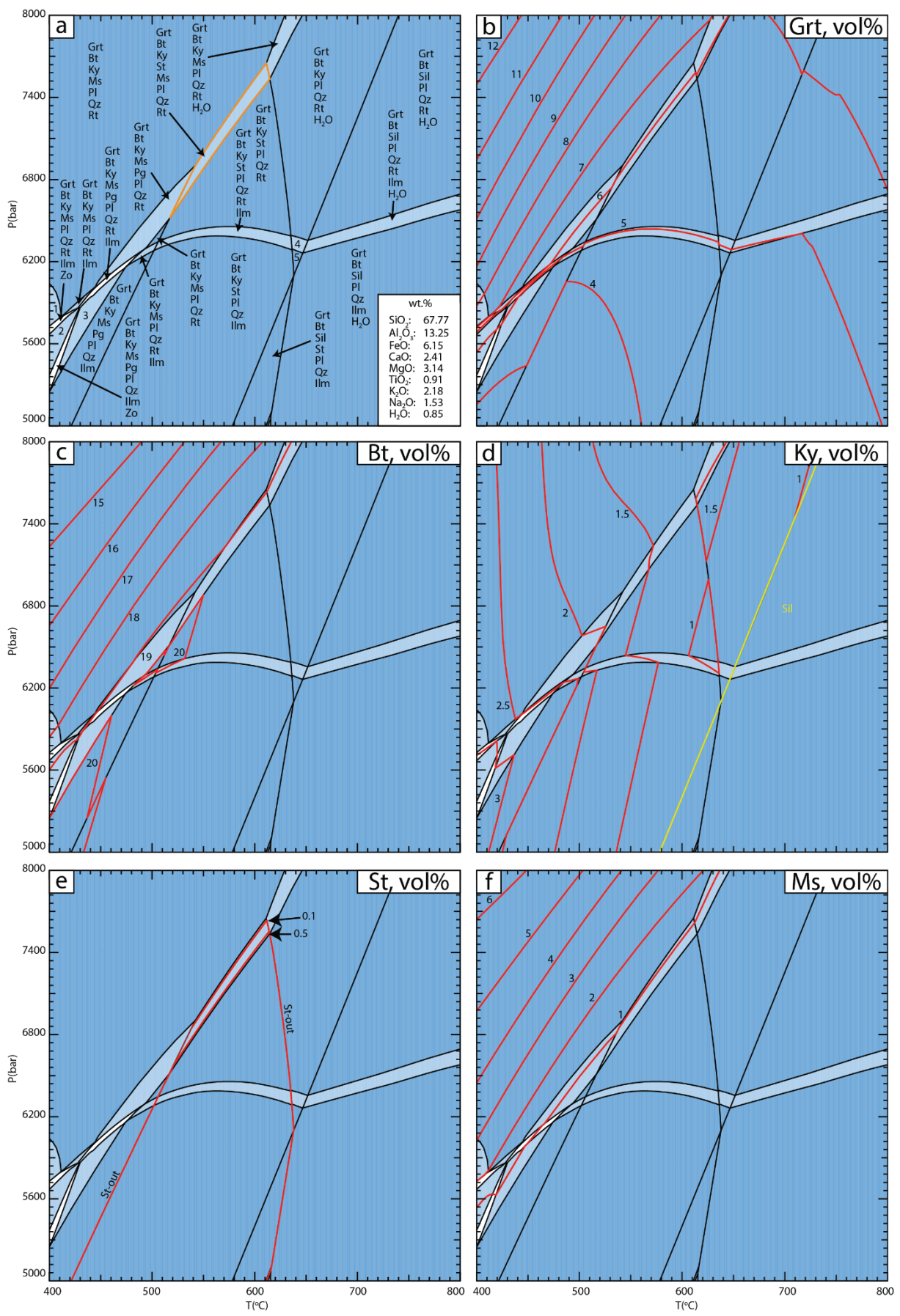


Figure 4.19 Results from modelling in Perple_X (Connolly, 1990). a) PT-pseudosection for the garnet mica schist (Lin_14-19 and Lin_15-19). The degree of freedom increases with darker colours, the white fields are divalent. Phase assemblages represented by numbers are: (1) Grt-Bt-Ky-Ms-Pl-Qz-Rt-Zo; (2) Grt-Bt-Ky-Ms-Pl-Qz-Ilm-Zo; (3) Grt-Bt-Ky-Ms-Pg-Pl-Qz-Ilm; (4) Grt-Bt-Ky-Pl-Qz-Rt-Ilm-H₂O; (5) Grt-Bt-Ky-Pl-Ilm-H₂O. b) to f) Contour lines showing the vol.% of garnet, biotite, kyanite, staurolite and muscovite respectively.

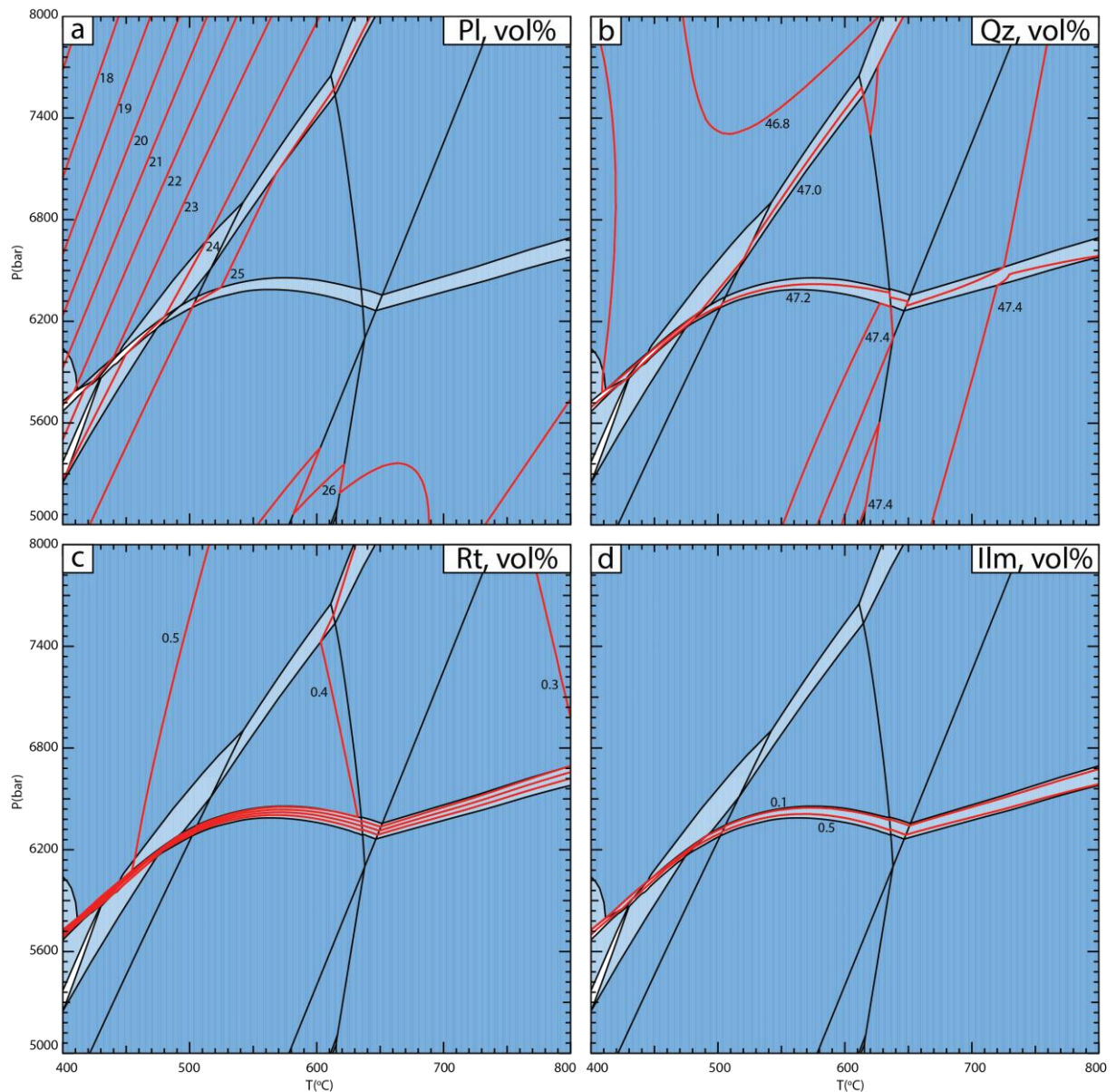


Figure 4.20 Results from modelling in Perple_X (Connolly, 1990). a), b), c), and d) Contour lines showing the vol.% of plagioclase, quartz, rutile, and ilmenite respectively.

4.6 Image analyses

The image analysis in ImageJ Fiji (Schindelin et al., 2012) was done to estimate the mineral abundance in sample Lin_14-19. However, quartz, kyanite, staurolite and carbonate have similar BSE contrast and could therefore not be distinguished from each other. Similarly, also muscovite and plagioclase, and ilmenite and rutile could not be distinguished based on their BSE contrast and are colour coded as one phase (Fig 4.21). For the image analysis, the full thin section BSE map was subdivided into nine tiles that were analysed separately. Table 4.5 contains the number of pixels and calculated area% for the different phases (or combination of thereof) for the nine tiles, the calculated average abundance, and abundance normalized to 100% (indicated in brackets in the following). The counted pixels of quartz, kyanite and staurolite totals to 46.3 area% (52.0 area%). The counted pixels of plagioclase and muscovite is 20.9 area% (23.5 area%). The counted pixels of chlorite are equal to 0.8 area% (0.9 area%). The biotite pixels account for 15.4 area% (17.3 area%). Garnet abundance is 5.3 area% (5.9 area%). Counted pixels of combined rutile and ilmenite accounts for 0.34 area% (0.38 area%). Porosity is counted to 0.06 area% (0.07 area%). The total amount of pixels counted in Figure 4.11 was 89% of the total pixels. Thus, an uncertainty of 11% is therefore given to both the average and normalized area% values.

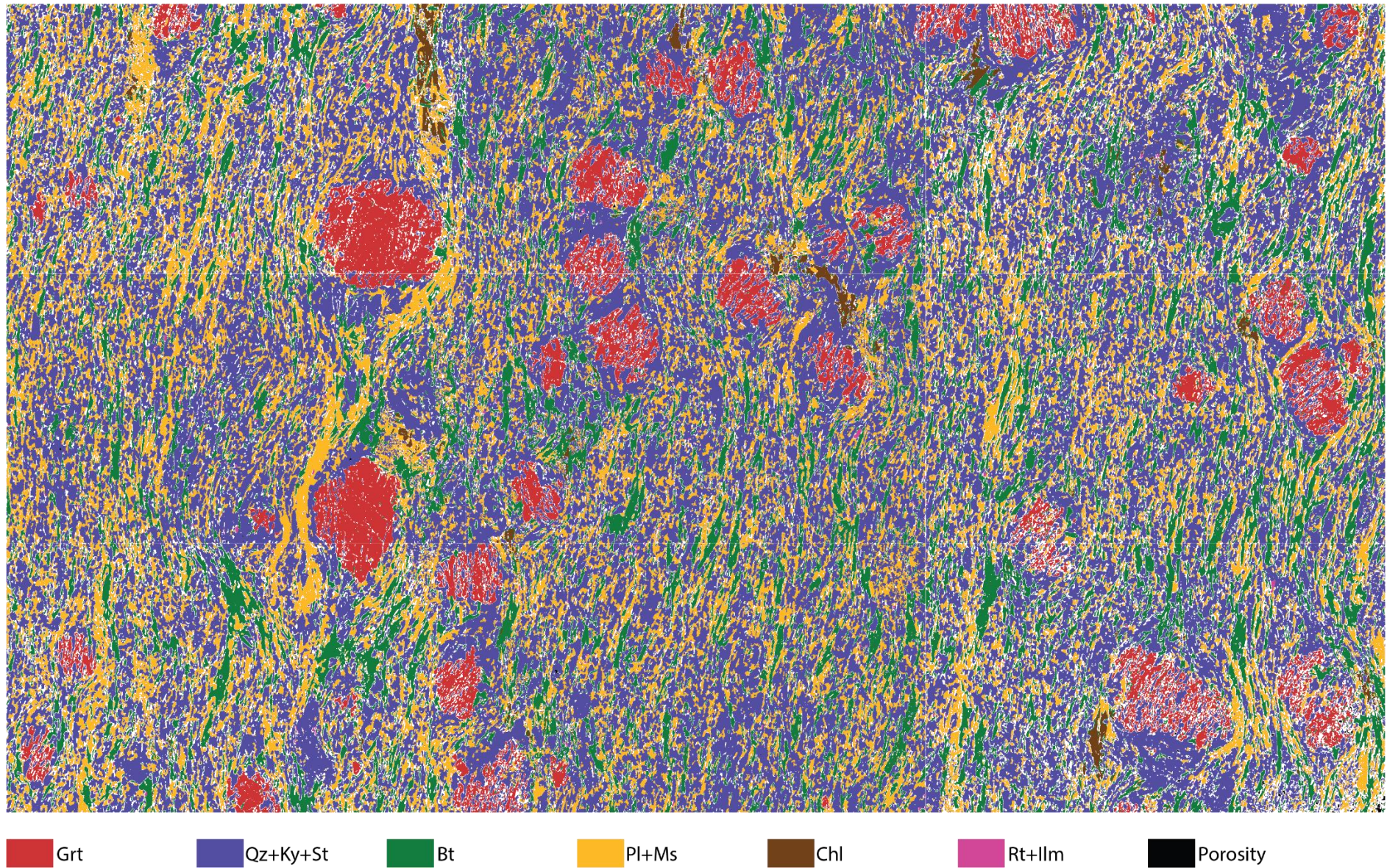


Figure 4.21 Result of the image analyses done in image processing package Fiji in the ImageJ distribution (Schindelin et al., 2012). Red represents garnet, green represents biotite, blue represents quartz, kyanite and staurolite, yellow represents plagioclase and muscovite, brown represents chlorite, pink represents rutile and ilmenite and black represents porosity in the rock

Table 4.5 Area percent for each of the mineral assemblages in Figure 4.11. Uncertainties for average area% and normalized area% are 11% of the values.

	Qz+Ky +St (%)	Pl+Ms (%)	Chl (%)	Bt (%)	Grt (%)	IIm+Rt (%)	Pore space (%)	Volume_{tot} (%)
Tile 1	37.1	25.0	1.52	12.3	8.02	0.36	0.04	83.9
Tile 2	54.8	17.8	1.03	14.4	6.67	0.35	0.05	94.6
Tile 3	48.3	15.1	1.61	15.7	3.74	0.54	0.05	84.5
Tile 4	46.8	25.9	0.26	13.2	4.87	0.42	0.06	91.0
Tile 5	53.4	19.1	0.95	14.9	6.69	0.34	0.02	95.1
Tile 6	43.3	21.4	0.26	18.4	4.96	0.32	0.01	88.2
Tile 7	39.4	24.7	0.09	15.8	4.90	0.24	0.08	84.8
Tile 8	51.6	22.9	0.30	16.0	2.72	0.26	0.05	93.6
Tile 9	41.7	16.3	0.93	17.5	4.98	0.18	0.22	81.4
Average area%	46.3	20.9	0.77	15.4	5.28	0.34	0.06	89.0
Uncertainty	5.11	2.31	0.09	1.69	0.58	0.04	0.00	
Normalized to 100%	52.0	23.5	0.87	17.2	5.94	0.38	0.07	100
Uncertainty	5.74	2.59	0.10	1.90	0.66	0.04	0.00	

CHAPTER 5: DISCUSSION

5.1 Thermobarometry, modelling and peak metamorphic conditions

Garnet-biotite garnet-biotite-aluminosilicate-quartz thermobarometry

128 spot analyses with the EMP were conducted on garnet, and 84 for the biotite. 7 pairs of garnet and biotite from the garnet mica schist were used to make a PT estimate. The average of the data population from the GB-GBAQ thermobarometer (Wu, 2017, Holdaway, 2000) is situated at a pressure of 7.03 kbar ± 0.17 kbar and a temperature of $593^{\circ}\text{C} \pm 8^{\circ}\text{C}$ (Fig 4.15a), with the uncertainties representing $2\sigma_{\text{mean}}$ of the data population. The uncertainty of each individual data point is 1.8 kbar and 25°C (Wu, 2017, Holdaway, 2000). When the average data population is compared with the pseudosection in Figure 4.20a, a clear correlation can be seen (Fig 5.1). At constant pressure the average data population plots 28°C higher than the field representing the peak metamorphic mineral assemblage. The coherency between the GB-GBAQ thermobarometer and the modelled pseudosection strengthens the credibility of both results. It is required that the mineral assemblage is equilibrated to use thermometers and/or barometers. Only garnet and biotite in direct contact were used, and it is therefore assumed that equilibrium was attained on the timescale of peak PT conditions. This assumption is strengthened when comparing Figure 4.15a with 4.15b. Figure 4.15b shows the PT estimates for both the results presented from the GB-GBAQ thermobarometer (Fig. 4.15a) and PT estimates for closely located, but not in direct contact, garnet and biotite pairs. The fact that the closely located garnet and biotite pairs do not touch each other makes them useless in constraining PT conditions. However, due to their PT results positioning in PT space, they indicate that the thin section has attained equilibrium on thin section scale. Another indication of the mineral assemblage representing equilibrium is the zonation of the garnet. Figure 4.10b shows that the garnet has a typical Mn-Ca-rich core with a Fe-Mg-rich rim, which suggest partial equilibrium during prograde growth (Winter, 2001, Cooke et al., 2000)

Ti-in-biotite thermometry

The PT range from the Ti-in-biotite thermometer (Wu and Chen, 2015) coupled with the GBAQ barometer (Wu, 2017) is large, thus plotting partly outside the pseudosection. Since the barometer is the same as in the GB-GBAQ thermobarometer, a slight lower temperature results in a significant lower pressure due to the temperature dependency of the GBAQ barometer. At the average pressure of 6.40 kbar, the temperature is $565^{\circ}\text{C} \pm 38^{\circ}\text{C}$ ($2\sigma_{\text{mean}}$) (Fig 5.1), with the minimum amount of Ti in biotite resulting in a temperature of 507°C , while the maximum

amount of Ti gives a temperature of 602°C, resulting in a temperature range of 95°C based on the content of Ti in biotite. Even with the of the 2σ of $\pm 37^\circ\text{C}$, the uncertainty is still significantly larger than the $2\sigma_{\text{mean}}$ (8°C) from the GB thermometer. However, with an uncertainty of 37°C , the temperature estimate overlaps with that of the GB thermometer. Keller and Ague (2018) applied the thermometer by only using the biotite with the highest recorded Ti content. The maximum Ti-in-biotite slope (Fig 4.17) crosses the average pressure slope at a pressure of 7.44 kbar ± 1.8 kbar and a temperature of $611^\circ\text{C} \pm 65^\circ\text{C}$. For comparison, the highest recorded PT estimate from the GB-GBAQ is $608^\circ\text{C} \pm 25^\circ\text{C}$ and 7.33 kbar ± 1.80 kbar. This shows that the biotite equilibrated with Ti at PT conditions like that of the PT estimate from the GB-GBAQ thermobarometer. The maximum Ti-in-biotite-GBAQ PT result contributes to solidify the peak PT conditions from the previous GB-GBAQ results and shows that the biotite has equilibrated at a temperature around 600°C , not only based on the Mg-Fe exchange, but also regarding the Ti content. The large temperature range from the Ti-in-biotite thermometry (Wu and Chen, 2015) may be a result of local re-equilibrium in the rock on the retrogression path (Henry et al., 2005). The composition of biotite can change rapidly if a late fluid phase is present, while altered biotite may go through cation exchange on the retrogressive path (Henry et al., 2005).

Zr in rutile thermometry

As with the Ti in biotite thermometer (Wu and Chen, 2015) coupled with the GBAQ barometer (Wu, 2017), the ZiR-GBAQ thermobarometer (Kohn, 2020, Wu, 2017) defines a wide pressure range but a relatively narrow temperature range (Fig 4.18). The intersect between the average pressure and temperature slopes are located at a pressure of 6.07 kbar and 551°C . With an uncertainty of 15°C , the temperature estimates from the ZiR thermometer (Kohn, 2020) overlaps with the temperature estimate based on the average concentration of Ti in biotite from the Ti-in-biotite thermometer (Wu and Chen, 2015) and GBAQ barometer (Wu, 2015). The pressure of 6.07 kbar has a ~ 0.9 kbar difference compared to the results from the GB-GBAQ thermobarometer. By comparing the ZiR-GBAQ results with the thermodynamic modelling, the average PT estimate from the ZiR thermometer and the GBAQ barometer is inconsistent with the pseudosection and plots outside the stability field of rutile. This raises a question about the reliability of the temperature estimate from the ZiR thermometer by Kohn (2020). Since the ZiR-GBAQ thermobarometer both gives the lowest PT estimates, and plots outside the stability field of rutile, it is reasonable to assume that the PT conditions are underestimated. Following the temperature slope from the ZiR thermometer, it crosses the rutile-out line at approximately 553°C and 6.38 kbar. By looking at the pseudosection (Fig 5.1), this should be the lowest PT

estimate possible for the ZiR-GBAQ thermobarometer. If this was the case, it would plot next to the average PT estimate from the Ti-in-biotite thermometer and GBAQ barometer and those two thermobarometers would agree on the minimum PT conditions.

The reason why the ZiR thermometer gives lower temperature estimates than the other two thermometers may come from the fact that the Zr in rutile analyses were conducted on rutile situated in the matrix. The first calibration of the ZiR thermometer was done by Zack et al. (2004). When calibrating the Zr in rutile thermometer, Zack et al. (2004) excluded the matrix rutile since it had a systematically lower Zr concentration compared to rutile occurring as inclusions. Zack et al. (2004) suggest that rutile inclusions in garnet are shielded from Zr diffusion since the rutile is kept away from fluids, and that Zr diffusion in the garnet crystal lattice is too slow to allow diffusion of Zr between the rutile inclusion and the garnet host. Analysing the concentration of Zr in inclusions of rutile in garnet was attempted. Due to large variations in the measured concentration of Zr when the two external standards NIST610 and R632 were used, these results were not reliable.

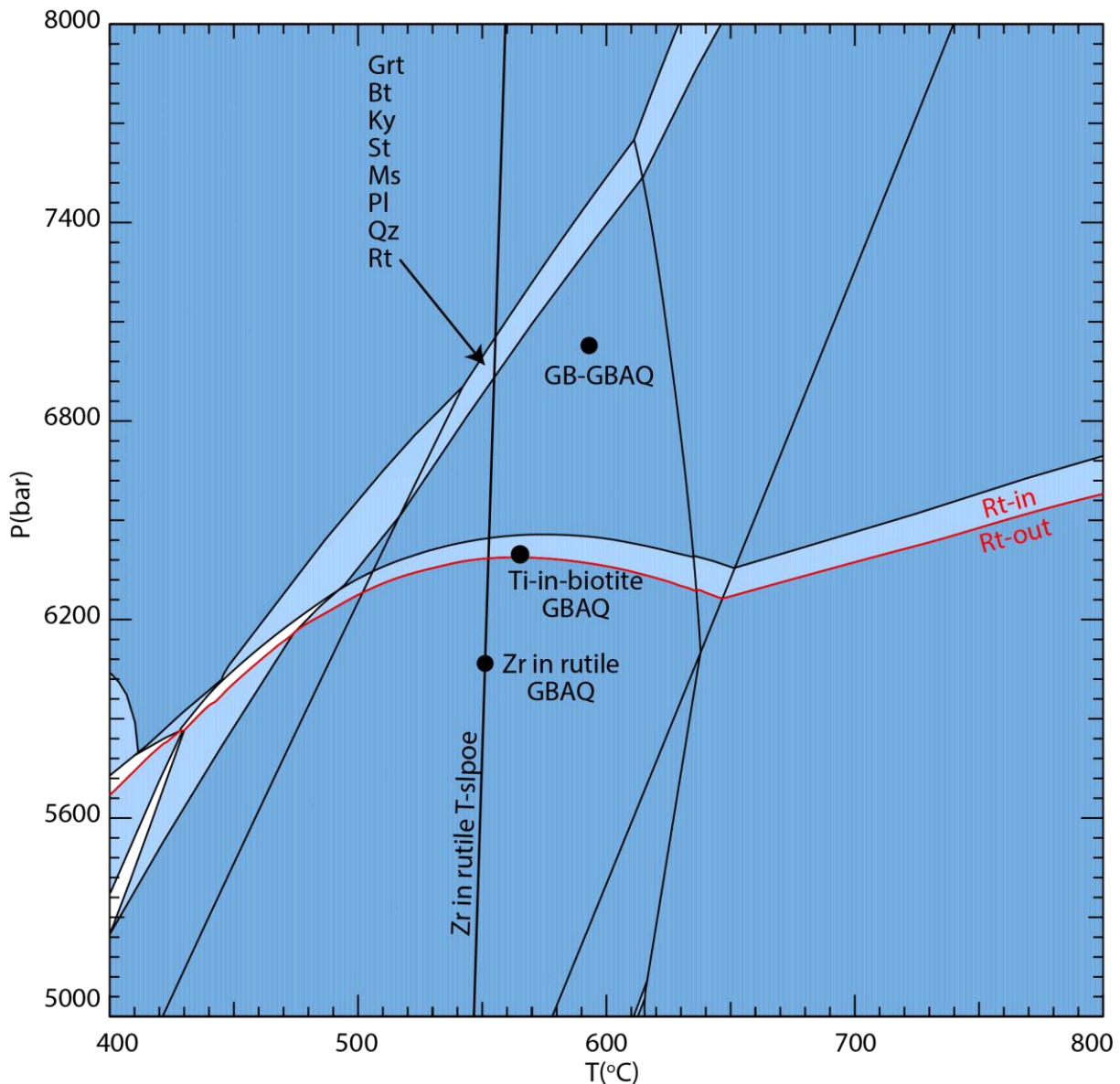


Figure 5.1 Location of PT results from all three thermobarometers compared with the pseudosection and the stability field of rutile. Uncertainties for PT estimates, see Figure 4.12a, Figure 4.14 and 4.15.

Contour lines and image analysis

The set of contour plots that were generated with Perple_X (Connolly, 1990) (Fig. 4.19b-f, Fig 4.20a-d) can be compared with the mineral abundance (area%) of Lin_14-19 (Table 4.5), which was acquired through the image analyses with ImageJ Fiji (Schindelin et al., 2012). To be able to compare area%, which is a 2-dimensional unit, with vol.%, which is a 3-dimensional unit, it is required to assume that the values from the area% are representative for the whole rock.

Figure 4.19b shows that there is supposed to be approximately 6 vol.% of garnet in Lin_14-19, if the rock has experienced peak metamorphic conditions corresponding to PT values of the outlined field in Figure 4.19a. The estimated area%, hence vol.%, of garnet in Lin_14-19 is

$5.94\% \pm 0.66\%$, which is well within the modelled value of approximately 6 vol.%. The modelled mineral abundance of quartz, kyanite and staurolite in Lin_14-19 is 47%, 1%-2%, and 0.1%-0.5% respectively. Due to the similarities in the BSE contrast for these three phases, they are all included in one phase in the image analysis. The minimum abundance of these three phases are ~ 48.1 vol.%, while their maximum abundance is ~ 49.5 vol.%. This matches with the results from the image analysis where all three mineral phases combined account for $52\% \pm 5.74\%$. The vol.% of garnet is thought to be highly accurate due to the limited number of crystals and the size of them, which limits the loss of counted pixels. Since the vol.% of garnet is close to 6, it can, with great certainty, be stated that the vol.% of kyanite does not exceed 2 vol.%, based on the number of crystals and their size. The amount of staurolite can also be confirmed to not exceed the amount of kyanite due to both fewer and generally smaller crystals. Comparing the exact vol.% of both kyanite and staurolite to the modelled abundance is impossible with the data from the image analysis, but the modelled vol.% seems consistent based on petrographic observation.

The modelled abundance of biotite resulted in a vol.% between 19 vol.% and 20 vol.%. The image analysis gave a value of 17.23 area% ± 1.90 area%. Chlorite accounts for 0.87 area% ± 0.10 area%, while the modelling suggests that it should not be stable. Figure 4.4d shows chlorite replacing biotite, which is a reaction seen in all four thin sections of the garnet mica-schist and indicates that the chlorite is a secondary mineral. Chlorite can also be formed by alteration of garnet and staurolite, which makes it difficult to predict what mineral phase the chlorite was formed by. Plagioclase and muscovite, which are represented as one phase in Figure 4.18 have a combined area% of $23.5\% \pm 2.59\%$. The results from the modelled contour lines show that muscovite is supposed to have a vol.% of approximately 1%, while plagioclase is supposed to have a vol.% between 24% and 25%. These two phases should constitute 25 vol.% to 26 vol.% together, which is within the estimated area% from the image analysis. Rutile and ilmenite are estimated to constitute 0.38 area% ± 0.04 area% combined. Based on petrographic observations, the 0.38 area% is approximately evenly distributed between the two phases. Figure 4.20c shows that rutile is supposed to have a value ranging between 0.4 vol.% and 0.5 vol.%, while Figure 4.19a and Figure 4.20d shows that ilmenite is not stable in the field representing peak metamorphic conditions. If peak assemblage was set to where rutile and ilmenite coexist, the rock should not have had any muscovite in the mineral assemblage. Since muscovite is present in the rock, the field outlined in yellow in Figure 4.19a was chosen to represent peak metamorphic mineral assemblage. The formation of rutile happens at the

expense of ilmenite (Angiboust and Harlov, 2017). If this reaction had completed, all the ilmenite would have turned into rutile. The area% of rutile, which is approximately 0.18 area% is close to the supposed value from the modelling.

If the result from the image analysis (Fig 4.21) is placed on top of a BSE image of Lin_14-19, it is clearly seen that a lot of the empty space in Figure 4.21 is placed along grain boundaries of all mineral phases present in the thin section. The empty space which is not related to grain boundaries is often located where small crystals of biotite are situated. These crystals were too small to be preserved through all the steps in the image analysis and therefore ended up as empty space in Figure 4.21. If the image analysis was able to detect closer to 100% of the total number of pixels in the thin section, it is believed that the only mineral which would have a slight increase to the total vol.% would be biotite. The other phases present would have had a uniform increase in vol.%, and therefore not change the abundance relative to each other. The coherency between the supposed vol.% of the mineral phases from the modelling and the actual area% from image analysis further strengthens the reliability in the PT estimate from the pseudosection.

Peak PT conditions

Combined results from all thermobarometers show that the pressure estimates range from 6.07 kbar to 7.03 kbar, while the temperatures estimate range between 551°C and 593°C. The peak conditions for both pressure and temperature are derived from the GB-GBAQ geothermobarometer. The GB-GBAQ thermobarometer also gave the PT estimate closest to the modelled stability field in the pseudosection which correlates with the abundance of all present mineral phases.

5.2 Linnajavri PT estimate in the context of regional PT estimates

Few studies have previously estimated PT conditions for rocks in the Köli Nappe in the local area (Crowley and Spear, 1987). Studies making PT estimates in the regional Köli Nappe are more abundant, but these studies tend to be from areas quite far away from the Linnajavri area (e.g. Beckholmen, 1983, Bergman, 1992, McClellan, 2004).

The study of Crowley and Spear (1987) investigated peak PT conditions for two local nappes, Langvatn Nappe and Marko Nappe, situated within the Köli Nappe. The study area, approximately 57 km N-NE of Kvifjell, may be the closest PT estimate for Köli rocks in the area. Crowley and Spear (1987) used both the GB thermometer by Ferry and Spear (1978) and

the recalibrated garnet-muscovite-biotite-plagioclase (GMBP) barometer by Hodges and Crowley (1985) on 10 samples of pelitic schists from both nappes.

Crowley and Spear (1987) reported results ranging between 528°C and 6.6 kbar to 620°C and 8.8 kbar, with an average at $567 \pm 32^\circ\text{C}$ and 8.0 ± 0.9 kbar. A temperature of 567°C is within the uncertainty of all three temperature estimates that this study has generated and correlates with the average temperature from the Ti in biotite thermometer (565°C). The pressure, however, is 1-2 kbars above the average pressure estimates from the GBAQ barometer, and approximately 0.35 kbars above the maximum pressure where the mineral assemblage is stable according to the pseudosection. Due to the large uncertainty of the GBAQ barometer (1.8 kbar), 8 kbar is still within the error bars of all the calculated pressures.

Bergman (1992) conducted a PT estimate with the calibration of the GB thermometer by Perchuk and Lavrent'eva (1983), and the calibration of the GMBP barometer by Hoisch (1990) on metapelites occurring together with ophiolite fragments from Bunnerviken lens in the Tännforsfältet area in Sweden, approximately 480 km S-SW of the Linnajavri area. The metapelitic rock samples Bergman (1992) collected from Bunnerviken lens were composed of biotite, muscovite, quartz, plagioclase and garnet, \pm hornblende \pm clinozoisite \pm chlorite \pm carbonate, with accessory ilmenite, tourmaline, apatite and zircon. The results from the thermobarometry in Bergman (1992) yielded temperatures from 490°C to 570°C , and pressures from 6 kbar to 9.5 kbar.

Based on the mineral composition that Bergman (1992) describes, the samples do not match either Lin_14-19 or Lin_15-19. The presence of hornblende, clinozoesite and apatite, and the absence of kyanite, staurolite and rutile make it incomparable with the garnet mica schist petrology wise. On the other hand, it does resemble the mineral assemblage found in the metagreywacke from the Linnajavri area. Except for the presence of apatite, and the absence of rutile, all other phases are observed in the metagreywacke.

The upper limit of the temperature estimate from Bergman (1992) correlates with the estimate from the Ti in biotite thermometer, and is slightly lower than the results from the GB thermometer, which shows the highest recorded temperature. The pressure, which covers 3.5 kbar, does match up with all the recorded pressures in this study. The PT estimate by Bergman (1992) resembles the PT estimate from the garnet mica schist more than the metagreywacke, while the mineralogy matches the metagreywacke, and not so much the garnet mica schist.

Only 7-8 km west of the study area of Bergman (1992), Beckholmen (1983) made a PT estimate on Saxvallklumpen metabasite, which is surrounded by metasediments from the Köli Nappe. The PT estimate was made based on index minerals in the metabasite. The setting of an ophiolite surrounded by metasediments is identical to the setting of the Kvifjell ultramafic body at Linnajavri. Through the index minerals, the temperature was estimated to be in the range of 500°C -550°C, while the pressure was estimated to be more than 7 kbar.

The whole temperature range by Beckholmen (1983) is approximately 50°C lower than the temperatures observed at Linnajavri. The pressure, however, is similar to the recorded pressure from the GB-GBAQ results. Though this is a PT estimate based on index minerals, it is consistent with the thermobarometric results from Bergman (1992), and shows that the Köli rocks in the Tännforsfältet area in Sweden have experienced similar peak metamorphic conditions as the Köli rocks in the Linnajavri area.

Approximately 660 km S-SW of the Linnajavri area, McClellan (2004) investigated the metamorphic conditions at the Seve-Köli Nappe boundary in the southern Trondheim region. Temperature calculations were obtained by applying five GB thermometers (Ferry and Spear (1978), Hodges and Spear (1982), Perchuk and Lavrent'eva (1983), Ferry and Spear (1978) with the mixing model of Berman (1990), and Kleemann and Reinhardt (1994)) on nine samples of pelitic schist from both the Köli and Seve Nappe. Due to the lack of a mineral assemblage appropriate for pressure estimation, the pressure was not quantified (McClellan, 2004). The metapelites are though assumed by McClellan (2004) to have experienced a moderate pressure due to the chemistry of both the muscovite and amphibole. The results from the GB thermometer by Kleemann and Reinhardt (1994), which, according to Wu and Cheng (2006), is the best GB thermometer together with Holdaway (2000) due to their small errors in reproducing experimental temperatures, shows a temperature ranging between 516°C and 570°C (McClellan, 2004). While also this temperature range is lower than the temperature range at Linnajavri, all temperatures in McClellan (2004) were calculated at a pressure of 6 kbar due to the assumption of a moderate pressure. Calculating the temperature at a pressure of 7 kbar instead, which is the highest pressure recorded at Linnajavri, would raise the temperature range from McClellan (2004) to match better with the temperature estimate from Kvifjell.

All the studies agree that rocks from the far stretching Köli Nappe have experienced PT conditions of 550°C, while some also estimate that the temperature could have reached 570°C and 620°C. The studies also agree on a pressure in the range of 6-7 kbar, while Crowley and Spear (1987) and Bergman (1992) report that the pressures could have reached 8.8 kbar and 9.5

kbar respectively. The general agreement that the Köl Nappe has reached lower amphibolite facies also includes the rocks found next to Kvifjell. The pressure estimates are in general quite similar to the peak pressure conditions found at Kvifjell, while the temperature estimates are slightly lower, with the exception of Crowley and Spear (1987) who report temperatures similar to the peak temperature conditions.

5.3 Limitations

Different thermometers and barometers have a set of requirements which must be met in order to be able to use them. This also applies to the barometer and thermometers used in this thesis.

All PT estimates in this thesis are located within the calibration range of the GB-GBAQ thermobarometer, which is calibrated in the broad PT range of 450-950°C and 1-17 kbar (Wu, 2017). The rocks the GB thermometer is applied to require coexisting garnet and biotite, while the GBAQ barometer also requires additional aluminosilicate and quartz, since all four phases are involved in the net-transfer reactions (Eq. 3.2 and Eq.3.3) (Wu, 2017).

The PT results from the Ti in biotite thermometer by Wu and Chen (2015) fall well within the thermometers calibration range of 450-840°C and 1-19 kbar. The requirements in order to apply the thermometer are fulfilled, where rutile and/or ilmenite coexist with the biotite (Fig 4.6b), and the biotite has an X_{Ti} between 0.02 and 0.14 (Wu and Chen, 2015).

The temperature estimate from the ZrR thermometer (Kohn, 2020) also plots inside the calibration range of the thermometer (480-725°C and 3.5-31.5 kbar). According to Eq. 3.6 (Kohn, 2020), zircon must coexist together with rutile in order to apply the ZrR thermometer to rock samples. As seen in Figure 4.6e, zircon occurs in the garnet mica schist samples together with rutile and makes this a suitable thermometer.

5.4 Decarbonation

The PT estimate constrained in this thesis contributes to when decarbonation in mountain collisions may initiate. The decarbonation process at Kvifjell ultramafic body has occurred at shallower depths than previously recorded decarbonation processes, such as in the Scottish Highlands and in the Southern Alps, New Zealand (Skelton, 2011, Menzies et al., 2018). While ultramafic rocks can be present in mountain collision settings, they are more often related to subduction zones. Due to the decarbonation process at Kvifjell occurring in ultramafic rocks, the temperature estimate can be transferred to subduction zones to indicate when the decarbonation process may start in the different subduction zone settings of Peacock (1990)

(Fig 5.2a). At the fixed temperature of 565°C-593°C, decarbonation may occur in 5 Ma subducted slabs at depths of approximately 21-22 km (Fig 5.2b). For slabs with the age of 10 Ma, decarbonation may initiate at depths of approximately 29-31 km, approximately 66-70 km for mature slabs with the age of 50 Ma, and approximately 134-142 km for the oldest slabs with the age of 200 Ma (Fig 5.2b). This contradicts Kerrick and Connolly (1998), which concluded that decarbonation in ophiocarbonates is minimal, or does not happen at or before sub-arc depths.

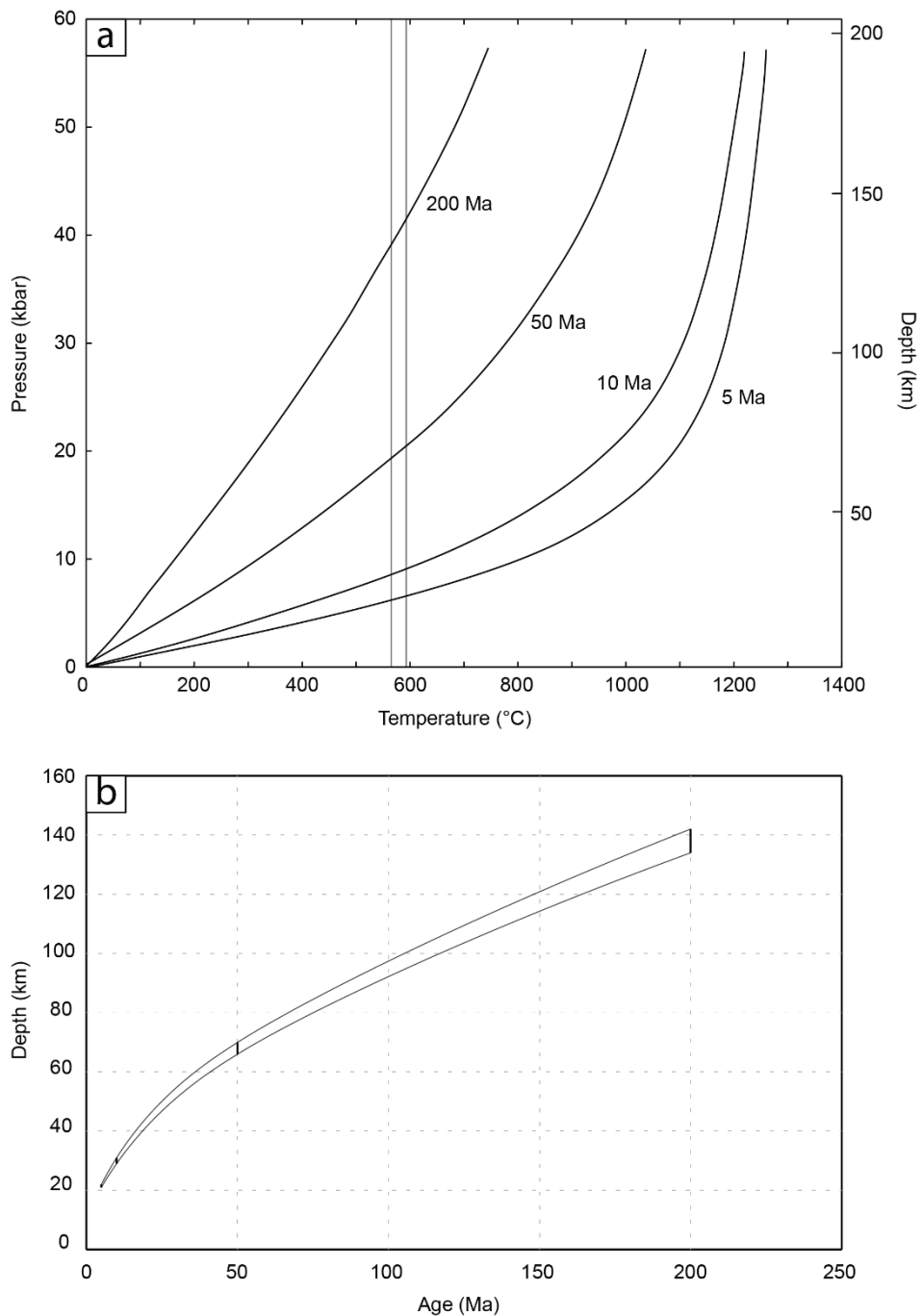


Figure 5.2 a) Pressure-temperature-time (P-T-t) for top of the lithosphere in subduction zones as a function of the age. Straight lines represent temperatures of 565°C and 593°C respectively. Redrawn from Peacock (1990). b) Depths at which decarbonation may occur at temperatures of 565°C-593°C based on the age of the subducted lithosphere.

CHAPTER 6: CONCLUSION

Based on conventional thermobarometry, trace element thermometry, thermodynamic modelling, and image analysis, this study provides new insights into the peak metamorphic conditions at which decarbonation at Kvitfjell ultramafic body occurred:

- Decarbonation at Kvitfjell ultramafic complex occurred at a maximum PT condition of $593^{\circ}\text{C} \pm 8^{\circ}\text{C}$ and $7.03 \text{ kbar} \pm 0.17 \text{ kbar}$, while it could have been as low as $565^{\circ}\text{C} \pm 37^{\circ}\text{C}$ and $6.40 \text{ kbar} \pm 0.09 \text{ kbar}$.
- Transferring the temperature estimate from Kvitfjell ultramafic body to subduction zones indicates that decarbonation may occur at shallower depths than previously proposed.

CHAPTER 7: FUTURE WORK

Even though an estimate has been made on the peak PT conditions at which decarbonation occurred at Kvifjell ultramafic body, it would be interesting to see what pressures another barometer would give. Especially if the Raman quartz barometer by Kohn (2014) was coupled with the ZiR thermometer (Kohn, 2020), where inclusions of both quartz and rutile within the same garnet were analysed and coupled together. Would the rutile inclusions in garnet show higher concentrations of Zr, and thus a higher temperature estimate? The rutile could also be dated to investigate if some are inherited.

An important question regarding the decarbonation at Linnajavri is the timescale at which the decarbonation occurred. The carbonation of the ophiolites at Linnajavri was a fast reaction happening at a timescale of 10-100 years (Beinlich et al., 2020). Further investigation on the timescale at which the decarbonation occurred would be interesting.

Another question regarding the decarbonation at Linnajavri is, where does the carbon go? Does the released carbon go into the rocks adjacent to Kvifjell ultramafic body, or does it escape completely from the rock sequences in the area? This is an important question which will further improve the understanding of the decarbonation process at Linnajavri.

REFERENCES:

- ANGIBOUST, S. & HARLOV, D. 2017. Ilmenite breakdown and rutile-titanite stability in metagranitoids: Natural observations and experimental results. *American Mineralogist: Journal of Earth and Planetary Materials*, 102, 1696-1708.
- ARMSTRONG, J. T. 1988. Quantitative analysis of silicates and oxide minerals: comparison of Monte-Carlo, ZAF and Phi-Rho-Z procedures. *Microbe. Anal.*, 239–246.
- AXELSSON, E., PAPE, J., BERNDT, J., CORFU, F., MEZGER, K. & RAITH, M. M. 2018. Rutile R632—A new natural reference material for U-Pb and Zr determination. *Geostandards and Geoanalytical Research*, 42, 319-338.
- BEBOUT, G. E. 1995. The impact of subduction-zone metamorphism on mantle-ocean chemical cycling. *Chemical Geology*, 126, 191-218.
- BECKHOLMEN, M. 1983. Petrography, petrochemistry and regional significance of the Saxvallklumpen metabasite, Köli Nappe Complex, Tännforsfältet, central Swedish Caledonides. *Geologiska Föreningen i Stockholm Förhandlingar*, 104, 293-303.
- BEINLICH, A., JOHN, T., VRIJMOED, J. C., TOMINAGA, M., MAGNA, T. & PODLADCHIKOV, Y. Y. 2020. Instantaneous rock transformations in the deep crust driven by reactive fluid flow. *Nature Geoscience*, 13, 307-311.
- BEINLICH, A., PLÜMPER, O., HÖVELMANN, J., AUSTRHEIM, H. & JAMTVEIT, B. 2012. Massive serpentinite carbonation at Linnajavri, N-Norway. *Terra Nova*, 24, 446-455.
- BERGMAN, S. 1992. P-T paths in the Handöl area, central Scandinavia: record of Caledonian accretion of outboard rocks to the Baltoscandian margin. *Journal of Metamorphic Geology*, 10, 265-281.
- BERMAN, R. G. 1990. Mixing properties of Ca-Mg-Fe-Mn garnets. *American Mineralogist*, 75, 328-344.
- BRATTLI, B. & PRESTVIK, T. 1987a. *Linnajavrre, bedrock geology map 2230 III, scale 1:50,000*. preliminary edition: Norges geologiske undersøkelse.
- BRATTLI, B. & PRESTVIK, T. 1987b. Tysfjord granite and overlying rocks in the area of Linnajavrre, central-north Norway. *Bulletin-Norges geologiske undersøkelse*, 65-72.
- BREKKE, H., FURNES, H., NORDÅS, J. & HERTOGEN, J. 1984. Lower Palaeozoic convergent plate margin volcanism on Bømlo, SW Norway, and its bearing on the tectonic environments of the Norwegian Caledonides. *Journal of the Geological Society*, 141, 1015-1032.
- BUCHER-NURMINEN, K. 1991. Mantle fragments in the Scandinavian Caledonides. *Tectonophysics*, 190, 173-192.
- CONNOLLY, J. 1990. Multivariable phase diagrams; an algorithm based on generalized thermodynamics. *American Journal of Science*, 290, 666-718.
- COOKE, R., O'BRIEN, P. & CARSWELL, D. 2000. Garnet zoning and the identification of equilibrium mineral compositions in high-pressure-temperature granulites from the Moldanubian Zone, Austria. *Journal of Metamorphic Geology*, 18, 551-569.
- CORFU, F., ROBERTS, R. J., TORSVIK, T. H., ASHWAL, L. D. & RAMSAY, D. M. 2007. Peri-Gondwanan elements in the Caledonian Nappes of Finnmark, Northern Norway: Implications for the paleogeographic framework of the Scandinavian Caledonides. *American Journal of Science*, 307, 434-458.
- CROWLEY, P. D. & SPEAR, F. S. 1987. The P-T evolution of the Middle Kli Nappe Complex, Scandinavian Caledonides (68°N) and its tectonic implications. *Contributions to mineralogy and petrology*, 95, 512-522.
- DEER, W. A., HOWIE, R. A. & ZUSSMAN, J. 1992. *An introduction to the rock-forming minerals*, Harlow, Pearson Prentice Hall.

- DONOVAN, J. J., LOWERS, H. A. & RUSK, B. G. 2011. Improved electron probe microanalysis of trace elements in quartz. *American Mineralogist*, 96, 274-282.
- DONOVAN, J. J., SNYDER, D. A. & RIVERS, M. L. An improved interference correction for trace element analysis. Proceedings of the Annual Meeting-Electron Microscopy Society of America, 1992. San francisco press, 1646-1646.
- FERRY, J. T. & SPEAR, F. 1978. Experimental calibration of the partitioning of Fe and Mg between biotite and garnet. *Contributions to mineralogy and petrology*, 66, 113-117.
- FOSSEN, H. & HURICH, C. A. 2005. The Hardangerfjord Shear Zone in SW Norway and the North Sea: a large-scale low-angle shear zone in the Caledonian crust. *Journal of the Geological Society*, 162, 675-687.
- HENRY, D. J. & GUIDOTTI, C. V. 2002. Titanium in biotite from metapelitic rocks: Temperature effects, crystal-chemical controls, and petrologic applications. *American Mineralogist*, 87, 375-382.
- HENRY, D. J., GUIDOTTI, C. V. & THOMSON, J. A. 2005. The Ti-saturation surface for low-to-medium pressure metapelitic biotites: Implications for geothermometry and Ti-substitution mechanisms. *American mineralogist*, 90, 316-328.
- HODGES, K. & CROWLEY, P. T. 1985. Error estimation and empirical geothermobarometry for pelitic systems. *American Mineralogist*, 70, 702-709.
- HODGES, K. & SPEAR, F. S. 1982. Geothermometry, geobarometry and the Al₂SiO₅ triple point at Mt. Moosilauke, New Hampshire. *American mineralogist*, 67, 1118-1134.
- HOISCH, T. D. 1990. Empirical calibration of six geobarometers for the mineral assemblage quartz+ muscovite+ biotite+ plagioclase+ garnet. *Contributions to Mineralogy and Petrology*, 104, 225-234.
- HOLDAWAY, M. 2000. Application of new experimental and garnet Margules data to the garnet-biotite geothermometer. *American mineralogist*, 85, 881-892.
- HOLLAND, T. & POWELL, R. 1991. A compensated-Redlich-Kwong (CORK) equation for volumes and fugacities of CO₂ and H₂O in the range 1 bar to 50 kbar and 100–1600 C. *Contributions to Mineralogy and Petrology*, 109, 265-273.
- HOLLAND, T. & POWELL, R. 1998. An internally consistent thermodynamic data set for phases of petrological interest. *Journal of metamorphic Geology*, 16, 309-343.
- JENNINGS, E. S. & HOLLAND, T. J. B. 2015. A Simple Thermodynamic Model for Melting of Peridotite in the System NCFMASOCr. *Journal of Petrology*, 56, 869-892.
- KELEMEN, P. B. & MANNING, C. E. 2015. Reevaluating carbon fluxes in subduction zones, what goes down, mostly comes up. *Proceedings of the National Academy of Sciences*, 112, E3997-E4006.
- KELLER, D. S. & AGUE, J. J. 2018. High-pressure granulite facies metamorphism (~ 1.8 GPa) revealed in silica-undersaturated garnet-spinel-corundum gneiss, Central Maine Terrane, Connecticut, USA. *American Mineralogist: Journal of Earth and Planetary Materials*, 103, 1851-1868.
- KERRICK, D. & CONNOLLY, J. 1998. Subduction of ophicarbonates and recycling of CO₂ and H₂O. *Geology*, 26, 375-378.
- KERRICK, D. & CONNOLLY, J. 2001. Metamorphic devolatilization of subducted marine sediments and the transport of volatiles into the Earth's mantle. *Nature*, 411, 293-296.
- KLEEMANN, U. & REINHARDT, J. 1994. Garnet-biotite thermometry revisited: The effect of AlVI and Ti in biotite. *European Journal of Mineralogy*, 925-942.
- KOHN, M. J. 2014. “Thermoba-Raman-try”: Calibration of spectroscopic barometers and thermometers for mineral inclusions. *Earth and Planetary Science Letters*, 388, 187-196.
- KOHN, M. J. 2020. A refined zirconium-in-rutile thermometer. *American Mineralogist: Journal of Earth and Planetary Materials*, 105, 963-971.

- LAETSCH, T. & DOWNS, R. Software for identification and refinement of cell parameters from powder diffraction data of minerals using the RRUFF Project and American Mineralogist Crystal Structure Databases. 19th General Meeting of the International Mineralogical Association, Kobe, Japan, 2006. e28.
- LI, X., ZHANG, C., BEHRENS, H. & HOLTZ, F. 2020a. Calculating amphibole formula from electron microprobe analysis data using a machine learning method based on principal components regression. *Lithos*, 362, 105469.
- LI, X., ZHANG, C., BEHRENS, H. & HOLTZ, F. 2020b. Calculating biotite formula from electron microprobe analysis data using a machine learning method based on principal components regression. *Lithos*, 356, 105371.
- LINDAHL, I. & NILSSON, L. P. 2008. Geology of the soapstone deposits of the Linnajavri area, Hamarøy, Nordland, north Norwegian Caledonides—Norway's largest reserves of soapstone. *Geol. Soc., Geol. Sur. Nor. Spec. Publ.*, 11, 19-35.
- LONGERICH, H. P., JACKSON, S. E. & GÜNTHER, D. 1996. Inter-laboratory note. Laser ablation inductively coupled plasma mass spectrometric transient signal data acquisition and analyte concentration calculation. *Journal of analytical atomic spectrometry*, 11, 899-904.
- MCCLELLAN, E. A. 2004. Metamorphic conditions across the Seve-Köli Nappe boundary, southeastern Trondheim region, Norwegian Caledonides: Comparison of garnet-biotite thermometry and amphibole chemistry. *Norwegian Journal of Geology/Norsk Geologisk Forening*, 84.
- MENZIES, C. D., WRIGHT, S. L., CRAW, D., JAMES, R. H., ALT, J. C., COX, S. C., PITCAIRN, I. K. & TEAGLE, D. A. 2018. Carbon dioxide generation and drawdown during active orogenesis of siliciclastic rocks in the Southern Alps, New Zealand. *Earth and Planetary Science Letters*, 481, 305-315.
- MIYASHIRO, A. & SHIDO, F. 1985. Tschermark substitution in low-and middle-grade pelitic schists. *Journal of Petrology*, 26, 449-487.
- PATON, C., HELLSTROM, J., PAUL, B., WOODHEAD, J. & HERGT, J. 2011. Iolite: Freeware for the visualisation and processing of mass spectrometric data. *Journal of Analytical Atomic Spectrometry*, 26, 2508-2518.
- PEACOCK, S. A. 1990. Fluid processes in subduction zones. *Science*, 248, 329-337.
- PEDERSEN, R., BRUTON, D. & FURNES, H. 1992. Ordovician faunas, island arcs and ophiolites in the Scandinavian Caledonides. *Terra Nova*, 4, 217-222.
- PERCHUK, L. & LAVRENT'EVA, I. 1983. Experimental investigation of exchange equilibria in the system cordierite-garnet-biotite. *Kinetics and equilibrium in mineral reactions*. Springer.
- PICKARD, C. J. & NEEDS, R. J. 2015. Structures and stability of calcium and magnesium carbonates at mantle pressures. *Physical Review B*, 91, 104101.
- PINCHON, M., PASQUET, L. & BONNET, N. 2005. *IMAGEJ PLUGINS* [Online]. Available: https://imagej.nih.gov/ij/plugins/inserm514/#shading_correction [Accessed 14.09 2021].
- REHNSTRÖM, E. F. & CORFU, F. 2004. Palaeoproterozoic U-Pb ages of autochthonous and allochthonous granites from the northern Swedish Caledonides—regional and palaeogeographic implications. *Precambrian Research*, 132, 363-378.
- ROBERTS, D. 2003. The Scandinavian Caledonides: event chronology, palaeogeographic settings and likely modern analogues. *Tectonophysics*, 365, 283-299.
- ROBERTS, D. & GEE, D. G. 1985. An introduction to the structure of the Scandinavian Caledonides. *The Caledonide Orogen: Scandinavia and Related Areas*. New York: John Wiley & Sons Ltd.

- ROBERTS, D., NORDGULEN, O. & MELEZHIK, V. 2007. The Uppermost Allochthon in the Scandinavian Caledonides: From a Laurentian ancestry through Taconian orogeny to Scandian crustal growth on Baltica. *MEMOIRS-GEOLOGICAL SOCIETY OF AMERICA*, 200, 357.
- SCHINDELIN, J., ARGANDA-CARRERAS, I., FRISE, E., KAYNIG, V., LONGAIR, M., PIETZSCH, T., PREIBISCH, S., RUEDEN, C., SAALFELD, S. & SCHMID, B. 2012. Fiji: an open-source platform for biological-image analysis. *Nature methods*, 9, 676-682.
- SKELTON, A. 2011. Flux rates for water and carbon during greenschist facies metamorphism. *Geology*, 39, 43-46.
- SLAMA, J. & PEDERSEN, R. B. 2015. Zircon provenance of SW Caledonian phyllites reveals a distant Timanian sediment source. *Journal of the Geological Society*, 172, 465-478.
- STEPHENS, M., GUSTAVSON, M., RAMBERG, I. & ZACHRISSON, E. 1985. The Caledonides of central-north Scandinavia—a tectonostratigraphic overview. *The Caledonide orogen—Scandinavia and related areas*, 135-162.
- STEWART, E. & AGUE, J. J. 2020. Pervasive subduction zone devolatilization recycles CO₂ into the forearc. *Nature communications*, 11, 1-8.
- STROBL, L. A. 2021. *Decarbonation of Carbonated Serpentinites at Linnajavri, Norway: Insights from Petrology and Geochemistry. Part II*. Msc, University of Utrecht.
- STROBL, L. A., PLÜMPER, O., OHL, M. & BEINLICH, A. 2021. Shallow-Depth Slab Decarbonation as a control on the Deep Carbon Cycle. *Goldschmidt2021• Virtual* 4-9 July.
- SUNDBLAD, K. 1986. The Stipok allochthon—an exotic terrane in the northern Swedish Caledonides. *Geologiska Föreningen i Stockholm Förhandlingar*, 108, 309-311.
- TAYLOR, S. R. & MCLENNAN, S. M. 1985. The continental crust: its composition and evolution.
- TOMINAGA, M., BEINLICH, A., LIMA, E. A., TIVEY, M. A., HAMPTON, B. A., WEISS, B. & HARIGANE, Y. 2017. Multi-scale magnetic mapping of serpentinite carbonation. *Nature communications*, 8, 1-10.
- TROITZSCH, U. & ELLIS, D. J. 2004. High-PT study of solid solutions in the system ZrO₂-TiO₂: The stability of srilankite. *European Journal of Mineralogy*, 16, 577-584.
- WHITE, R. W., POWELL, R., HOLLAND, T. J. B., JOHNSON, T. E. & GREEN, E. C. R. 2014. New mineral activity–composition relations for thermodynamic calculations in metapelitic systems. *Journal of Metamorphic Geology*, 32, 261-286.
- WINTER, J. 2001. *An Introduction to Igneous and Metamorphic Petrology*, New Jersey, Prentice-Hall Inc.
- WU, C.-M. & CHEN, H.-X. 2015. Revised Ti-in-biotite geothermometer for ilmenite-or rutile-bearing crustal metapelites. *Science Bulletin*, 60, 116-121.
- WU, C.-M. & CHENG, B.-H. 2006. Valid garnet–biotite (GB) geothermometry and garnet–aluminum silicate–plagioclase–quartz (GASP) geobarometry in metapelitic rocks. *Lithos*, 89, 1-23.
- WU, C. 2015. Revised empirical garnet–biotite–muscovite–plagioclase geobarometer in metapelites. *Journal of Metamorphic Geology*, 33, 167-176.
- WU, C. M. 2017. Calibration of the garnet–biotite–Al₂SiO₅–quartz geobarometer for metapelites. *Journal of Metamorphic geology*, 35, 983-998.
- ZACK, T., MORAES, R. & KRONZ, A. 2004. Temperature dependence of Zr in rutile: empirical calibration of a rutile thermometer. *Contributions to Mineralogy and Petrology*, 148, 471-488.

APPENDICES

Appendix 1 – Perple_X build file

Appendix 2 – EDS analysis

Appendix 3 – Bulk rock chemical composition

Appendix 4 – EMP analysis

Appendix 5 – EMPA areas

Appendix 6 – LA-ICP-MS analysis

Appendix 1 – Perple_X build file

hp04ver.dat thermodynamic data file

no_print | print generates print output

plot | obsolete 6.8.4+

solution_model.dat | solution model file, blank = none

Lin_14-19

perplex_option.dat | Perple_X option file

5 calculation type: 0- composition, 1- Schreinemakers, 3- Mixed, 4- swash, 5- gridded min, 7- 1d fract, 8- gwash, 9- 2d fract, 10- 7 w/file input, 11- 9 w/file input, 12- 0d infiltration

0 unused place holder, post 06

0 number component transformations

15 number of components in the data base

1 component amounts, 0 - mole, 1 mass

0 unused place holder, post 06

0 unused place holder, post 06

0 unused place holder, post 05

5 ifug EoS for saturated phase

2 gridded minimization dimension (1 or 2)

0 special dependencies: 0 - P and T independent, 1 - P(T), 2 - T(P)

0.00000 0.00000 0.00000 0.00000 0.00000 Geothermal gradient polynomial coeffs.

begin thermodynamic component list

SIO2 1 67.7700 0.00000 0.00000 mass amount

AL2O3 1 13.2500 0.00000 0.00000 mass amount

FEO 1 6.15000 0.00000 0.00000 mass amount

```

CAO 1 2.41000 0.00000 0.00000 mass amount
MGO 1 3.14000 0.00000 0.00000 mass amount
TIO2 1 0.91000 0.00000 0.00000 mass amount
K2O 1 2.18000 0.00000 0.00000 mass amount
NA2O 1 1.53000 0.00000 0.00000 mass amount
H2O 1 0.85000 0.00000 0.00000 mass amount
end thermodynamic component list

begin saturated component list
end saturated component list

begin saturated phase component list
end saturated phase component list

begin independent potential/fugacity/activity list
end independent potential list

begin excluded phase list
ab
san
osm1
end excluded phase list

begin solution phase list
Bi(W)
Gt(W)
Chl(W)
Pl(JH)
Mica(W)
St(W)
end solution phase list

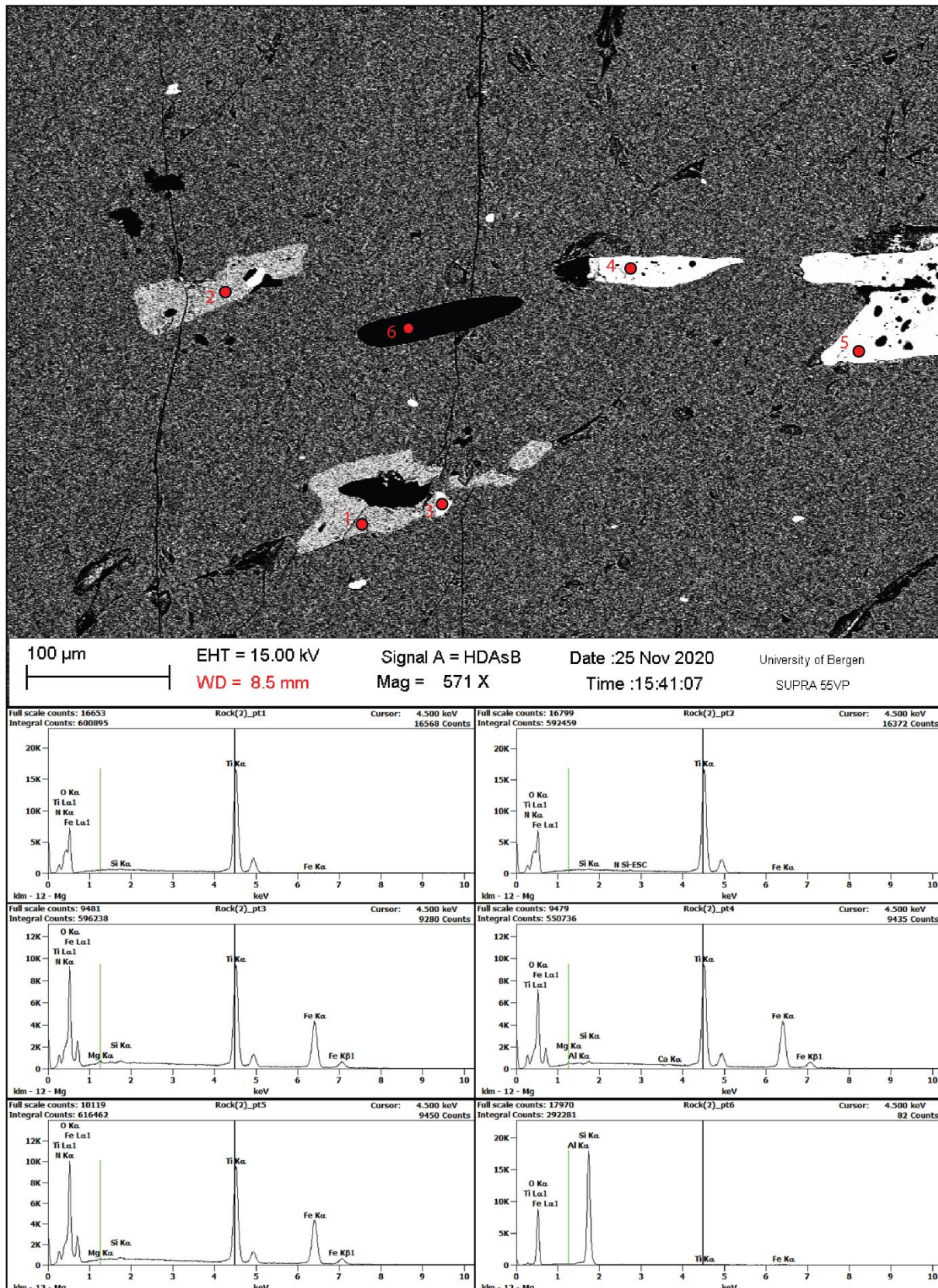
 8000.00    1073.00    0.00000    0.00000    0.00000    max p, t, xco2, mu_1, mu_2
 5000.00     673.000    0.00000    0.00000    0.00000    min p, t, xco2, mu_1, mu_2
 0.00000    0.00000    0.00000    0.00000    0.00000    unused place holder post 06

```

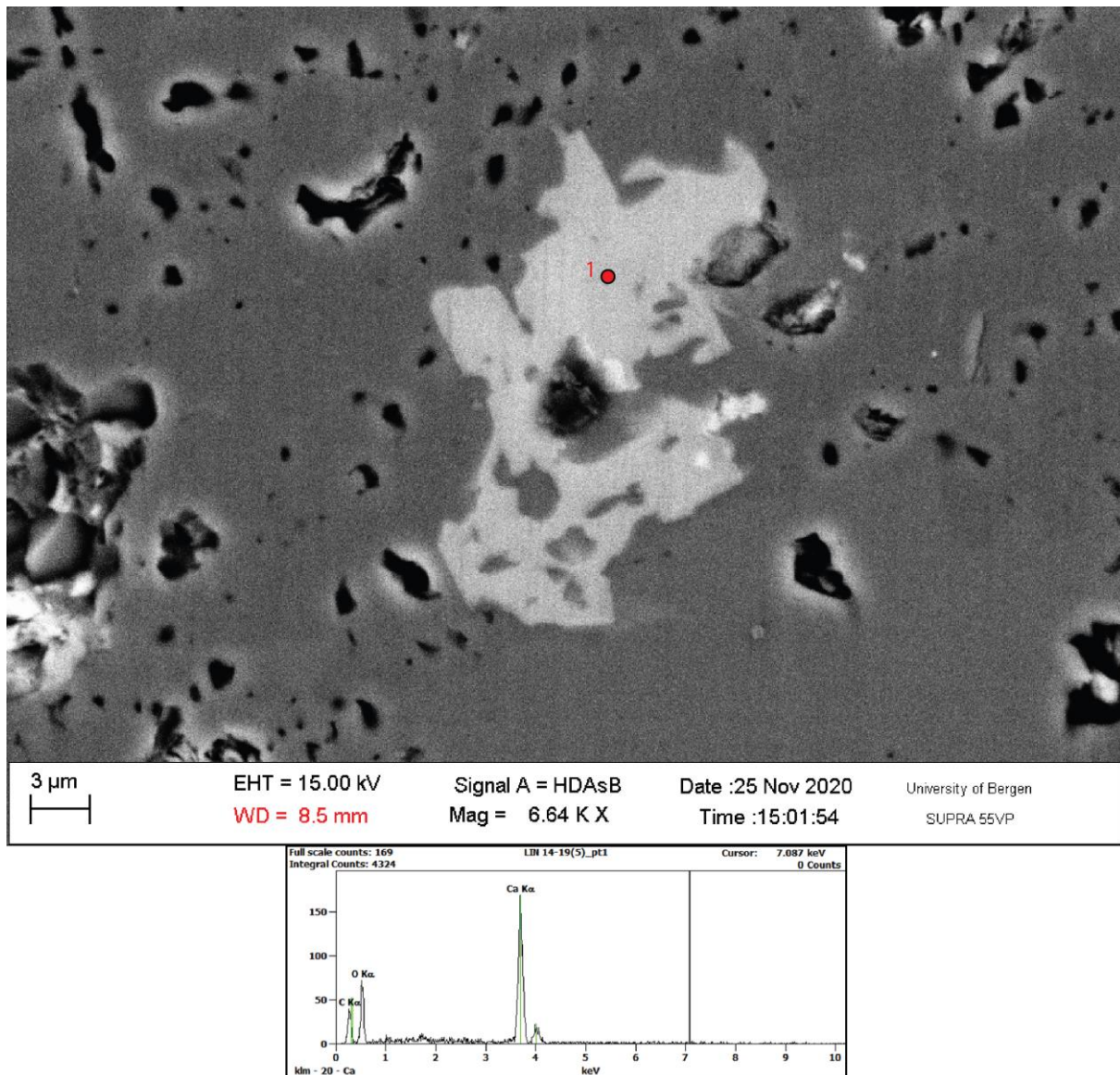
2 1 4 5 3 indices of 1st & 2nd independent & sectioning variables

Appendix 2 – EDS analysis

EDS analysis for rutile, ilmenite, and quartz in Lin_14-19



EDS analysis for calcite in Lin_14-19



Appendix 3 – Bulk rock chemical composition

Sample	Major elements (Wt%)																			LOI	H ₂ O	CO ₂	Total		
	SiO ₂	Al ₂ O ₃	Fe ₂ O ₃	FeO	CaO	MgO	MnO	TiO ₂	V ₂ O ₅	SO ₃	P ₂ O ₅	K ₂ O	Na ₂ O	SrO	Cr ₂ O ₃	As	Co	Cu	Ni	Zn	Cl				
Lin_12a-19	46,04	14,53	7,57	9,36	9,03	5,8	0,271	2,157	0,101	0,04	0,18	0,199	3,54	0,05	0,008	b.d.l.	0,005	0,015	0,004	0,014	b.d.l.	0,23	0,17	0,06	99,14
Lin_13-19	41,01	16,01	5,51	10	12,18	8,88	0,234	2,044	0,09	0,175	0,071	0,191	2,04	0,06	0,028	b.d.l.	0,007	0,021	0,011	0,012	0,001	0,81	0,67	0,14	99,38
Lin_14-19	67,77	13,25	0,54	5,75	2,41	3,14	0,096	0,915	0,019	0,015	0,137	2,18	2,15	0,02	0,017	b.d.l.	0,002	0,003	0,005	0,008	b.d.l.	1,09	0,93	0,16	99,52
Lin_15-19	67,99	13,98	1,52	4,79	1,99	3,07	0,07	0,915	0,021	0,012	0,143	2,57	1,53	0,02	0,016	b.d.l.	0,002	0,002	0,004	0,008	b.d.l.	0,77	0,7	0,07	99,42
Lin_16-19	61,81	14,37	2,94	4,03	3,81	3,82	0,129	0,858	0,022	0,01	0,186	3,4	1,64	0,02	0,014	b.d.l.	0,002	0,003	0,005	0,009	b.d.l.	2,2	1,82	0,38	99,28
Trace elements (ppm)																									
Sample	Ag	As	Bi	Cd	Ce	Co	Cr	Cu	Dy	Er	Eu	Ga	Gd	Ge	Hf	Ho	La	Lu	Mo	Nb	Nd	Ni			
Lin_12a-19	0,3	0,6	b.d.l.	0,1	6,54	47,3	61	140	4,52	2,66	1,19	20,2	3,72	1,4	1,01	0,95	2,26	0,36	0,6	1,03	7,76	34			
Lin_13-19	b.d.l.	1	b.d.l.	0,2	6,12	53,9	204	192	5,73	3,48	1,42	21,7	5,02	1,9	1,32	1,24	1,52	0,45	0,6	0,8	9,21	96			
Lin_14-19	0,1	0,4	0,26	b.d.l.	75,4	18,6	129	32	5,78	3,35	1,38	16,5	6,25	1,3	6,53	1,24	37,6	0,52	1	15	35,5	58			
Lin_15-19	0,1	0,2	0,2	b.d.l.	79,6	20,6	127	22	6,18	3,29	1,44	18,8	6,21	1,75	6,73	1,2	39,1	0,47	0,6	15,8	37	48			
Lin_16-19	b.d.l.	0,4	0,24	b.d.l.	73,7	19,4	105	28	5,44	3,32	1,4	19,9	6,08	1,75	5,67	1,12	36,3	0,5	0,8	14,7	34,2	48			
Sample	Pb	Pr	Rb	Re	Sb	Sc	Sm	Sn	Sr	Ta	Tb	Te	Th	Tl	Tm	U	V	W	Y	Yb	Zn	Zr			
Lin_12a-19	2	1,27	1,45	b.d.l.	0,2	54,3	2,73	0,6	305	0,09	0,69	b.d.l.	0,03	b.d.l.	0,38	0,01	554	b.d.l.	22,6	2,47	115	30			
Lin_13-19	3	1,4	1,65	b.d.l.	0,9	57,8	3,68	0,8	383	0,05	0,91	b.d.l.	b.d.l.	b.d.l.	0,5	0,05	504	1	29,8	3,11	100	27			
Lin_14-19	17	9,38	91,7	b.d.l.	b.d.l.	17,9	6,71	3	104	1,18	0,95	b.d.l.	11,5	0,2	0,51	2,2	117	0,5	30,9	3,5	75	241			
Lin_15-19	12	10,1	110	b.d.l.	b.d.l.	17,5	8,14	3	96	1,24	0,97	b.d.l.	12,2	0,4	0,47	2,28	113	1	29,7	2,94	75	242			
Lin_16-19	14	9,13	136	b.d.l.	b.d.l.	17,8	6,86	2,6	124	1,11	0,95	b.d.l.	11,5	0,6	0,53	2,23	125	1,5	29,5	3,18	85	208			

b.d.l. = below detection limit (<0,01 wt.%)

Appendix 4 – EMP analysis

EMP error

	Grt (n=128)		Bt (n=84)		Mu (n=33)		Pl (n=59)		Amp (n=10)	
	Avg %ERR	2σ	Avg %ERR	2σ	Avg %ERR	2σ	Avg %ERR	2σ	Avg %ERR	2σ
Si	0,364	0,004	0,409	0,083	0,376	0,072	0,281	0,010	0,342	0,003
Ti	25,2	61,7	2,55	0,696	7,57	6,88	-246	2977	5,94	1,09
Al	0,328	0,004	0,384	0,077	0,275	0,048	0,287	0,014	0,391	0,008
Fe	0,373	0,019	0,576	0,110	1,95	1,27	23,9	72,7	0,508	0,019
Mn	4,28	8,52	61,5	318	24,8	549	272	3384	4,88	0,481
Mg	0,940	0,205	0,479	0,120	1,97	0,912	335	6730	0,494	0,016
Ca	0,542	0,072	-39,1	991	37,9	193	0,551	0,152	0,429	0,017
Na	93,2	857	9,98	6,80	2,72	0,687	0,595	0,048	1,43	0,081
K	-95890	2169897	0,472	0,100	0,475	0,101	9,75	4,40	2,82	0,206
F	91,5	1636	6,07	2,23	14,6	6,77	19,0	10,6	10,4	2,84
Cr	-16,0	1445	69,5	218	39,6	214	-49,2	815	294	1383
Cl	-179	3970	54,3	643	216	2929	-1355316	20821699	-960	6603

SAMPLE	14-S1-A1_grt	14-S1-A1_plg	14-S1-A2_plg	14-S1-A2_bt	14-S1-A3_bt	14-S1-A3_grt	14-S1-A4_grt traverse_rim-to-core	14-S1-A4_grt traverse_rim-to-core	14-S1-A4_grt traverse_rim-to-core	14-S1-A4_grt traverse_rim-to-core	14-S1-A4_grt traverse_rim-to-core
SiO2 WT%	38,01	62,67	60,46	37,69	36,27	38,18	37,38	37,76	37,73	37,93	37,75
TiO2 WT%	0,05	0,00	0,04	1,98	2,06	0,05	0,09	0,10	0,08	0,09	0,38
Al2O3 WT%	21,84	23,95	25,40	19,68	19,53	21,84	21,94	21,88	21,82	21,89	21,91
FeO WT%	31,36	0,16	0,03	15,64	15,79	31,29	31,15	31,18	31,80	31,62	31,87
MnO WT%	0,70	0,02	0,00	0,02	0,03	0,35	0,34	0,34	0,37	0,41	0,42
MgO WT%	3,28	0,00	0,00	11,96	11,42	3,12	3,01	2,90	2,86	2,70	2,82
CaO WT%	5,66	4,83	6,50	0,01	0,05	6,31	6,68	6,68	6,45	6,70	6,05
Na2O WT%	0,01	8,25	7,42	0,10	0,15	0,00	0,01	0,00	0,01	0,01	0,02
K2O WT%	0,00	0,05	0,05	9,51	9,31	0,01	0,02	0,00	0,00	0,02	0,00
F WT%	0,04	0,09	0,05	0,34	0,40	0,04	0,05	0,01	0,03	0,08	0,03
Cr2O3 WT%	0,00	0,01	0,00	0,03	0,03	0,03	0,01	0,03	0,02	0,02	0,00
Cl WT%	0,00	0,00	0,00	0,00	0,00	0,00	0,00	0,01	0,01	0,00	0,01
O WT%	0,00	0,00	0,00	0,00	0,00	0,00	0,00	0,00	0,00	0,00	0,00
H2O WT%	0,00	0,00	0,00	4,06	4,04	0,00	0,00	0,00	0,00	0,00	0,00
Total	100,95	100,04	99,89	101,03	99,07	101,22	100,68	100,87	101,17	101,49	101,27
O≡Cl,F				0,18	0,21						
TOTAL				100,85	98,86						
FORMULA	24,00	24,00	24,00	24,00	24,00	24,00	24,00	24,00	24,00	24,00	24,00
BASIS	O	O	O	O	O	O	O	O	O	O	O
Si FORMULA	5,98	8,31	8,06	5,52	5,44	5,99	5,91	5,95	5,95	5,96	5,94
Ti FORMULA	0,01	0,00	0,00	0,22	0,23	0,01	0,01	0,01	0,01	0,01	0,05
Al FORMULA	4,05	3,74	3,99	3,40	3,45	4,04	4,09	4,07	4,05	4,05	4,06
Fe FORMULA	4,13	0,02	0,00	1,92	1,98	4,11	4,12	4,11	4,19	4,16	4,19
Mn FORMULA	0,09	0,00	0,00	0,00	0,00	0,05	0,05	0,04	0,05	0,05	0,06
Mg FORMULA	0,77	0,00	0,00	2,61	2,55	0,73	0,71	0,68	0,67	0,63	0,66
Ca FORMULA	0,95	0,69	0,93	0,00	0,01	1,06	1,13	1,13	1,09	1,13	1,02
Na FORMULA	0,00	2,12	1,92	0,03	0,04	0,00	0,00	0,00	0,00	0,00	0,01
K FORMULA	0,00	0,01	0,01	1,78	1,78	0,00	0,00	0,00	0,00	0,00	0,00
F FORMULA	0,02	0,04	0,02	0,16	0,19	0,02	0,03	0,00	0,02	0,04	0,01
Cr FORMULA	0,00	0,00	0,00	0,00	0,00	0,00	0,00	0,00	0,00	0,00	0,00
Cl FORMULA	0,00	0,00	0,00	0,00	0,00	0,00	0,00	0,00	0,00	0,00	0,00
O FORMULA	24,00	24,00	24,00	24,00	24,00	24,00	24,00	24,00	24,00	24,00	24,00
H FORMULA	0,00	0,00	0,00	3,97	4,05	0,00	0,00	0,00	0,00	0,00	0,00
X-POS	32,31	32,34	32,16	32,02	31,69	31,62	30,51	30,51	30,52	30,52	30,53
Y-POS	8,37	8,40	7,80	7,78	7,77	7,78	9,26	9,24	9,19	9,11	9,03

SAMPLE	14-S1-A4_grt traverse_rim-to-core	14-S1-A4_grt traverse_rim-to-core	14-S1-A4_grt traverse_rim-to-core	14-S1-A4_grt traverse_rim-to-core	14-S1-A4_grt traverse_rim-to-core	14-S1-A4_grt single-rim	14-S1-A4_grt single-mid	14-S1-A4_plg	14-S1-A4_plg	14-S1-A4_plg	14-S1-A4_bt
SiO2 WT%	37,75	37,64	37,85	37,73	37,74	37,77	37,73	61,83	61,88	61,14	35,84
TiO2 WT%	0,07	0,07	0,07	0,06	0,08	0,10	0,07	0,01	0,01	0,01	1,77
Al2O3 WT%	21,92	21,97	21,87	21,76	21,89	21,88	21,88	24,98	24,57	25,10	19,67
FeO WT%	31,66	31,52	31,45	31,41	31,85	30,84	31,37	0,22	0,17	0,09	15,69
MnO WT%	0,51	0,61	0,58	0,61	0,65	0,73	0,46	0,02	0,00	0,00	0,01
MgO WT%	2,64	2,58	2,53	2,46	2,52	2,83	2,65	0,00	0,01	0,00	11,49
CaO WT%	6,35	6,55	6,67	6,34	6,18	6,60	6,66	5,38	5,17	5,89	0,03
Na2O WT%	0,02	0,03	0,01	0,02	0,00	0,01	0,03	8,02	7,96	7,64	0,10
K2O WT%	0,00	0,00	0,00	0,00	0,00	0,00	0,00	0,10	0,07	0,07	9,50
F WT%	0,00	0,00	0,00	0,00	0,01	0,01	0,02	0,06	0,10	0,09	0,35
Cr2O3 WT%	0,01	0,02	0,00	0,02	0,02	0,01	0,01	0,01	0,00	0,00	0,02
Cl WT%	0,00	0,00	0,01	0,00	0,00	0,00	0,00	0,00	0,01	0,00	0,01
O WT%	0,00	0,00	0,00	0,00	0,00	0,00	0,00	0,00	0,00	0,00	0,00
H2O WT%	0,00	0,00	0,00	0,00	0,00	0,00	0,00	0,00	0,00	0,00	4,04
Total	100,93	100,95	101,04	100,42	100,95	100,78	100,88	100,61	99,96	100,03	98,53
O≡Cl,F											0,19
TOTAL											98,34
FORMULA	24,00	24,00	24,00	24,00	24,00	24,00	24,00	24,00	24,00	24,00	24,00
BASIS	O	O	O	O	O	O	O	O	O	O	O
Si FORMULA	5,96	5,94	5,97	5,99	5,96	5,96	5,96	8,17	8,22	8,13	5,41
Ti FORMULA	0,01	0,01	0,01	0,01	0,01	0,01	0,01	0,00	0,00	0,00	0,20
Al FORMULA	4,08	4,09	4,06	4,07	4,08	4,07	4,07	3,89	3,85	3,93	3,50
Fe FORMULA	4,18	4,16	4,15	4,17	4,21	4,07	4,14	0,02	0,02	0,01	1,98
Mn FORMULA	0,07	0,08	0,08	0,08	0,09	0,10	0,06	0,00	0,00	0,00	0,00
Mg FORMULA	0,62	0,61	0,59	0,58	0,59	0,67	0,62	0,00	0,00	0,00	2,58
Ca FORMULA	1,07	1,11	1,13	1,08	1,05	1,12	1,13	0,76	0,74	0,84	0,00
Na FORMULA	0,01	0,01	0,00	0,01	0,00	0,00	0,01	2,06	2,05	1,97	0,03
K FORMULA	0,00	0,00	0,00	0,00	0,00	0,00	0,00	0,02	0,01	0,01	1,83
F FORMULA	0,00	0,00	0,00	0,00	0,00	0,01	0,01	0,02	0,04	0,04	0,17
Cr FORMULA	0,00	0,00	0,00	0,00	0,00	0,00	0,00	0,00	0,00	0,00	0,00
Cl FORMULA	0,00	0,00	0,00	0,00	0,00	0,00	0,00	0,00	0,00	0,00	0,00
O FORMULA	24,00	24,00	24,00	24,00	24,00	24,00	24,00	24,00	24,00	24,00	24,00
H FORMULA	0,00	0,00	0,00	0,00	0,00	0,00	0,00	0,00	0,00	0,00	4,07
X-POS	30,53	30,55	30,56	30,56	30,56	30,32	30,38	30,23	30,36	30,40	30,45
Y-POS	8,97	8,81	8,72	8,68	8,61	9,34	9,10	9,47	9,39	9,66	9,29

SAMPLE	14-S1-A4_bt	14-S1-A5_bt	14-S1-A5_bt	14-S1-A5_grt	14-S1-A5_grt	14-S1-A6_plg	14-S2-A1_plg	14-S2-A1_plg	14-S2-A1_musc	14-S2-A2_grt left-to-right	14-S2-A2_grt left-to-right
SiO2 WT%	35,32	36,48	36,51	37,89	37,53	66,05	60,56	60,78	45,93	38,07	37,89
TiO2 WT%	1,75	2,22	1,42	0,05	0,03	0,00	0,03	0,00	0,42	0,08	0,08
Al2O3 WT%	19,78	19,52	20,73	21,82	21,87	21,57	25,46	25,16	36,90	21,83	21,89
FeO WT%	16,10	16,24	16,14	31,74	31,76	0,07	0,02	0,06	1,01	31,38	31,02
MnO WT%	0,03	0,06	0,00	0,44	0,40	0,01	0,02	0,00	0,00	0,43	0,41
MgO WT%	11,54	11,71	11,86	3,48	3,55	0,00	0,00	0,00	0,88	3,29	2,80
CaO WT%	0,03	0,00	0,02	5,19	5,15	1,90	6,33	5,83	0,01	5,75	6,83
Na2O WT%	0,05	0,07	0,12	0,00	0,02	9,94	7,45	7,80	0,78	0,02	0,04
K2O WT%	9,36	9,80	9,70	0,01	0,00	0,07	0,07	0,07	10,18	0,00	0,00
F WT%	0,31	0,35	0,38	0,01	0,02	0,09	0,10	0,08	0,10	0,03	0,05
Cr2O3 WT%	0,05	0,02	0,02	0,00	0,01	0,00	0,00	0,00	0,01	0,01	0,01
Cl WT%	0,01	0,00	0,00	0,00	0,01	0,00	0,00	0,01	0,00	0,01	0,00
O WT%	0,00	0,00	0,00	0,00	0,00	0,00	0,00	0,00	0,00	0,00	0,00
H2O WT%	4,03	4,03	4,04	0,00	0,00	0,00	0,00	0,00	4,53	0,00	0,00
Total	98,37	100,51	100,94	100,61	100,35	99,68	100,04	99,73	100,73	100,88	101,01
O≡Cl,F	0,17	0,18	0,20							0,05	
TOTAL	98,20	100,33	100,74							100,68	
FORMULA	24,00	24,00	24,00	24,00	24,00	24,00	24,00	24,00	24,00	24,00	24,00
BASIS	O	O	O	O	O	O	O	O	O	O	O
Si FORMULA	5,35	5,42	5,38	5,98	5,94	8,71	8,06	8,11	6,05	5,99	5,97
Ti FORMULA	0,20	0,25	0,16	0,01	0,00	0,00	0,00	0,00	0,04	0,01	0,01
Al FORMULA	3,53	3,42	3,60	4,06	4,08	3,35	4,00	3,96	5,73	4,05	4,06
Fe FORMULA	2,04	2,02	1,99	4,19	4,21	0,01	0,00	0,01	0,11	4,13	4,08
Mn FORMULA	0,00	0,01	0,00	0,06	0,05	0,00	0,00	0,00	0,00	0,06	0,05
Mg FORMULA	2,61	2,59	2,61	0,82	0,84	0,00	0,00	0,00	0,17	0,77	0,66
Ca FORMULA	0,00	0,00	0,00	0,88	0,87	0,27	0,90	0,83	0,00	0,97	1,15
Na FORMULA	0,02	0,02	0,03	0,00	0,01	2,54	1,92	2,02	0,20	0,01	0,01
K FORMULA	1,81	1,86	1,82	0,00	0,00	0,01	0,01	0,01	1,71	0,00	0,00
F FORMULA	0,15	0,16	0,18	0,00	0,01	0,04	0,04	0,03	0,04	0,01	0,02
Cr FORMULA	0,01	0,00	0,00	0,00	0,00	0,00	0,00	0,00	0,00	0,00	0,00
Cl FORMULA	0,00	0,00	0,00	0,00	0,00	0,00	0,00	0,00	0,00	0,00	0,00
O FORMULA	24,00	24,00	24,00	24,00	24,00	24,00	24,00	24,00	24,00	24,00	24,00
H FORMULA	4,07	3,99	3,97	0,00	0,00	0,00	0,00	0,00	3,98	0,00	0,00
X-POS	30,48	29,14	29,16	29,17	29,16	28,96	39,20	39,27	39,30	39,08	38,98
Y-POS	9,28	8,83	8,74	8,70	8,69	9,54	4,91	4,99	5,02	5,44	5,55

SAMPLE	14-S2-A2_grt left-to-right	14-S2-A2_grt left-to-right	14-S2-A2_grt left-to-right	14-S2- A2_musc	14-S2-A2_plg	14-S2-A3_grt left-to-right	14-S2-A3_grt left-to-right	14-S2-A3_grt left-to-right	14-S2-A3_bt	14-S2-A3_plg	14-S2-A4_grt
SiO2 WT%	37,68	36,28	35,40	45,45	59,86	37,76	37,55	37,80	35,24	61,47	37,50
TiO2 WT%	0,06	2,10	1,90	0,63	0,02	0,06	0,01	0,14	2,03	0,00	0,06
Al2O3 WT%	21,84	19,86	19,65	36,98	25,67	21,80	21,89	21,73	19,70	24,43	21,83
FeO WT%	31,17	16,23	15,90	0,97	0,05	32,13	31,81	29,74	15,69	0,19	31,65
MnO WT%	0,26	0,02	0,04	0,00	0,00	1,10	0,76	2,09	0,02	0,00	1,05
MgO WT%	3,41	11,71	11,88	0,73	0,00	3,10	2,93	2,07	11,49	0,01	2,41
CaO WT%	5,89	0,05	0,11	0,00	6,46	4,94	5,63	7,60	0,05	5,06	6,31
Na2O WT%	0,03	0,06	0,10	0,79	7,26	0,01	0,00	0,00	0,10	8,10	0,01
K2O WT%	0,00	9,54	9,34	10,21	0,07	0,01	0,00	0,00	9,36	0,07	0,00
F WT%	0,06	0,39	0,40	0,19	0,10	0,03	0,06	0,00	0,43	0,11	0,00
Cr2O3 WT%	0,02	0,05	0,02	0,02	0,00	0,00	0,00	0,04	0,03	0,00	0,02
Cl WT%	0,00	0,00	0,01	0,00	0,00	0,00	0,00	0,00	0,00	0,00	0,00
O WT%	0,00	0,00	0,00	0,00	0,00	0,00	0,00	0,00	0,00	0,00	0,00
H2O WT%	0,00	4,03	4,03	4,52	0,00	0,00	0,00	0,00	4,04	0,00	0,00
Total	100,42	100,33	98,77	100,49	99,46	100,92	100,62	101,11	98,18	99,44	100,79
O≡Cl,F	0,20	0,21	0,10						0,22		
TOTAL	100,13	98,56	100,39						97,96		
FORMULA	24,00	24,00	24,00	24,00	24,00	24,00	24,00	24,00	24,00	24,00	24,00
BASIS	O	O	O	O	O	O	O	O	O	O	O
Si FORMULA	5,96	5,39	5,34	6,01	8,02	5,97	5,95	5,96	5,34	8,21	5,94
Ti FORMULA	0,01	0,23	0,22	0,06	0,00	0,01	0,00	0,02	0,23	0,00	0,01
Al FORMULA	4,07	3,48	3,49	5,76	4,05	4,06	4,09	4,04	3,52	3,85	4,08
Fe FORMULA	4,12	2,02	2,01	0,11	0,01	4,25	4,22	3,92	1,99	0,02	4,19
Mn FORMULA	0,04	0,00	0,01	0,00	0,00	0,15	0,10	0,28	0,00	0,00	0,14
Mg FORMULA	0,80	2,59	2,67	0,14	0,00	0,73	0,69	0,49	2,60	0,00	0,57
Ca FORMULA	1,00	0,01	0,02	0,00	0,93	0,84	0,96	1,28	0,01	0,72	1,07
Na FORMULA	0,01	0,02	0,03	0,20	1,89	0,00	0,00	0,00	0,03	2,10	0,00
K FORMULA	0,00	1,81	1,80	1,72	0,01	0,00	0,00	0,00	1,81	0,01	0,00
F FORMULA	0,03	0,18	0,19	0,08	0,04	0,02	0,03	0,00	0,21	0,04	0,00
Cr FORMULA	0,00	0,01	0,00	0,00	0,00	0,00	0,00	0,00	0,00	0,00	0,00
Cl FORMULA	0,00	0,00	0,00	0,00	0,00	0,00	0,00	0,00	0,00	0,00	0,00
O FORMULA	24,00	24,00	24,00	24,00	24,00	24,00	24,00	24,00	24,00	24,00	24,00
H FORMULA	0,00	3,99	4,06	3,99	0,00	0,00	0,00	0,00	4,08	0,00	0,00
X-POS	38,98	39,12	39,01	39,23	39,08	38,54	38,52	38,45	38,35	38,56	38,08
Y-POS	5,80	5,40	5,83	5,56	5,92	4,75	4,91	5,20	4,66	4,73	5,14

SAMPLE	14-S2-A4_grt	14-S2-A4_grt	14-S2-A5_musc top-to-bottom	14-S2-A5_musc top-to-bottom	14-S2-A6_grt	14-S2-A6_grt	14-S2-A6_bt	14-S2-A6_bt	14-S2-A6_musc top-to-bottom	14-S2-A6_musc top-to-bottom	14-S2-A6_plg top-to-bottom
SiO2 WT%	37,28	37,51	45,58	46,34	37,74	37,61	35,77	35,56	45,83	45,76	60,79
TiO2 WT%	0,08	0,07	0,42	0,51	0,09	0,06	1,72	1,80	0,44	0,48	0,00
Al2O3 WT%	21,79	21,75	36,52	36,16	21,71	21,95	19,83	19,89	37,07	36,08	24,50
FeO WT%	31,62	31,61	1,04	1,15	31,23	31,60	15,95	15,60	1,05	1,11	0,12
MnO WT%	0,99	1,11	0,02	0,00	0,60	0,38	0,06	0,03	0,00	0,00	0,02
MgO WT%	2,48	2,43	0,88	1,02	3,23	3,43	11,83	11,91	0,86	1,07	0,01
CaO WT%	6,08	6,31	0,06	0,02	5,83	5,84	0,07	0,11	0,03	0,01	5,17
Na2O WT%	0,03	0,01	0,76	0,74	0,00	0,02	0,13	0,12	0,76	0,70	7,99
K2O WT%	0,00	0,00	10,09	10,16	0,00	0,01	9,35	9,32	10,10	10,19	0,08
F WT%	0,00	0,00	0,25	0,18	0,01	0,04	0,35	0,39	0,15	0,14	0,12
Cr2O3 WT%	0,05	0,03	0,00	0,04	0,01	0,02	0,04	0,03	0,07	0,04	0,00
Cl WT%	0,00	0,00	0,01	0,00	0,00	0,00	0,02	0,00	0,00	0,00	0,00
O WT%	0,00	0,00	0,00	0,00	0,00	0,00	0,00	0,00	0,00	0,00	0,00
H2O WT%	0,00	0,00	4,52	4,52	0,00	0,00	4,04	4,04	4,53	4,52	0,00
Total	100,37	100,82	100,15	100,83	100,44	100,94	99,14	98,80	100,88	100,07	98,81
O≡Cl,F			0,13	0,10			0,19	0,20	0,08	0,07	
TOTAL			100,01	100,74			98,96	98,59	100,80	99,99	0,00
FORMULA	24,00	24,00	24,00	24,00	24,00	24,00	24,00	24,00	24,00	24,00	24,00
BASIS	O	O	O	O	O	O	O	O	O	O	O
Si FORMULA	5,93	5,95	6,05	6,10	5,97	5,93	5,37	5,35	6,03	6,07	8,18
Ti FORMULA	0,01	0,01	0,04	0,05	0,01	0,01	0,19	0,20	0,04	0,05	0,00
Al FORMULA	4,09	4,06	5,71	5,61	4,05	4,08	3,51	3,53	5,75	5,64	3,89
Fe FORMULA	4,21	4,19	0,12	0,13	4,13	4,16	2,00	1,96	0,12	0,12	0,01
Mn FORMULA	0,13	0,15	0,00	0,00	0,08	0,05	0,01	0,00	0,00	0,00	0,00
Mg FORMULA	0,59	0,57	0,17	0,20	0,76	0,80	2,65	2,67	0,17	0,21	0,00
Ca FORMULA	1,04	1,07	0,01	0,00	0,99	0,99	0,01	0,02	0,00	0,00	0,74
Na FORMULA	0,01	0,00	0,19	0,19	0,00	0,01	0,04	0,03	0,19	0,18	2,08
K FORMULA	0,00	0,00	1,71	1,71	0,00	0,00	1,79	1,79	1,70	1,72	0,01
F FORMULA	0,00	0,00	0,11	0,08	0,01	0,02	0,17	0,19	0,06	0,06	0,05
Cr FORMULA	0,01	0,00	0,00	0,00	0,00	0,00	0,00	0,00	0,01	0,00	0,00
Cl FORMULA	0,00	0,00	0,00	0,00	0,00	0,00	0,01	0,00	0,00	0,00	0,00
O FORMULA	24,00	24,00	24,00	24,00	24,00	24,00	24,00	24,00	24,00	24,00	24,00
H FORMULA	0,00	0,00	4,00	3,97	0,00	0,00	4,04	4,06	3,97	4,01	0,00
X-POS	38,07	38,09	37,92	38,13	37,34	37,57	37,35	37,44	37,34	37,49	37,18
Y-POS	5,14	5,15	6,07	6,07	5,66	5,77	5,80	5,79	5,93	6,08	5,84

SAMPLE	14-S2-A6_plg top-to-bottom	14-S2-A7_plg top-to-bottom	14-S2-A7_plg top-to-bottom	15-S1_A1_musc	15-S1_A2_grt	15-S1_A2_grt	15-S1_A2_grt	15-S1_A2_plg	15-S1_A2_plg	15-S1_A2_bt	15-S1_A2_bt
SiO2 WT%	61,02	60,27	60,24	44,85	37,31	37,34	36,99	57,61	58,04	35,24	34,84
TiO2 WT%	0,00	0,00	0,00	0,61	0,05	0,07	0,07	0,02	0,06	2,01	1,92
Al2O3 WT%	24,30	24,73	24,46	35,35	21,81	21,76	21,75	26,30	25,99	19,71	20,15
FeO WT%	0,05	0,04	0,02	2,45	30,21	30,37	30,46	0,17	0,20	16,45	15,89
MnO WT%	0,00	0,01	0,00	0,00	0,84	1,52	0,68	0,01	0,01	0,05	0,02
MgO WT%	0,00	0,00	0,00	1,07	3,36	2,75	3,16	0,00	0,00	11,75	11,91
CaO WT%	5,02	5,36	5,15	0,00	6,02	6,51	6,52	7,09	6,70	0,03	0,04
Na2O WT%	8,07	7,82	7,94	0,49	0,03	0,02	0,03	6,87	7,20	0,12	0,11
K2O WT%	0,09	0,08	0,08	10,56	0,01	0,00	0,00	0,07	0,06	9,52	9,19
F WT%	0,09	0,09	0,12	0,17	0,02	0,00	0,00	0,11	0,12	0,41	0,32
Cr2O3 WT%	0,00	0,00	0,00	0,00	0,03	0,02	0,00	0,03	0,00	0,01	0,02
Cl WT%	0,00	0,00	0,00	0,01	0,01	0,00	0,00	0,01	0,00	0,01	0,01
O WT%	0,00	0,00	0,00	0,00	0,00	0,00	0,00	0,00	0,00	0,00	0,00
H2O WT%	0,00	0,00	0,00	4,48	0,00	0,00	0,00	0,00	0,00	4,01	4,04
Total	98,61	98,38	97,98	100,00	99,69	100,31	99,66	98,27	98,37	99,34	98,47
O≡Cl,F					0,09					0,22	0,17
TOTAL					99,91					99,12	98,30
FORMULA	24,00	24,00	24,00	24,00	24,00	24,00	24,00	24,00	24,00	24,00	24,00
BASIS	O	O	O	O	O	O	O	O	O	O	O
Si FORMULA	8,22	8,14	8,17	6,02	5,94	5,93	5,91	7,85	7,89	5,31	5,27
Ti FORMULA	0,00	0,00	0,00	0,06	0,01	0,01	0,01	0,00	0,01	0,23	0,22
Al FORMULA	3,86	3,94	3,91	5,59	4,09	4,07	4,09	4,22	4,16	3,50	3,59
Fe FORMULA	0,01	0,00	0,00	0,28	4,02	4,04	4,07	0,02	0,02	2,07	2,01
Mn FORMULA	0,00	0,00	0,00	0,00	0,11	0,20	0,09	0,00	0,00	0,01	0,00
Mg FORMULA	0,00	0,00	0,00	0,21	0,80	0,65	0,75	0,00	0,00	2,64	2,69
Ca FORMULA	0,72	0,78	0,75	0,00	1,03	1,11	1,12	1,03	0,98	0,01	0,01
Na FORMULA	2,11	2,05	2,09	0,13	0,01	0,01	0,01	1,81	1,90	0,03	0,03
K FORMULA	0,02	0,01	0,01	1,81	0,00	0,00	0,00	0,01	0,01	1,83	1,77
F FORMULA	0,04	0,04	0,05	0,07	0,01	0,00	0,00	0,05	0,05	0,20	0,15
Cr FORMULA	0,00	0,00	0,00	0,00	0,00	0,00	0,00	0,00	0,00	0,00	0,00
Cl FORMULA	0,00	0,00	0,00	0,00	0,00	0,00	0,00	0,00	0,00	0,00	0,00
O FORMULA	24,00	24,00	24,00	24,00	24,00	24,00	24,00	24,00	24,00	24,00	24,00
H FORMULA	0,00	0,00	0,00	4,01	0,00	0,00	0,00	0,00	0,00	4,03	4,07
X-POS	37,26	35,97	36,41	-2,05	-1,94	-1,77	-1,88	-1,93	-2,00	-1,76	-1,74
Y-POS	6,07	5,73	5,81	8,49	9,16	9,15	9,51	9,56	9,15	9,75	9,73

SAMPLE	<i>15-SI_A3_bt</i>	<i>15-SI_A3_bt</i>	<i>15-SI_A4_grt</i>	<i>15-SI_A4_grt</i>	<i>15-SI_A5_grt</i>	<i>15-SI_A5_grt</i>	<i>15-SI_A5_plg</i>	<i>15-SI_A5_plg</i>	<i>15-SI_A6_grt</i> <i>left_to_right</i>	<i>15-SI_A6_grt</i>	<i>15-SI_A6_grt</i>
SiO2 WT%	35,29	34,63	36,91	36,88	36,94	36,98	58,63	58,23	36,96	36,76	36,72
TiO2 WT%	2,06	2,28	0,09	0,08	0,05	0,08	0,00	0,02	0,04	0,06	0,12
Al2O3 WT%	19,91	19,55	21,67	21,82	21,89	21,70	24,98	25,42	22,00	21,86	21,84
FeO WT%	16,69	17,20	29,46	29,71	31,28	30,87	0,19	0,07	30,87	31,60	31,47
MnO WT%	0,01	0,02	2,82	2,50	0,32	0,33	0,01	0,01	0,61	0,34	0,15
MgO WT%	11,57	11,57	2,08	2,26	3,61	3,55	0,00	0,00	3,19	3,16	3,39
CaO WT%	0,01	0,01	7,15	7,21	5,77	6,12	5,81	6,08	6,21	6,05	5,94
Na2O WT%	0,13	0,12	0,05	0,04	0,02	0,01	7,58	7,52	0,02	0,02	0,00
K2O WT%	9,52	9,06	0,00	0,00	0,00	0,00	0,05	0,04	0,00	0,00	0,01
F WT%	0,40	0,36	0,00	0,00	0,01	0,05	0,10	0,09	0,00	0,00	0,09
Cr2O3 WT%	0,01	0,00	0,00	0,00	0,00	0,02	0,00	0,00	0,03	0,01	0,01
Cl WT%	0,01	0,01	0,00	0,00	0,00	0,00	0,00	0,00	0,00	0,00	0,00
O WT%	0,00	0,00	0,00	0,00	0,00	0,00	0,00	0,00	0,00	0,00	0,00
H2O WT%	4,01	4,01	0,00	0,00	0,00	0,00	0,00	0,00	0,00	0,00	0,00
Total	99,61	98,83	100,09	100,40	99,90	99,72	97,36	97,47	99,93	99,84	99,72
O≡Cl,F	0,21	0,19									
TOTAL	99,40	98,64									
FORMULA	24,00	24,00	24,00	24,00	24,00	24,00	24,00	24,00	24,00	24,00	24,00
BASIS	<i>O</i>	<i>O</i>	<i>O</i>	<i>O</i>	<i>O</i>	<i>O</i>	<i>O</i>	<i>O</i>	<i>O</i>	<i>O</i>	<i>O</i>
Si FORMULA	5,30	5,25	5,90	5,88	5,88	5,90	8,03	7,97	5,89	5,87	5,87
Ti FORMULA	0,23	0,26	0,01	0,01	0,01	0,01	0,00	0,00	0,01	0,01	0,01
Al FORMULA	3,53	3,50	4,08	4,10	4,11	4,08	4,03	4,10	4,13	4,12	4,12
Fe FORMULA	2,10	2,18	3,94	3,96	4,17	4,12	0,02	0,01	4,11	4,22	4,21
Mn FORMULA	0,00	0,00	0,38	0,34	0,04	0,05	0,00	0,00	0,08	0,05	0,02
Mg FORMULA	2,59	2,62	0,50	0,54	0,86	0,84	0,00	0,00	0,76	0,75	0,81
Ca FORMULA	0,00	0,00	1,22	1,23	0,99	1,05	0,85	0,89	1,06	1,04	1,02
Na FORMULA	0,04	0,04	0,01	0,01	0,01	0,00	2,01	2,00	0,01	0,01	0,00
K FORMULA	1,83	1,75	0,00	0,00	0,00	0,00	0,01	0,01	0,00	0,00	0,00
F FORMULA	0,19	0,17	0,00	0,00	0,01	0,03	0,04	0,04	0,00	0,00	0,05
Cr FORMULA	0,00	0,00	0,00	0,00	0,00	0,00	0,00	0,00	0,00	0,00	0,00
Cl FORMULA	0,00	0,00	0,00	0,00	0,00	0,00	0,00	0,00	0,00	0,00	0,00
O FORMULA	24,00	24,00	24,00	24,00	24,00	24,00	24,00	24,00	24,00	24,00	24,00
H FORMULA	4,02	4,06	0,00	0,00	0,00	0,00	0,00	0,00	0,00	0,00	0,00
X-POS	-1,24	-1,21	0,01	0,01	0,01	0,01	0,01	0,01	0,00	0,00	0,00
Y-POS	7,93	7,93	8,99	8,89	9,93	9,91	9,92	9,97	8,76	8,92	8,39

SAMPLE	<i>15-S1_A6_plg</i>	<i>15-S1_A6_plg</i>	<i>15-S1_A6_bt</i>	<i>15-S1_A6_bt</i>	<i>15-S1_A6_bt</i>	<i>15-S1_A7_musc</i>	<i>15-S1_A7_musc</i>	<i>15-S2_A1_grt</i>	<i>15-S2_A2_musc</i>	<i>15-S2_A2_musc</i>	<i>15-S2_A2_musc</i>
SiO ₂ WT%	58,29	58,06	35,01	34,20	34,62	43,53	43,93	36,39	43,12	42,96	42,08
TiO ₂ WT%	0,00	0,00	2,06	1,81	2,25	0,30	0,51	0,07	0,27	0,42	0,52
Al ₂ O ₃ WT%	25,79	25,89	19,73	20,18	20,03	36,70	35,43	21,98	36,63	36,68	36,31
FeO WT%	0,23	0,07	16,42	16,19	16,62	1,82	1,85	30,77	1,66	1,90	1,76
MnO WT%	0,00	0,00	0,02	0,04	0,00	0,00	0,00	0,42	0,00	0,00	0,00
MgO WT%	0,00	0,01	11,93	11,75	11,61	0,80	1,04	3,47	0,63	0,72	0,64
CaO WT%	6,30	6,28	0,04	0,05	0,02	0,00	0,01	5,78	0,02	0,02	0,02
Na ₂ O WT%	7,45	7,43	0,14	0,17	0,12	0,76	0,63	0,04	0,85	0,80	0,74
K ₂ O WT%	0,08	0,09	9,40	9,38	9,48	10,17	10,21	0,02	9,96	10,06	9,88
F WT%	0,09	0,08	0,33	0,35	0,35	0,11	0,13	0,03	0,12	0,12	0,13
Cr ₂ O ₃ WT%	0,01	0,00	0,05	0,06	0,07	0,04	0,03	0,02	0,01	0,03	0,03
Cl WT%	0,00	0,00	0,00	0,01	0,01	0,00	0,00	0,00	0,00	0,00	0,00
O WT%	0,00	0,00	0,00	0,00	0,00	0,00	0,00	0,00	0,00	0,00	0,00
H ₂ O WT%	0,00	0,00	4,02	4,02	4,01	4,50	4,50	0,00	4,51	4,49	4,50
Total	98,19	97,87	99,14	98,20	99,18	98,71	98,25	99,00	97,76	98,21	96,61
O≡Cl,F			0,17	0,18	0,18	0,06	0,07		0,06	0,06	0,07
TOTAL			98,97	98,02	99,00	98,65	98,18		97,70	98,14	96,54
FORMULA	24,00	24,00	24,00	24,00	24,00	24,00	24,00	24,00	24,00	24,00	24,00
BASIS	<i>O</i>	<i>O</i>	<i>O</i>	<i>O</i>	<i>O</i>	<i>O</i>	<i>O</i>	<i>O</i>	<i>O</i>	<i>O</i>	<i>O</i>
Si FORMULA	7,93	7,92	5,28	5,21	5,23	5,89	5,97	5,85	5,88	5,85	5,82
Ti FORMULA	0,00	0,00	0,23	0,21	0,26	0,03	0,05	0,01	0,03	0,04	0,05
Al FORMULA	4,14	4,16	3,51	3,62	3,57	5,85	5,68	4,16	5,89	5,89	5,91
Fe FORMULA	0,03	0,01	2,07	2,06	2,10	0,21	0,21	4,14	0,19	0,22	0,20
Mn FORMULA	0,00	0,00	0,00	0,00	0,00	0,00	0,00	0,06	0,00	0,00	0,00
Mg FORMULA	0,00	0,00	2,68	2,67	2,62	0,16	0,21	0,83	0,13	0,15	0,13
Ca FORMULA	0,92	0,92	0,01	0,01	0,00	0,00	0,00	1,00	0,00	0,00	0,00
Na FORMULA	1,96	1,96	0,04	0,05	0,03	0,20	0,17	0,01	0,22	0,21	0,20
K FORMULA	0,01	0,02	1,81	1,82	1,83	1,75	1,77	0,00	1,73	1,75	1,74
F FORMULA	0,04	0,04	0,16	0,17	0,17	0,05	0,06	0,02	0,05	0,05	0,06
Cr FORMULA	0,00	0,00	0,01	0,01	0,01	0,00	0,00	0,00	0,00	0,00	0,00
Cl FORMULA	0,00	0,00	0,00	0,00	0,00	0,00	0,00	0,00	0,00	0,00	0,00
O FORMULA	24,00	24,00	24,00	24,00	24,00	24,00	24,00	24,00	24,00	24,00	24,00
H FORMULA	0,00	0,00	4,04	4,08	4,04	4,06	4,08	0,00	4,10	4,08	4,15
X-POS	0,00	0,00	0,00	0,00	0,00	0,64	0,54	-10,87	-10,85	-10,86	-10,89
Y-POS	8,73	8,67	8,49	8,48	8,33	9,66	9,57	13,39	11,33	11,37	11,34

SAMPLE	<i>15-S2_A3_grt</i>	<i>15-S2_A3_bt</i>	14-S2-A4_grt redo	14-S2-A7_plg top-to-bottom	14-S2-A7_plg top-to-bottom	15-S1_A1_musc	15-S1_A2_grt lower	15-S1_A2_grt upper	15-S1_A2_grt left	15-S1_A2_plg left	15-S1_A2_plg
SiO2 WT%	36,62	34,50	37,90	62,99	61,72	45,61	37,63	37,73	37,37	58,98	59,47
TiO2 WT%	0,04	1,18	0,05	0,00	0,00	0,93	0,09	0,05	0,09	0,00	0,01
Al2O3 WT%	22,06	20,43	22,01	24,34	24,56	35,83	22,13	21,84	21,96	26,22	25,41
FeO WT%	30,42	16,02	31,68	0,05	0,01	2,49	30,92	30,03	31,25	0,15	0,15
MnO WT%	1,49	0,05	1,05	0,00	0,00	0,01	0,93	1,28	1,02	0,02	0,01
MgO WT%	2,83	12,37	2,49	0,00	0,00	1,05	3,25	2,87	3,10	0,00	0,00
CaO WT%	6,26	0,05	6,25	5,15	5,32	0,02	6,05	6,80	5,78	7,17	6,79
Na2O WT%	0,02	0,14	0,03	8,85	8,70	0,59	0,05	0,01	0,01	7,65	7,69
K2O WT%	0,01	9,27	0,00	0,09	0,07	10,48	0,01	0,00	0,01	0,06	0,04
F WT%	0,00	0,41	0,02	0,09	0,08	0,13	0,00	0,02	0,01	0,12	0,08
Cr2O3 WT%	0,00	0,03	0,01	0,00	0,00	0,01	0,02	0,00	0,00	0,00	0,00
Cl WT%	0,01	0,01	0,00	0,00	0,00	0,00	0,00	0,01	0,00	0,00	0,00
O WT%	0,00	0,00	0,00	0,00	0,00	0,00	0,00	0,00	0,00	0,00	0,00
H2O WT%	0,00	4,03	0,00	0,00	0,00	4,48	0,00	0,00	0,00	0,00	0,00
Total	99,73	98,49	101,48	101,53	100,44	101,62	101,07	100,63	100,60	100,38	99,62
O≡Cl,F		0,21				0,07					
TOTAL		98,28				101,55					
FORMULA	24,00	24,00	24,00	24,00	24,00	24,00	24,00	24,00	24,00	24,00	24,00
BASIS	<i>O</i>	<i>O</i>	O	O	O	O	O	O	O	O	O
Si FORMULA	5,86	5,23	5,96	8,25	8,18	6,02	5,92	5,96	5,92	7,88	7,99
Ti FORMULA	0,00	0,13	0,01	0,00	0,00	0,09	0,01	0,01	0,01	0,00	0,00
Al FORMULA	4,16	3,65	4,08	3,76	3,84	5,57	4,10	4,07	4,10	4,13	4,02
Fe FORMULA	4,07	2,03	4,17	0,01	0,00	0,27	4,07	3,97	4,14	0,02	0,02
Mn FORMULA	0,20	0,01	0,14	0,00	0,00	0,00	0,12	0,17	0,14	0,00	0,00
Mg FORMULA	0,67	2,80	0,58	0,00	0,00	0,21	0,76	0,68	0,73	0,00	0,00
Ca FORMULA	1,07	0,01	1,05	0,72	0,76	0,00	1,02	1,15	0,98	1,03	0,98
Na FORMULA	0,01	0,04	0,01	2,25	2,24	0,15	0,01	0,00	0,00	1,98	2,00
K FORMULA	0,00	1,79	0,00	0,02	0,01	1,76	0,00	0,00	0,00	0,01	0,01
F FORMULA	0,00	0,19	0,01	0,04	0,03	0,05	0,00	0,01	0,00	0,05	0,03
Cr FORMULA	0,00	0,00	0,00	0,00	0,00	0,00	0,00	0,00	0,00	0,00	0,00
Cl FORMULA	0,00	0,00	0,00	0,00	0,00	0,00	0,00	0,00	0,00	0,00	0,00
O FORMULA	24,00	24,00	24,00	24,00	24,00	24,00	24,00	24,00	24,00	24,00	24,00
H FORMULA	0,00	4,07	0,00	0,00	0,00	3,94	0,00	0,00	0,00	0,00	0,00
X-POS	-10,47	-10,51	38,00	35,92	36,36	-2,10	-2,03	-1,88	-1,91	-1,98	-2,07
Y-POS	11,71	11,64	5,19	5,78	5,87	8,61	9,20	9,19	9,53	9,68	9,29

SAMPLE	15-S1_A2_bt	15-S1_A2_bt upper	14-S2-A4_grt redo	14-S2-A4_grt redo	14-S2-A4_grt redo	15-S1_A3_bt	15-S1_A3_bt	15-S1_A4_grt	15-S1_A4_grt	15-S1_A5_grt	15-S1_A5_grt
SiO2 WT%	36,10	36,23	37,32	37,27	37,61	36,04	36,38	37,01	37,37	37,51	37,45
TiO2 WT%	2,07	1,92	0,09	0,08	0,10	2,16	1,81	0,12	0,07	0,08	0,04
Al2O3 WT%	18,98	19,08	21,69	21,82	21,61	19,65	19,77	21,36	21,44	21,59	21,63
FeO WT%	16,84	15,76	31,73	31,21	32,03	16,51	16,32	29,18	29,92	31,00	31,09
MnO WT%	0,01	0,01	1,10	1,20	1,01	0,00	0,02	2,47	1,66	0,25	0,22
MgO WT%	11,43	11,37	2,44	2,46	2,48	11,13	11,38	2,21	2,58	3,57	3,66
CaO WT%	0,03	0,06	6,21	6,37	6,09	0,01	0,03	7,18	6,71	5,92	5,89
Na2O WT%	0,12	0,11	0,02	0,02	0,03	0,16	0,18	0,04	0,00	0,03	0,02
K2O WT%	9,72	9,32	0,00	0,00	0,00	9,68	9,67	0,00	0,00	0,01	0,00
F WT%	0,41	0,39	0,00	0,01	0,04	0,38	0,39	0,00	0,00	0,02	0,05
Cr2O3 WT%	0,00	0,01	0,02	0,01	0,00	0,02	0,03	0,02	0,02	0,03	0,02
Cl WT%	0,02	0,01	0,00	0,00	0,01	0,01	0,00	0,00	0,00	0,00	0,00
O WT%	0,00	0,00	0,00	0,00	0,00	0,00	0,00	0,00	0,00	0,00	0,00
H2O WT%	4,01	4,04	0,00	0,00	0,00	4,02	4,03	0,00	0,00	0,00	0,00
Total	99,73	98,32	100,62	100,45	101,01	99,77	100,01	99,51	99,75	100,02	100,08
O≡Cl,F	0,22	0,21				0,20	0,20				
TOTAL	99,52	98,11				99,57	99,80				
FORMULA	24,00	24,00	24,00	24,00	24,00	24,00	24,00	24,00	24,00	24,00	24,00
BASIS	O	O	O	O	O	O	O	O	O	O	O
Si FORMULA	5,42	5,47	5,93	5,93	5,96	5,40	5,43	5,94	5,97	5,95	5,94
Ti FORMULA	0,23	0,22	0,01	0,01	0,01	0,24	0,20	0,01	0,01	0,01	0,00
Al FORMULA	3,36	3,40	4,07	4,09	4,04	3,47	3,48	4,04	4,04	4,04	4,05
Fe FORMULA	2,12	1,99	4,22	4,15	4,24	2,07	2,04	3,92	4,00	4,12	4,13
Mn FORMULA	0,00	0,00	0,15	0,16	0,14	0,00	0,00	0,34	0,23	0,03	0,03
Mg FORMULA	2,56	2,56	0,58	0,58	0,59	2,49	2,53	0,53	0,61	0,85	0,87
Ca FORMULA	0,00	0,01	1,06	1,09	1,03	0,00	0,00	1,23	1,15	1,01	1,00
Na FORMULA	0,04	0,03	0,01	0,01	0,01	0,05	0,05	0,01	0,00	0,01	0,01
K FORMULA	1,86	1,80	0,00	0,00	0,00	1,85	1,84	0,00	0,00	0,00	0,00
F FORMULA	0,20	0,19	0,00	0,01	0,02	0,18	0,18	0,00	0,00	0,01	0,02
Cr FORMULA	0,00	0,00	0,00	0,00	0,00	0,00	0,00	0,00	0,00	0,00	0,00
Cl FORMULA	0,00	0,00	0,00	0,00	0,00	0,00	0,00	0,00	0,00	0,00	0,00
O FORMULA	24,00	24,00	24,00	24,00	24,00	24,00	24,00	24,00	24,00	24,00	24,00
H FORMULA	4,02	4,08	0,00	0,00	0,00	4,02	4,01	0,00	0,00	0,00	0,00
X-POS	-1,84	-1,80	38,01	38,06	37,99	-1,29	-1,30	0,01	0,00	0,01	0,01
Y-POS	9,85	9,84	5,17	5,20	5,17	8,03	8,05	9,00	8,90	10,01	10,02

SAMPLE	15-S1_A5_plg	15-S1_A5_plg	15-S1_A6_grt middle	15-S1_A6_grt left	15-S1_A6_grt right	15-S1_A6_plg	15-S1_A6_plg right	15-S1_A6_bt top_to_bottom	15-S1_A6_bt top_to_bottom	15-S1_A6_bt top_to_bottom	15-S1_A7_musc
SiO2 WT%	60,75	60,34	37,54	37,60	37,67	60,28	60,25	36,36	35,44	35,59	45,13
TiO2 WT%	0,00	0,02	0,07	0,08	0,09	0,00	0,01	2,14	1,84	2,31	0,27
Al2O3 WT%	24,34	24,55	21,69	21,68	21,50	24,85	24,78	18,87	19,33	18,70	36,07
FeO WT%	0,15	0,08	31,10	31,38	31,42	0,25	0,08	16,40	16,44	16,66	1,78
MnO WT%	0,00	0,00	0,52	0,31	0,15	0,01	0,00	0,03	0,01	0,01	0,01
MgO WT%	0,00	0,00	3,12	3,13	3,26	0,00	0,00	11,55	11,44	11,22	0,67
CaO WT%	5,85	6,02	6,17	6,22	6,10	6,37	6,36	0,07	0,05	0,07	0,01
Na2O WT%	8,25	8,16	0,03	0,03	0,03	7,95	7,85	0,16	0,19	0,14	0,86
K2O WT%	0,07	0,06	0,01	0,00	0,01	0,07	0,08	9,65	9,45	9,50	10,19
F WT%	0,11	0,09	0,01	0,11	0,07	0,10	0,09	0,42	0,37	0,33	0,15
Cr2O3 WT%	0,01	0,01	0,00	0,02	0,01	0,00	0,00	0,06	0,12	0,08	0,04
Cl WT%	0,00	0,01	0,00	0,00	0,00	0,00	0,00	0,01	0,00	0,01	0,00
O WT%	0,00	0,00	0,00	0,00	0,00	0,00	0,00	0,00	0,00	0,00	0,00
H2O WT%	0,00	0,00	0,00	0,00	0,00	0,00	0,00	4,02	4,02	4,01	4,50
Total	99,49	99,34	100,25	100,56	100,30	99,90	99,47	99,73	98,68	98,62	99,67
O≡Cl,F											
TOTAL											
FORMULA	24,00	24,00	24,00	24,00	24,00	24,00	24,00	24,00	24,00	24,00	24,00
BASIS	O	O	O	O	O	O	O	O	O	O	O
Si FORMULA	8,15	8,11	5,96	5,95	5,97	8,07	8,09	5,45	5,37	5,40	6,04
Ti FORMULA	0,00	0,00	0,01	0,01	0,01	0,00	0,00	0,24	0,21	0,26	0,03
Al FORMULA	3,85	3,89	4,06	4,05	4,02	3,92	3,92	3,33	3,45	3,35	5,69
Fe FORMULA	0,02	0,01	4,13	4,16	4,17	0,03	0,01	2,06	2,08	2,11	0,20
Mn FORMULA	0,00	0,00	0,07	0,04	0,02	0,00	0,00	0,00	0,00	0,00	0,00
Mg FORMULA	0,00	0,00	0,74	0,74	0,77	0,00	0,00	2,58	2,58	2,54	0,13
Ca FORMULA	0,84	0,87	1,05	1,06	1,04	0,91	0,91	0,01	0,01	0,01	0,00
Na FORMULA	2,15	2,13	0,01	0,01	0,01	2,06	2,04	0,05	0,05	0,04	0,22
K FORMULA	0,01	0,01	0,00	0,00	0,00	0,01	0,01	1,84	1,83	1,84	1,74
F FORMULA	0,05	0,04	0,01	0,06	0,03	0,04	0,04	0,20	0,18	0,16	0,06
Cr FORMULA	0,00	0,00	0,00	0,00	0,00	0,00	0,00	0,01	0,01	0,01	0,00
Cl FORMULA	0,00	0,00	0,00	0,00	0,00	0,00	0,00	0,00	0,00	0,00	0,00
O FORMULA	24,00	24,00	24,00	24,00	24,00	24,00	24,00	24,00	24,00	24,00	24,00
H FORMULA	0,00	0,00	0,00	0,00	0,00	0,00	0,00	4,02	4,06	4,06	4,02
X-POS	0,01	0,01	0,00	0,00	0,00	0,00	0,00	0,00	0,00	0,00	0,60
Y-POS	10,03	10,07	8,87	9,03	8,50	8,84	8,78	8,60	8,59	8,43	9,74

SAMPLE	15-S1_A7_musc	15-S2_A1_grt	15-S2_A1_musc	15-S2_A2_musc	15-S2_A2_musc	15-S2_A2_musc	15-S2_A3_grt	15-S2_A3_bt	15-S2_A4_grt	15-S2_A5_grt lower	15-S2_A5_grt upper
SiO2 WT%	46,20	37,09	45,80	44,35	45,50	44,38	37,63	35,45	37,21	37,00	37,09
TiO2 WT%	0,52	0,06	0,15	0,18	0,42	0,57	0,03	1,29	0,16	0,08	0,05
Al2O3 WT%	34,10	21,60	36,66	35,40	36,21	35,09	21,55	19,89	21,52	21,24	21,16
FeO WT%	1,88	30,40	1,98	1,69	1,84	1,85	30,36	16,09	27,97	30,79	30,75
MnO WT%	0,00	0,41	0,00	0,04	0,01	0,00	1,48	0,00	2,98	0,84	0,72
MgO WT%	1,08	3,47	0,83	0,68	0,65	0,70	2,84	12,24	1,83	3,15	3,29
CaO WT%	0,01	6,08	0,02	0,02	0,02	0,02	6,19	0,10	7,87	5,67	5,64
Na2O WT%	0,66	0,03	0,81	0,82	0,81	0,74	0,02	0,14	0,05	0,03	0,00
K2O WT%	10,40	0,02	10,25	10,09	9,96	10,24	0,01	9,06	0,00	0,01	0,01
F WT%	0,12	0,05	0,16	0,11	0,14	0,12	0,01	0,47	0,00	0,03	0,06
Cr2O3 WT%	0,02	0,00	0,03	0,01	0,04	0,02	0,00	0,01	0,01	0,01	0,02
Cl WT%	0,01	0,00	0,01	0,00	0,01	0,00	0,01	0,02	0,00	0,00	0,00
O WT%	0,00	0,00	0,00	0,00	0,00	0,00	0,00	0,00	0,00	0,00	0,00
H2O WT%	4,50	0,00	4,50	4,51	4,51	4,50	0,00	4,03	0,00	0,00	0,00
Total	99,50	99,21	101,18	97,89	100,12	98,23	100,13	98,79	99,49	98,85	98,80
O=Cl,F											
TOTAL											
FORMULA	24,00	24,00	24,00	24,00	24,00	24,00	24,00	24,00	24,00	24,00	24,00
BASIS	O	O	O	O	O	O	O	O	O	O	O
Si FORMULA	6,20	5,94	6,04	6,04	6,05	6,03	5,98	5,34	5,96	5,96	5,98
Ti FORMULA	0,05	0,01	0,01	0,02	0,04	0,06	0,00	0,15	0,02	0,01	0,01
Al FORMULA	5,39	4,07	5,70	5,68	5,68	5,62	4,04	3,53	4,06	4,03	4,02
Fe FORMULA	0,21	4,07	0,22	0,19	0,20	0,21	4,04	2,03	3,75	4,15	4,14
Mn FORMULA	0,00	0,06	0,00	0,00	0,00	0,00	0,20	0,00	0,40	0,11	0,10
Mg FORMULA	0,22	0,83	0,16	0,14	0,13	0,14	0,67	2,75	0,44	0,76	0,79
Ca FORMULA	0,00	1,04	0,00	0,00	0,00	0,00	1,05	0,02	1,35	0,98	0,97
Na FORMULA	0,17	0,01	0,21	0,22	0,21	0,20	0,01	0,04	0,01	0,01	0,00
K FORMULA	1,78	0,00	1,73	1,75	1,69	1,78	0,00	1,74	0,00	0,00	0,00
F FORMULA	0,05	0,03	0,07	0,05	0,06	0,05	0,00	0,23	0,00	0,02	0,03
Cr FORMULA	0,00	0,00	0,00	0,00	0,00	0,00	0,00	0,00	0,00	0,00	0,00
Cl FORMULA	0,00	0,00	0,00	0,00	0,00	0,00	0,00	0,00	0,00	0,00	0,00
O FORMULA	24,00	24,00	24,00	24,00	24,00	24,00	24,00	24,00	24,00	24,00	24,00
H FORMULA	4,03	0,00	3,96	4,09	4,00	4,08	0,00	4,06	0,00	0,00	0,00
X-POS	0,51	-10,93	-10,95	-10,90	-10,91	-10,94	-10,52	-10,55	-10,27	-10,10	-10,06
Y-POS	9,64	13,52	13,58	11,44	11,49	11,45	11,83	11,76	12,51	13,70	13,68

SAMPLE	15-S2_A5_bt lower	15-S2_A5_bt upper	15-S2_A5_plg	15-S2_A5_plg	15-S2_A5_plg	15-S2_A6_grt	15-S2_A6_bt left_to_right	15-S2_A6_bt left_to_right	15-S2_A6_bt left_to_right	15-S2_A6_bt right_of_last_bt	15-S2_A6_plg
SiO2 WT%	36,21	36,34	60,00	60,06	61,05	37,81	35,79	35,94	36,38	36,93	59,61
TiO2 WT%	1,66	1,48	0,03	0,00	0,01	0,05	1,19	2,03	2,32	2,24	0,00
Al2O3 WT%	19,39	18,92	25,34	25,20	24,36	21,69	19,60	19,10	18,88	18,70	25,04
FeO WT%	15,84	16,01	0,07	0,10	0,23	30,68	16,11	16,33	15,97	15,79	0,10
MnO WT%	0,02	0,02	0,00	0,00	0,01	0,40	0,02	0,01	0,02	0,02	0,00
MgO WT%	11,99	12,07	0,00	0,00	0,03	3,47	12,13	11,52	11,79	11,90	0,00
CaO WT%	0,01	0,01	6,58	6,59	5,73	6,02	0,05	0,04	0,02	0,02	6,83
Na2O WT%	0,17	0,16	7,83	7,75	8,18	0,00	0,16	0,12	0,13	0,15	7,63
K2O WT%	9,55	9,64	0,05	0,05	0,08	0,00	9,47	9,74	9,81	9,76	0,07
F WT%	0,38	0,34	0,09	0,09	0,06	0,04	0,37	0,38	0,37	0,46	0,09
Cr2O3 WT%	0,05	0,01	0,03	0,02	0,00	0,00	0,00	0,03	0,05	0,00	0,03
Cl WT%	0,00	0,01	0,00	0,01	0,01	0,00	0,01	0,00	0,01	0,02	0,00
O WT%	0,00	0,00	0,00	0,00	0,00	0,00	0,00	0,00	0,00	0,00	0,00
H2O WT%	4,04	4,03	0,00	0,00	0,00	0,00	4,03	4,02	4,03	4,03	0,00
Total	99,30	99,06	100,00	99,82	99,73	100,13	98,94	99,25	99,76	100,03	99,37
O≡Cl,F	0,20	0,18					0,20				
TOTAL	99,11	98,87					98,74				
FORMULA	24,00	24,00	24,00	24,00	24,00	24,00	24,00	24,00	24,00	24,00	24,00
BASIS	O	O	O	O	O	O	O	O	O	O	O
Si FORMULA	5,43	5,47	8,02	8,04	8,16	5,98	5,39	5,41	5,44	5,50	8,02
Ti FORMULA	0,19	0,17	0,00	0,00	0,00	0,01	0,14	0,23	0,26	0,25	0,00
Al FORMULA	3,43	3,35	3,99	3,97	3,84	4,05	3,48	3,39	3,33	3,28	3,97
Fe FORMULA	1,99	2,01	0,01	0,01	0,03	4,06	2,03	2,06	2,00	1,97	0,01
Mn FORMULA	0,00	0,00	0,00	0,00	0,00	0,05	0,00	0,00	0,00	0,00	0,00
Mg FORMULA	2,68	2,71	0,00	0,00	0,01	0,82	2,72	2,59	2,63	2,64	0,00
Ca FORMULA	0,00	0,00	0,94	0,95	0,82	1,02	0,01	0,01	0,00	0,00	0,99
Na FORMULA	0,05	0,05	2,03	2,01	2,12	0,00	0,05	0,03	0,04	0,04	1,99
K FORMULA	1,83	1,85	0,01	0,01	0,01	0,00	1,82	1,87	1,87	1,86	0,01
F FORMULA	0,18	0,16	0,04	0,04	0,02	0,02	0,18	0,18	0,18	0,22	0,04
Cr FORMULA	0,01	0,00	0,00	0,00	0,00	0,00	0,00	0,00	0,01	0,00	0,00
Cl FORMULA	0,00	0,00	0,00	0,00	0,00	0,00	0,00	0,00	0,00	0,00	0,00
O FORMULA	24,00	24,00	24,00	24,00	24,00	24,00	24,00	24,00	24,00	24,00	24,00
H FORMULA	4,04	4,05	0,00	0,00	0,00	0,00	4,05	4,04	4,02	4,01	0,00
X-POS	-10,04	-9,98	-10,15	-10,14	-10,11	-10,25	-10,27	-10,27	-10,20	-10,20	-10,05
Y-POS	13,72	13,72	13,73	13,74	13,74	11,76	11,71	11,54	11,51	11,52	11,63

SAMPLE	15-S2_A7_grt	15-S2_A7_grt	15-S2_A7_grt	15-S2_A8_musc	15-S2_A8_musc	15-S3_A1_plg	15-S3_A1_plg	15-S3_A1_bt	15-S3_A1_bt	15-S3_A2_grt	15-S3_A2_grt
	left_to_right										
SiO2 WT%	37,36	37,24	37,15	45,88	44,91	59,37	59,63	36,73	36,23	37,73	37,26
TiO2 WT%	0,06	0,07	0,08	0,52	0,35	0,00	0,01	2,09	2,00	0,04	0,10
Al2O3 WT%	21,16	21,16	21,31	34,20	35,71	25,09	25,23	19,31	19,35	21,98	21,50
FeO WT%	30,55	30,82	30,82	1,86	1,76	0,10	0,14	16,05	15,94	30,89	31,24
MnO WT%	0,94	0,92	0,93	0,00	0,00	0,02	0,00	0,00	0,03	1,13	0,46
MgO WT%	2,75	2,79	2,80	1,20	0,81	0,01	0,00	11,78	11,56	3,18	3,17
CaO WT%	6,33	6,20	6,40	0,00	0,02	6,61	6,53	0,07	0,05	5,57	6,05
Na2O WT%	0,02	0,02	0,03	0,65	0,77	7,70	7,58	0,19	0,16	0,01	0,01
K2O WT%	0,01	0,00	0,00	10,51	10,39	0,04	0,05	9,63	9,51	0,00	0,00
F WT%	0,00	0,02	0,01	0,15	0,18	0,06	0,10	0,41	0,40	0,00	0,02
Cr2O3 WT%	0,02	0,03	0,04	0,06	0,02	0,01	0,00	0,02	0,03	0,03	0,02
Cl WT%	0,00	0,00	0,00	0,00	0,00	0,01	0,00	0,01	0,01	0,00	0,01
O WT%	0,00	0,00	0,00	0,00	0,00	0,00	0,00	0,00	0,00	0,00	0,00
H2O WT%	0,00	0,00	0,00	4,50	4,50	0,00	0,00	4,03	4,03	0,00	0,00
Total	99,20	99,26	99,57	99,49	99,41	99,02	99,26	100,33	99,31	100,56	99,82
O≡Cl,F				0,08	0,10			0,22	0,21		
TOTAL				99,42	99,31			100,11	99,10		
FORMULA	24,00	24,00	24,00	24,00	24,00	24,00	24,00	24,00	24,00	24,00	24,00
BASIS	O	O	O	O	O	O	O	O	O	O	O
Si FORMULA	6,00	5,98	5,95	6,16	6,04	8,01	8,02	5,45	5,43	5,96	5,94
Ti FORMULA	0,01	0,01	0,01	0,05	0,04	0,00	0,00	0,23	0,23	0,01	0,01
Al FORMULA	4,00	4,01	4,02	5,41	5,66	3,99	4,00	3,38	3,42	4,09	4,04
Fe FORMULA	4,10	4,14	4,13	0,21	0,20	0,01	0,02	1,99	2,00	4,08	4,17
Mn FORMULA	0,13	0,13	0,13	0,00	0,00	0,00	0,00	0,00	0,00	0,15	0,06
Mg FORMULA	0,66	0,67	0,67	0,24	0,16	0,00	0,00	2,61	2,58	0,75	0,75
Ca FORMULA	1,09	1,07	1,10	0,00	0,00	0,96	0,94	0,01	0,01	0,94	1,03
Na FORMULA	0,01	0,01	0,01	0,17	0,20	2,02	1,98	0,06	0,05	0,00	0,00
K FORMULA	0,00	0,00	0,00	1,80	1,78	0,01	0,01	1,82	1,82	0,00	0,00
F FORMULA	0,00	0,01	0,01	0,06	0,08	0,02	0,04	0,19	0,19	0,00	0,01
Cr FORMULA	0,00	0,00	0,01	0,01	0,00	0,00	0,00	0,00	0,00	0,00	0,00
Cl FORMULA	0,00	0,00	0,00	0,00	0,00	0,00	0,00	0,00	0,00	0,00	0,00
O FORMULA	24,00	24,00	24,00	24,00	24,00	24,00	24,00	24,00	24,00	24,00	24,00
H FORMULA	0,00	0,00	0,00	4,03	4,03	0,00	0,00	3,99	4,04	0,00	0,00
X-POS	-9,65	-9,66	-9,68	-9,06	-8,80	-7,04	-7,04	-7,00	-7,01	-7,26	-7,06
Y-POS	12,80	12,83	12,86	13,81	13,65	30,40	30,39	30,27	30,24	29,10	29,04

SAMPLE	15-S3_A2_grt left_to_right	15-S3_A2_bt middle	15-S3_A2_bt lower	15-S3_A1_plg	15-S3_A1_plg	15-S3_A1_bt	15-S3_A1_bt	15-S3_A2_grt	15-S3_A2_grt	15-S3_A2_grt	15-S3_A2_bt
SiO2 WT%	37,58	36,17	35,55	60,40	59,76	36,31	37,06	38,07	37,56	37,76	37,41
TiO2 WT%	0,06	2,23	2,14	0,00	0,02	2,31	1,98	0,08	0,08	0,11	2,17
Al2O3 WT%	21,97	19,38	19,44	25,38	25,32	18,79	19,39	21,47	21,29	21,57	19,52
FeO WT%	30,88	16,71	16,89	0,07	0,12	16,45	16,01	31,53	31,76	31,35	15,96
MnO WT%	0,47	0,02	0,03	0,00	0,01	0,03	0,02	0,79	0,41	0,46	0,04
MgO WT%	3,39	11,65	11,62	0,01	0,00	11,73	11,80	3,36	3,26	3,45	11,00
CaO WT%	6,16	0,05	0,03	6,92	6,69	0,02	0,07	5,91	6,10	6,07	0,39
Na2O WT%	0,01	0,09	0,06	7,86	8,05	0,14	0,17	0,03	0,01	0,02	0,47
K2O WT%	0,01	9,59	9,65	0,06	0,04	9,48	9,43	0,00	0,00	0,01	9,28
F WT%	0,05	0,29	0,39	0,11	0,09	0,35	0,43	0,00	0,05	0,03	0,35
Cr2O3 WT%	0,04	0,07	0,05	0,01	0,00	0,05	0,02	0,03	0,03	0,01	0,06
Cl WT%	0,00	0,01	0,01	0,00	0,00	0,01	0,01	0,00	0,00	0,00	0,01
O WT%	0,00	0,00	0,00	0,00	0,00	0,00	0,00	0,00	0,00	0,00	0,00
H2O WT%	0,00	4,02	4,01	0,00	0,00	4,02	4,04	0,00	0,00	0,00	4,05
Total	100,61	100,29	99,86	100,81	100,09	99,71	100,45	101,26	100,56	100,83	100,73
O≡Cl,F		0,15	0,20			0,19	0,22				0,18
TOTAL		100,13	99,66			99,53	100,23				100,54
FORMULA	24,00	24,00	24,00	24	24	24	24	24	24	24	24
BASIS	O	O	O	O	O	O	O	O	O	O	O
Si FORMULA	5,93	5,39	5,34	8,02	8,00	5,44	5,48	5,99	5,96	5,96	5,52
Ti FORMULA	0,01	0,25	0,24	0,00	0,00	0,26	0,22	0,01	0,01	0,01	0,24
Al FORMULA	4,09	3,40	3,44	3,97	3,99	3,32	3,38	3,98	3,98	4,01	3,39
Fe FORMULA	4,08	2,08	2,12	0,01	0,01	2,06	1,98	4,15	4,21	4,14	1,97
Mn FORMULA	0,06	0,00	0,00	0,00	0,00	0,00	0,00	0,10	0,05	0,06	0,01
Mg FORMULA	0,80	2,59	2,60	0,00	0,00	2,62	2,60	0,79	0,77	0,81	2,42
Ca FORMULA	1,04	0,01	0,00	0,98	0,96	0,00	0,01	1,00	1,04	1,03	0,06
Na FORMULA	0,00	0,03	0,02	2,02	2,09	0,04	0,05	0,01	0,00	0,01	0,14
K FORMULA	0,00	1,82	1,85	0,01	0,01	1,81	1,78	0,00	0,00	0,00	1,75
F FORMULA	0,02	0,14	0,18	0,04	0,04	0,17	0,20	0,00	0,02	0,02	0,16
Cr FORMULA	0,00	0,01	0,01	0,00	0,00	0,01	0,00	0,00	0,00	0,00	0,01
Cl FORMULA	0,00	0,00	0,00	0,00	0,00	0,00	0,00	0,00	0,00	0,00	0,00
O FORMULA	24,00	24,00	24,00	24,00	24,00	24,00	24,00	24,00	24,00	24,00	24,00
H FORMULA	0,00	4,00	4,01	0,00	0,00	4,02	3,99	0,00	0,00	0,00	3,98
X-POS	-7,14	-7,20	-7,25	-7,28	-7,14	-7,21	-7,12	-7,36	-7,16	-7,24	-7,30
Y-POS	28,84	28,86	28,83	30,32	30,35	30,31	30,22	29,05	28,99	28,78	28,83

SAMPLE	15-S3_A2_bt	15-S3_A2_bt	15-S3_A2_plg	15-S3_A2_plg	15-S3_A3_grt rim-to-core						
SiO2 WT%	36,02	36,15	60,08	58,54	37,53	37,67	37,74	37,98	37,98	37,71	37,89
TiO2 WT%	2,13	1,99	0,00	0,00	0,09	0,13	0,10	0,09	0,13	0,09	0,07
Al2O3 WT%	19,74	19,54	25,63	26,77	21,19	21,31	21,24	21,34	21,34	21,40	21,36
FeO WT%	17,17	16,74	0,20	0,20	31,04	30,47	30,79	29,36	29,09	28,91	29,09
MnO WT%	0,04	0,03	0,00	0,00	0,49	0,87	1,43	1,75	1,94	2,03	2,20
MgO WT%	11,37	11,70	0,00	0,00	3,39	3,05	2,93	2,57	2,38	2,33	2,28
CaO WT%	0,16	0,03	6,82	8,23	6,34	6,91	6,28	7,62	8,08	8,06	7,74
Na2O WT%	0,16	0,09	8,01	7,30	0,02	0,02	0,01	0,02	0,02	0,00	0,00
K2O WT%	9,14	9,77	0,04	0,04	0,02	0,00	0,00	0,00	0,00	0,01	0,00
F WT%	0,34	0,33	0,04	0,10	0,02	0,01	0,00	0,00	0,00	0,00	0,00
Cr2O3 WT%	0,05	0,04	0,00	0,00	0,02	0,00	0,01	0,00	0,01	0,03	0,00
Cl WT%	0,01	0,01	0,00	0,00	0,00	0,00	0,00	0,01	0,00	0,00	0,00
O WT%	0,00	0,00	0,00	0,00	0,00	0,00	0,00	0,00	0,00	0,00	0,00
H2O WT%	4,02	4,02	0,00	0,00	0,00	0,00	0,00	0,00	0,00	0,00	0,00
Total	100,35	100,42	100,84	101,19	100,16	100,44	100,49	100,69	100,86	100,51	100,62
O≡Cl,F	0,18	0,17									
TOTAL	100,17	100,25									
FORMULA	24	24	24	24	24	24	24	24	24	24	24
BASIS	O	O	O	O	O	O	O	O	O	O	O
Si FORMULA	5,37	5,39	7,98	7,78	5,97	5,97	5,99	6,00	5,99	5,98	6,00
Ti FORMULA	0,24	0,22	0,00	0,00	0,01	0,02	0,01	0,01	0,02	0,01	0,01
Al FORMULA	3,47	3,43	4,01	4,19	3,97	3,98	3,97	3,98	3,97	4,00	3,99
Fe FORMULA	2,14	2,09	0,02	0,02	4,13	4,04	4,09	3,88	3,84	3,83	3,85
Mn FORMULA	0,00	0,00	0,00	0,00	0,07	0,12	0,19	0,23	0,26	0,27	0,30
Mg FORMULA	2,53	2,60	0,00	0,00	0,80	0,72	0,69	0,60	0,56	0,55	0,54
Ca FORMULA	0,03	0,00	0,97	1,17	1,08	1,17	1,07	1,29	1,37	1,37	1,31
Na FORMULA	0,05	0,02	2,06	1,88	0,01	0,01	0,00	0,01	0,01	0,00	0,00
K FORMULA	1,74	1,86	0,01	0,01	0,00	0,00	0,00	0,00	0,00	0,00	0,00
F FORMULA	0,16	0,15	0,02	0,04	0,01	0,01	0,00	0,00	0,00	0,00	0,00
Cr FORMULA	0,01	0,00	0,00	0,00	0,00	0,00	0,00	0,00	0,00	0,00	0,00
Cl FORMULA	0,00	0,00	0,00	0,00	0,00	0,00	0,00	0,00	0,00	0,00	0,00
O FORMULA	24,00	24,00	24,00	24,00	24,00	24,00	24,00	24,00	24,00	24,00	24,00
H FORMULA	3,99	3,99	0,00	0,00	0,00	0,00	0,00	0,00	0,00	0,00	0,00
X-POS	-7,32	-7,37	-7,40	-7,41	-6,60	-6,57	-6,54	-6,53	-6,52	-6,51	-6,49
Y-POS	28,83	28,81	29,03	29,09	30,45	30,34	30,19	30,16	30,14	30,12	30,09

SAMPLE	15-S3_A3_grt rim-to-core	15-S3_A3_grt rim-to-core	15-S3_A3_grt rim-to-core	15-S3_A3_grt rim-to-core	15-S3_A3_grt rim-to-core	15-S3_A3_bt rim-to-core	15-S3_A3_bt rim-to-core	15-S3_A3_bt rim-to-core	15-S3_A3_bt rim-to-core	15-S3_A3_bt rim-to-core
SiO2 WT%	37,67	37,87	37,52	37,48	37,75	36,10	36,27	35,99	36,17	36,25
TiO2 WT%	0,16	0,15	0,11	0,14	0,17	1,56	1,62	1,87	1,89	1,96
Al2O3 WT%	21,24	21,30	21,29	21,06	21,19	19,64	19,39	19,34	19,32	19,29
FeO WT%	29,48	29,23	29,10	28,66	29,35	16,31	16,07	16,40	16,35	16,40
MnO WT%	2,56	2,99	3,14	3,37	2,88	0,04	0,05	0,00	0,04	0,02
MgO WT%	2,20	2,03	1,98	1,83	1,94	12,00	12,22	12,02	11,82	11,96
CaO WT%	7,53	7,58	7,63	7,92	7,54	0,03	0,01	0,00	0,03	0,00
Na2O WT%	0,05	0,04	0,03	0,01	0,01	0,13	0,13	0,13	0,15	0,17
K2O WT%	0,00	0,01	0,00	0,01	0,01	9,69	9,57	9,68	9,59	9,68
F WT%	0,00	0,00	0,00	0,00	0,00	0,36	0,37	0,34	0,38	0,42
Cr2O3 WT%	0,04	0,02	0,04	0,00	0,01	0,04	0,00	0,01	0,02	0,01
Cl WT%	0,00	0,01	0,00	0,00	0,00	0,01	0,00	0,01	0,00	0,00
O WT%	0,00	0,00	0,00	0,00	0,00	0,00	0,00	0,00	0,00	0,00
H2O WT%	0,00	0,00	0,00	0,00	0,00	4,02	4,03	4,02	4,02	4,03
Total	100,84	101,16	100,76	100,37	100,73	99,92	99,74	99,80	99,79	100,18
O=Cl,F						0,19	0,20	0,18	0,20	0,22
TOTAL						99,73	99,55	99,62	99,59	99,96
FORMULA	24	24	24	24	24	24	24	24	24	24
BASIS	O	O	O	O	O	O	O	O	O	O
Si FORMULA	5,97	5,99	5,96	5,98	5,99	5,39	5,42	5,39	5,41	5,41
Ti FORMULA	0,02	0,02	0,01	0,02	0,02	0,18	0,18	0,21	0,21	0,22
Al FORMULA	3,97	3,97	3,99	3,96	3,96	3,46	3,41	3,41	3,41	3,39
Fe FORMULA	3,91	3,86	3,87	3,82	3,90	2,04	2,01	2,05	2,05	2,05
Mn FORMULA	0,34	0,40	0,42	0,45	0,39	0,01	0,01	0,00	0,00	0,00
Mg FORMULA	0,52	0,48	0,47	0,44	0,46	2,67	2,72	2,68	2,64	2,66
Ca FORMULA	1,28	1,28	1,30	1,35	1,28	0,00	0,00	0,00	0,00	0,00
Na FORMULA	0,02	0,01	0,01	0,00	0,00	0,04	0,04	0,04	0,04	0,04
K FORMULA	0,00	0,00	0,00	0,00	0,00	1,85	1,82	1,85	1,83	1,84
F FORMULA	0,00	0,00	0,00	0,00	0,00	0,17	0,18	0,16	0,18	0,20
Cr FORMULA	0,01	0,00	0,00	0,00	0,00	0,00	0,00	0,00	0,00	0,00
Cl FORMULA	0,00	0,00	0,00	0,00	0,00	0,00	0,00	0,00	0,00	0,00
O FORMULA	24,00	24,00	24,00	24,00	24,00	24,00	24,00	24,00	24,00	24,00
H FORMULA	0,00	0,00	0,00	0,00	0,00	4,01	4,02	4,02	4,02	4,01
X-POS	-6,47	-6,45	-6,45	-6,45	-6,49	-6,61	-6,61	-6,64	-6,65	-6,64
Y-POS	29,99	29,95	29,92	29,73	29,52	30,49	30,51	30,55	30,57	30,59

SAMPLE	15-S3_A3_bt rim-to-core	15-S3_A3_bt rim-to-core	15-S3_A4_grt rim-to-core	15-S3_A4_grt rim-to-core	15-S3_A4_grt rim-to-core	15-S3_A4_grt rim-to-core	15-S3_A4_grt rim-to-core	15-S3_A4_plg rim-to-core	15-S3_A4_plg rim-to-core	15-S3_A4_plg rim-to-core	15-S3_A5_grt
SiO2 WT%	36,46	36,65	37,32	37,58	37,99	37,61	37,70	60,00	59,52	59,31	37,72
TiO2 WT%	2,06	2,05	0,05	0,08	0,07	0,07	0,08	0,00	0,00	0,00	0,08
Al2O3 WT%	19,04	18,96	21,23	21,40	21,43	21,34	21,14	25,11	25,36	25,45	21,16
FeO WT%	16,21	16,16	30,80	30,60	30,14	29,93	29,86	0,12	0,04	0,05	30,58
MnO WT%	0,04	0,03	1,03	1,24	1,66	1,82	1,92	0,01	0,00	0,00	1,19
MgO WT%	11,97	11,99	3,23	2,98	2,62	2,61	2,50	0,01	0,00	0,00	2,92
CaO WT%	0,02	0,01	5,94	6,63	7,21	7,26	7,27	6,71	6,93	6,87	6,56
Na2O WT%	0,16	0,16	0,01	0,04	0,01	0,01	0,02	7,83	7,76	7,76	0,01
K2O WT%	9,56	9,65	0,00	0,00	0,01	0,00	0,00	0,05	0,06	0,06	0,01
F WT%	0,35	0,40	0,00	0,00	0,00	0,00	0,00	0,11	0,10	0,11	0,00
Cr2O3 WT%	0,03	0,02	0,01	0,01	0,01	0,00	0,03	0,00	0,00	0,00	0,00
Cl WT%	0,00	0,00	0,00	0,01	0,00	0,00	0,01	0,00	0,00	0,00	0,00
O WT%	0,00	0,00	0,00	0,00	0,00	0,00	0,00	0,00	0,00	0,00	0,00
H2O WT%	4,03	4,03	0,00	0,00	0,00	0,00	0,00	0,00	0,00	0,00	0,00
Total	99,93	100,10	99,61	100,51	101,08	100,61	100,48	99,93	99,73	99,59	100,19
O≡Cl,F	0,18	0,21									
TOTAL	99,75	99,89									
FORMULA	24	24	24	24	24	24	24	24	24	24	24
BASIS	O	O	O	O	O	O	O	O	O	O	O
Si FORMULA	5,44	5,46	5,97	5,96	5,99	5,97	5,99	8,03	7,99	7,97	6,00
Ti FORMULA	0,23	0,23	0,01	0,01	0,01	0,01	0,01	0,00	0,00	0,00	0,01
Al FORMULA	3,35	3,33	4,00	4,00	3,98	3,99	3,96	3,96	4,01	4,03	3,97
Fe FORMULA	2,02	2,01	4,12	4,06	3,97	3,97	3,97	0,01	0,00	0,01	4,07
Mn FORMULA	0,01	0,00	0,14	0,17	0,22	0,24	0,26	0,00	0,00	0,00	0,16
Mg FORMULA	2,66	2,66	0,77	0,71	0,61	0,62	0,59	0,00	0,00	0,00	0,69
Ca FORMULA	0,00	0,00	1,02	1,13	1,22	1,23	1,24	0,96	1,00	0,99	1,12
Na FORMULA	0,05	0,05	0,00	0,01	0,00	0,00	0,01	2,03	2,02	2,02	0,00
K FORMULA	1,82	1,83	0,00	0,00	0,00	0,00	0,00	0,01	0,01	0,01	0,00
F FORMULA	0,16	0,19	0,00	0,00	0,00	0,00	0,00	0,05	0,04	0,05	0,00
Cr FORMULA	0,00	0,00	0,00	0,00	0,00	0,00	0,00	0,00	0,00	0,00	0,00
Cl FORMULA	0,00	0,00	0,00	0,00	0,00	0,00	0,00	0,00	0,00	0,00	0,00
O FORMULA	24,00	24,00	24,00	24,00	24,00	24,00	24,00	24,00	24,00	24,00	24,00
H FORMULA	4,01	4,00	0,00	0,00	0,00	0,00	0,00	0,00	0,00	0,00	0,00
X-POS	-6,64	-6,64	-6,12	-6,14	-6,16	-6,16	-6,14	-6,11	-6,09	-6,08	-5,42
Y-POS	30,65	30,66	30,54	30,51	30,45	30,41	30,38	30,61	30,67	30,69	29,79

SAMPLE	15-S3_A5_grt	15-S3_A5_bt	15-S3_A5_bt	15-S3_A5_plg	15-S3_A5_plg	15-S4_A1_grt lower	15-S4_A1_grt middle	15-S4_A1_grt upper	15-S4_A1_bt middle	15-S4_A1_bt lower	15-S4_A1_bt upper
SiO2 WT%	37,76	35,47	36,35	59,40	62,95	37,95	37,68	37,98	36,05	36,13	36,38
TiO2 WT%	0,10	1,83	1,89	0,00	0,00	0,05	0,06	0,04	2,06	2,08	2,04
Al2O3 WT%	21,24	18,59	19,13	25,11	23,39	21,34	21,53	21,55	19,28	19,26	19,15
FeO WT%	30,78	16,33	16,37	0,15	0,03	31,30	31,10	31,65	16,63	16,50	16,44
MnO WT%	0,87	0,04	0,04	0,01	0,02	0,11	0,10	0,09	0,04	0,02	0,02
MgO WT%	3,04	12,00	12,32	0,01	0,02	3,80	3,78	3,71	12,03	12,05	12,16
CaO WT%	6,40	0,04	0,02	6,81	4,32	5,92	6,11	5,96	0,02	0,00	0,01
Na2O WT%	0,01	0,12	0,10	7,93	9,27	0,03	0,02	0,02	0,12	0,12	0,12
K2O WT%	0,00	9,49	9,51	0,06	0,11	0,00	0,00	0,00	9,62	9,60	9,55
F WT%	0,01	0,41	0,41	0,11	0,12	0,06	0,04	0,08	0,34	0,37	0,35
Cr2O3 WT%	0,00	0,05	0,05	0,00	0,00	0,04	0,02	0,03	0,07	0,04	0,03
Cl WT%	0,00	0,00	0,01	0,00	0,00	0,00	0,00	0,01	0,01	0,01	0,01
O WT%	0,00	0,00	0,00	0,00	0,00	0,00	0,00	0,00	0,00	0,00	0,00
H2O WT%	0,00	4,02	4,02	0,00	0,00	0,00	0,00	0,00	4,02	4,02	4,03
Total	100,19	98,38	100,21	99,60	100,22	100,58	100,46	101,13	100,28	100,21	100,27
O≡Cl,F	0,21	0,22							0,18	0,20	0,18
TOTAL	98,17	99,99							100,10	100,01	100,09
FORMULA	24	24	24	24	24	24	24	24	24	24	24
BASIS	O	O	O	O	O	O	O	O	O	O	O
Si FORMULA	6,00	5,40	5,41	7,99	8,35	5,99	5,95	5,97	5,38	5,39	5,41
Ti FORMULA	0,01	0,21	0,21	0,00	0,00	0,01	0,01	0,00	0,23	0,23	0,23
Al FORMULA	3,98	3,33	3,36	3,98	3,66	3,97	4,01	3,99	3,39	3,39	3,36
Fe FORMULA	4,09	2,08	2,04	0,02	0,00	4,13	4,11	4,16	2,07	2,06	2,05
Mn FORMULA	0,12	0,00	0,01	0,00	0,00	0,01	0,01	0,01	0,00	0,00	0,00
Mg FORMULA	0,72	2,72	2,74	0,00	0,00	0,89	0,89	0,87	2,67	2,68	2,70
Ca FORMULA	1,09	0,01	0,00	0,98	0,61	1,00	1,03	1,00	0,00	0,00	0,00
Na FORMULA	0,00	0,04	0,03	2,07	2,38	0,01	0,01	0,01	0,04	0,04	0,03
K FORMULA	0,00	1,84	1,81	0,01	0,02	0,00	0,00	0,00	1,83	1,83	1,81
F FORMULA	0,01	0,20	0,19	0,04	0,05	0,03	0,02	0,04	0,16	0,18	0,17
Cr FORMULA	0,00	0,01	0,01	0,00	0,00	0,00	0,00	0,00	0,01	0,00	0,00
Cl FORMULA	0,00	0,00	0,00	0,00	0,00	0,00	0,00	0,00	0,00	0,00	0,00
O FORMULA	24,00	24,00	24,00	24,00	24,00	24,00	24,00	24,00	24,00	24,00	24,00
H FORMULA	0,00	4,07	4,00	0,00	0,00	0,00	0,00	0,00	4,00	4,00	4,00
X-POS	-5,52	-5,39	-5,42	-5,36	-5,21	-1,12	-1,06	0,01	-1,24	-1,30	-1,12
Y-POS	29,76	29,88	30,05	29,78	30,01	29,97	30,02	29,85	29,97	30,00	30,12

SAMPLE	15-S4_A1_plg	15-S4_A1_plg	15-S4_A1_plg	15-S4_A1_plg	15-S4_A1_plg	15-S4_A2_grt middle	15-S4_A2_grt upper	15-S4_A2_grt lower	15-S4_A2_bt	15-S4_A2_bt	15-S4_A2_plg
SiO2 WT%	59,55	60,28	61,79	60,25	59,85	38,04	37,93	37,72	36,23	36,29	58,64
TiO2 WT%	0,03	0,02	0,01	0,00	0,00	0,04	0,08	0,07	1,61	1,78	0,00
Al2O3 WT%	25,88	25,27	24,13	25,10	25,53	21,67	21,36	21,58	19,65	19,47	26,08
FeO WT%	0,46	0,07	0,04	0,11	0,04	31,29	31,32	31,53	15,74	15,93	0,22
MnO WT%	0,00	0,00	0,00	0,00	0,00	0,21	0,11	0,43	0,02	0,04	0,00
MgO WT%	0,02	0,00	0,00	0,01	0,00	3,94	3,69	3,78	12,32	12,05	0,00
CaO WT%	6,98	6,51	5,25	6,59	6,90	5,60	6,01	5,70	0,03	0,08	7,48
Na2O WT%	7,91	8,16	8,77	8,06	7,82	0,02	0,01	0,03	0,15	0,14	7,55
K2O WT%	0,09	0,06	0,08	0,07	0,06	0,01	0,01	0,00	9,50	9,39	0,04
F WT%	0,10	0,12	0,10	0,10	0,09	0,06	0,06	0,03	0,36	0,42	0,12
Cr2O3 WT%	0,01	0,00	0,01	0,00	0,00	0,00	0,02	0,00	0,04	0,04	0,01
Cl WT%	0,00	0,00	0,01	0,00	0,00	0,00	0,00	0,00	0,01	0,02	0,00
O WT%	0,00	0,00	0,00	0,00	0,00	0,00	0,00	0,00	0,00	0,00	0,00
H2O WT%	0,00	0,00	0,00	0,00	0,00	0,00	0,00	0,00	4,04	4,04	0,00
Total	101,04	100,45	100,18	100,29	100,24	100,86	100,61	100,87	99,71	99,68	100,12
O≡Cl,F									0,19	0,22	
TOTAL									99,52	99,46	
FORMULA	24	24	24	24	24	24	24	24	24	24	24
BASIS	O	O	O	O	O	O	O	O	O	O	O
Si FORMULA	7,92	8,03	8,22	8,04	7,99	5,98	5,99	5,95	5,40	5,42	7,87
Ti FORMULA	0,00	0,00	0,00	0,00	0,00	0,00	0,01	0,01	0,18	0,20	0,00
Al FORMULA	4,05	3,97	3,78	3,95	4,02	4,01	3,98	4,01	3,45	3,43	4,12
Fe FORMULA	0,05	0,01	0,00	0,01	0,00	4,11	4,14	4,16	1,96	1,99	0,02
Mn FORMULA	0,00	0,00	0,00	0,00	0,00	0,03	0,01	0,06	0,00	0,00	0,00
Mg FORMULA	0,00	0,00	0,00	0,00	0,00	0,92	0,87	0,89	2,74	2,68	0,00
Ca FORMULA	0,99	0,93	0,75	0,94	0,99	0,94	1,02	0,96	0,00	0,01	1,07
Na FORMULA	2,04	2,11	2,26	2,08	2,02	0,01	0,00	0,01	0,04	0,04	1,96
K FORMULA	0,02	0,01	0,01	0,01	0,01	0,00	0,00	0,00	1,81	1,79	0,01
F FORMULA	0,04	0,05	0,04	0,04	0,04	0,03	0,03	0,01	0,17	0,20	0,05
Cr FORMULA	0,00	0,00	0,00	0,00	0,00	0,00	0,00	0,00	0,00	0,00	0,00
Cl FORMULA	0,00	0,00	0,00	0,00	0,00	0,00	0,00	0,00	0,00	0,00	0,00
O FORMULA	24,00	24,00	24,00	24,00	24,00	24,00	24,00	24,00	24,00	24,00	24,00
H FORMULA	0,00	0,00	0,00	0,00	0,00	0,00	0,00	0,00	4,02	4,02	0,00
X-POS	-1,17	-1,38	-1,41	-1,46	-1,54	-1,63	-1,48	-1,65	-1,72	-1,75	-1,68
Y-POS	30,02	30,25	30,30	29,93	29,92	29,17	29,22	29,34	29,13	29,13	29,36

SAMPLE	15-S4_A2_plg	15-S4_A3_grt rim	15-S4_A3_grt	15-S4_A3_grt	15-S4_A3_grt	15-S4_A3_grt	15-S4_A3_grt	15-S4_A3_bt left	15-S4_A3_bt right	15-S4_A3_plg upper	15-S4_A3_plg lower
SiO2 WT%	58,80	38,02	38,00	38,06	38,05	38,19	38,06	35,92	35,74	60,06	60,34
TiO2 WT%	0,00	0,07	0,06	0,06	0,07	0,06	0,08	1,86	2,03	0,00	0,01
Al2O3 WT%	26,15	21,54	21,49	21,61	21,56	21,52	21,50	19,39	18,84	25,36	25,32
FeO WT%	0,01	31,24	31,16	31,04	31,12	31,56	30,96	16,20	16,40	0,20	0,19
MnO WT%	0,02	0,77	0,19	0,11	0,08	0,09	0,05	0,04	0,01	0,01	0,02
MgO WT%	0,00	3,59	4,06	4,02	4,02	4,01	3,84	12,15	11,97	0,02	0,01
CaO WT%	7,60	5,66	5,70	5,83	6,00	5,76	6,28	0,08	0,08	6,55	6,52
Na2O WT%	7,42	0,01	0,02	0,00	0,01	0,01	0,02	0,14	0,15	8,14	8,10
K2O WT%	0,04	0,00	0,00	0,00	0,00	0,00	0,00	9,48	9,51	0,05	0,06
F WT%	0,15	0,03	0,04	0,09	0,04	0,07	0,08	0,38	0,42	0,09	0,11
Cr2O3 WT%	0,00	0,01	0,05	0,02	0,04	0,01	0,03	0,07	0,04	0,00	0,02
Cl WT%	0,00	0,00	0,00	0,01	0,00	0,00	0,00	0,01	0,00	0,00	0,00
O WT%	0,00	0,00	0,00	0,00	0,00	0,00	0,00	0,00	0,00	0,00	0,00
H2O WT%	0,00	0,00	0,00	0,00	0,00	0,00	0,00	4,03	4,02	0,00	0,00
Total	100,17	100,95	100,77	100,84	100,96	101,28	100,88	99,75	99,22	100,47	100,69
O≡Cl,F								0,20	0,22		
TOTAL								99,56	99,00		
FORMULA	24	24	24	24	24	24	24	24	24	24	24
BASIS	O	O	O	O	O	O	O	O	O	O	O
Si FORMULA	7,88	5,99	5,98	5,98	5,97	5,98	5,98	5,37	5,39	8,00	8,02
Ti FORMULA	0,00	0,01	0,01	0,01	0,01	0,01	0,01	0,21	0,23	0,00	0,00
Al FORMULA	4,13	4,00	3,98	4,00	3,99	3,97	3,98	3,42	3,35	3,98	3,97
Fe FORMULA	0,00	4,11	4,10	4,08	4,09	4,14	4,07	2,03	2,07	0,02	0,02
Mn FORMULA	0,00	0,10	0,02	0,01	0,01	0,01	0,01	0,01	0,00	0,00	0,00
Mg FORMULA	0,00	0,84	0,95	0,94	0,94	0,94	0,90	2,71	2,69	0,00	0,00
Ca FORMULA	1,09	0,95	0,96	0,98	1,01	0,97	1,06	0,01	0,01	0,94	0,93
Na FORMULA	1,93	0,00	0,01	0,00	0,00	0,00	0,01	0,04	0,04	2,10	2,09
K FORMULA	0,01	0,00	0,00	0,00	0,00	0,00	0,00	1,81	1,83	0,01	0,01
F FORMULA	0,06	0,02	0,02	0,04	0,02	0,03	0,04	0,18	0,20	0,04	0,04
Cr FORMULA	0,00	0,00	0,01	0,00	0,00	0,00	0,00	0,01	0,00	0,00	0,00
Cl FORMULA	0,00	0,00	0,00	0,00	0,00	0,00	0,00	0,00	0,00	0,00	0,00
O FORMULA	24,00	24,00	24,00	24,00	24,00	24,00	24,00	24,00	24,00	24,00	24,00
H FORMULA	0,00	0,00	0,00	0,00	0,00	0,00	0,00	4,02	4,04	0,00	0,00
X-POS	-1,88	-1,62	-1,60	-1,58	-1,56	-1,55	-1,53	-1,65	-1,68	-1,65	-1,72
Y-POS	29,28	28,58	28,60	28,61	28,62	28,63	28,64	28,57	28,51	28,53	28,57

SAMPLE	15-S4_A3_musc left	15-S4_A3_musc right	15-S4_A3_musc right	15-S4_A4_grt	15-S4_A4_grt	15-S4_A4_grt	15-S4_A4_grt	15-S4_A4_grt	15-S4_A5_grt	15-S4_A5_grt	15-S4_A5_grt
SiO2 WT%	46,45	45,89	46,58	38,02	37,85	38,08	38,01	37,94	38,00	37,87	37,81
TiO2 WT%	0,49	0,57	0,58	0,08	0,05	0,08	0,06	0,09	0,08	0,11	0,08
Al2O3 WT%	34,67	34,35	33,74	21,43	21,49	21,37	21,56	21,55	21,39	21,44	21,29
FeO WT%	1,65	1,76	1,94	31,04	31,14	31,34	31,50	31,57	31,56	31,33	31,31
MnO WT%	0,02	0,00	0,01	0,20	0,19	0,14	0,16	0,15	0,46	0,45	0,46
MgO WT%	0,99	1,08	1,26	3,57	3,55	3,55	3,56	3,53	3,22	3,16	3,23
CaO WT%	0,01	0,02	0,02	6,17	6,39	6,13	6,05	5,96	6,23	6,54	6,46
Na2O WT%	0,76	0,73	0,69	0,02	0,01	0,02	0,01	0,03	0,01	0,00	0,02
K2O WT%	10,06	10,28	10,19	0,00	0,00	0,00	0,00	0,00	0,01	0,00	0,01
F WT%	0,13	0,17	0,15	0,03	0,01	0,05	0,01	0,07	0,05	0,00	0,05
Cr2O3 WT%	0,07	0,02	0,04	0,03	0,00	0,02	0,01	0,03	0,02	0,03	0,03
Cl WT%	0,01	0,01	0,00	0,00	0,00	0,00	0,00	0,01	0,01	0,00	0,00
O WT%	0,00	0,00	0,00	0,00	0,00	0,00	0,00	0,00	0,00	0,00	0,00
H2O WT%	4,52	4,50	4,51	0,00	0,00	0,00	0,00	0,00	0,00	0,00	0,00
Total	99,85	99,39	99,70	100,59	100,67	100,79	100,93	100,91	101,04	100,92	100,73
O≡Cl,F	0,07	0,09	0,08								
TOTAL	99,77	99,29	99,62								
FORMULA	24	24	24	24	24	24	24	24	24	24	24
BASIS	O	O	O	O	O	O	O	O	O	O	O
Si FORMULA	6,19	6,16	6,23	6,00	5,97	6,00	5,98	5,98	5,99	5,97	5,98
Ti FORMULA	0,05	0,06	0,06	0,01	0,01	0,01	0,01	0,01	0,01	0,01	0,01
Al FORMULA	5,44	5,44	5,32	3,98	4,00	3,97	4,00	4,00	3,97	3,99	3,97
Fe FORMULA	0,18	0,20	0,22	4,09	4,11	4,13	4,14	4,16	4,16	4,13	4,14
Mn FORMULA	0,00	0,00	0,00	0,03	0,03	0,02	0,02	0,02	0,06	0,06	0,06
Mg FORMULA	0,20	0,22	0,25	0,84	0,83	0,83	0,84	0,83	0,76	0,74	0,76
Ca FORMULA	0,00	0,00	0,00	1,04	1,08	1,03	1,02	1,01	1,05	1,11	1,09
Na FORMULA	0,20	0,19	0,18	0,01	0,00	0,01	0,00	0,01	0,00	0,00	0,00
K FORMULA	1,71	1,76	1,74	0,00	0,00	0,00	0,00	0,00	0,00	0,00	0,00
F FORMULA	0,06	0,07	0,06	0,01	0,01	0,03	0,00	0,03	0,03	0,00	0,02
Cr FORMULA	0,01	0,00	0,00	0,00	0,00	0,00	0,00	0,00	0,00	0,00	0,00
Cl FORMULA	0,00	0,00	0,00	0,00	0,00	0,00	0,00	0,00	0,00	0,00	0,00
O FORMULA	24,00	24,00	24,00	24,00	24,00	24,00	24,00	24,00	24,00	24,00	24,00
H FORMULA	4,01	4,03	4,02	0,00	0,00	0,00	0,00	0,00	0,00	0,00	0,00
X-POS	-1,70	-1,75	-1,77	-1,18	-1,19	-1,22	-1,25	-1,27	0,01	0,01	0,01
Y-POS	28,48	28,44	28,43	28,90	28,92	28,95	28,98	29,01	29,06	29,03	29,00

SAMPLE	15-S4_A6_grt	15-S4_A6_grt	15-S4_A6_grt	16_S1-A1_grt	16_S1-A1_plg musc?	16_S1-A1_bt	16_S1-A1_bt	16_S1-A1_musc	16_S1-A1_musc	16_S1-A2_grt right	16_S1-A2_grt
SiO2 WT%	37,76	37,90	37,82	38,06	44,63	36,96	36,50	45,74	45,28	37,82	37,82
TiO2 WT%	0,09	0,08	0,12	0,10	0,40	2,25	2,50	0,48	0,34	0,05	0,06
Al2O3 WT%	21,36	21,27	21,40	21,40	32,27	17,61	17,86	33,09	33,41	21,40	21,31
FeO WT%	31,48	31,46	31,33	28,93	4,31	15,50	15,28	3,38	3,58	26,34	29,24
MnO WT%	0,56	0,54	0,58	4,05	0,02	0,10	0,10	0,02	0,01	7,03	4,07
MgO WT%	3,13	3,09	3,15	3,94	1,32	13,41	13,00	1,21	1,06	3,55	3,84
CaO WT%	6,37	6,34	6,35	4,62	0,04	0,03	0,02	0,03	0,02	5,02	4,75
Na2O WT%	0,04	0,03	0,03	0,02	0,40	0,08	0,04	0,42	0,43	0,01	0,03
K2O WT%	0,00	0,00	0,00	0,01	10,77	9,87	9,91	10,83	10,87	0,01	0,00
F WT%	0,05	0,05	0,07	0,00	0,16	0,45	0,43	0,16	0,17	0,00	0,00
Cr2O3 WT%	0,03	0,03	0,03	0,04	0,01	0,02	0,01	0,02	0,01	0,02	0,01
Cl WT%	0,00	0,00	0,00	0,00	0,01	0,01	0,01	0,00	0,00	0,00	0,00
O WT%	0,00	0,00	0,00	0,00	0,00	0,00	0,00	0,00	0,00	0,00	0,00
H2O WT%	0,00	0,00	0,00	0,00	0,00	4,03	4,03	4,45	4,45	0,00	0,00
Total	100,86	100,78	100,86	101,05	94,33	100,30	99,70	99,81	99,63	100,97	100,96
O=Cl,F					0,08	0,24	0,23	0,08	0,09		
TOTAL					94,25	100,06	99,47	99,73	99,54		
FORMULA	24	24	24	24	24	24	24	24	24	24	24
BASIS	O	O	O	O	O	O	O	O	O	O	O
Si FORMULA	5,97	5,99	5,97	5,99	6,70	5,50	5,46	6,18	6,14	5,96	5,97
Ti FORMULA	0,01	0,01	0,01	0,01	0,05	0,25	0,28	0,05	0,03	0,01	0,01
Al FORMULA	3,98	3,96	3,99	3,97	5,71	3,09	3,15	5,27	5,34	3,98	3,96
Fe FORMULA	4,16	4,16	4,14	3,80	0,54	1,93	1,91	0,38	0,41	3,47	3,86
Mn FORMULA	0,08	0,07	0,08	0,54	0,00	0,01	0,01	0,00	0,00	0,94	0,54
Mg FORMULA	0,74	0,73	0,74	0,92	0,30	2,97	2,90	0,24	0,21	0,83	0,90
Ca FORMULA	1,08	1,07	1,08	0,78	0,01	0,00	0,00	0,00	0,00	0,85	0,80
Na FORMULA	0,01	0,01	0,01	0,00	0,12	0,02	0,01	0,11	0,11	0,00	0,01
K FORMULA	0,00	0,00	0,00	0,00	2,06	1,87	1,89	1,87	1,88	0,00	0,00
F FORMULA	0,02	0,02	0,03	0,00	0,07	0,21	0,21	0,07	0,07	0,00	0,00
Cr FORMULA	0,00	0,00	0,00	0,01	0,00	0,00	0,00	0,00	0,00	0,00	0,00
Cl FORMULA	0,00	0,00	0,00	0,00	0,00	0,00	0,00	0,00	0,00	0,00	0,00
O FORMULA	24,00	24,00	24,00	24,00	24,00	24,00	24,00	24,00	24,00	24,00	24,00
H FORMULA	0,00	0,00	0,00	0,00	0,00	4,00	4,02	4,02	4,02	0,00	0,00
X-POS	0,01	0,01	0,01	-37,03	-37,09	-37,53	-37,46	-37,42	-37,68	-36,79	-36,85
Y-POS	29,22	29,23	29,23	19,71	19,72	19,90	19,83	20,02	20,10	18,45	18,70

SAMPLE	16_S1-A2_bt upper	16_S1-A2_bt	16_S1-A3_grt	16_S1-A3_grt	16_S1-A3_grt	16_S1-A4_grt	16_S1-A4_bt	16_S1- A4_musc	16_S1-A5_grt	16_S1-A5_bt lower	16_S1-A5_bt
SiO2 WT%	38,39	37,06	37,69	37,88	37,79	38,03	36,16	45,36	37,79	36,76	36,74
TiO2 WT%	0,09	1,82	0,19	0,14	0,11	0,01	1,62	0,27	0,04	1,94	1,82
Al2O3 WT%	26,59	18,23	21,24	21,08	20,99	21,36	18,34	32,54	21,11	17,57	17,89
FeO WT%	9,44	15,90	28,49	28,82	28,85	27,53	15,77	4,26	26,60	15,65	15,47
MnO WT%	0,35	0,09	4,37	4,09	4,05	5,72	0,15	0,01	6,29	0,12	0,11
MgO WT%	0,09	12,99	3,65	3,84	3,84	3,50	12,93	1,47	3,37	13,16	13,30
CaO WT%	23,12	0,07	4,98	5,12	5,02	5,17	0,02	0,01	5,41	0,02	0,01
Na2O WT%	0,00	0,07	0,04	0,03	0,01	0,00	0,07	0,44	0,00	0,06	0,10
K2O WT%	0,00	9,73	0,00	0,00	0,00	0,00	10,04	10,79	0,03	9,81	9,78
F WT%	0,10	0,44	0,00	0,00	0,00	0,00	0,45	0,21	0,00	0,47	0,47
Cr2O3 WT%	0,03	0,05	0,01	0,01	0,02	0,00	0,00	0,03	0,02	0,03	0,07
Cl WT%	0,01	0,01	0,01	0,00	0,00	0,00	0,00	0,00	0,01	0,01	0,02
O WT%	0,00	0,00	0,00	0,00	0,00	0,00	0,00	0,00	0,00	0,00	0,00
H2O WT%	4,18	4,03	0,00	0,00	0,00	0,00	4,01	4,43	0,00	4,02	4,03
Total	102,39	100,47	100,55	100,85	100,53	101,14	99,57	99,82	100,44	99,62	99,80
O=Cl,F	0,06	0,23					0,23	0,11		0,25	0,25
TOTAL	102,33	100,24					99,34	99,71		99,38	99,55
FORMULA	24	24	24	24	24	24	24	24	24	24	24
BASIS	O	O	O	O	O	O	O	O	O	O	O
Si FORMULA	5,39	5,50	5,97	5,98	5,98	5,99	5,44	6,17	5,99	5,51	5,49
Ti FORMULA	0,01	0,20	0,02	0,02	0,01	0,00	0,18	0,03	0,00	0,22	0,20
Al FORMULA	4,40	3,19	3,96	3,92	3,92	3,96	3,25	5,21	3,94	3,10	3,15
Fe FORMULA	1,11	1,97	3,77	3,80	3,82	3,62	1,98	0,48	3,53	1,96	1,93
Mn FORMULA	0,04	0,01	0,59	0,55	0,54	0,76	0,02	0,00	0,84	0,02	0,01
Mg FORMULA	0,02	2,87	0,86	0,90	0,91	0,82	2,90	0,30	0,80	2,94	2,96
Ca FORMULA	3,48	0,01	0,84	0,87	0,85	0,87	0,00	0,00	0,92	0,00	0,00
Na FORMULA	0,00	0,02	0,01	0,01	0,00	0,00	0,02	0,12	0,00	0,02	0,03
K FORMULA	0,00	1,84	0,00	0,00	0,00	0,00	1,92	1,87	0,01	1,88	1,87
F FORMULA	0,05	0,20	0,00	0,00	0,00	0,00	0,21	0,09	0,00	0,22	0,22
Cr FORMULA	0,00	0,01	0,00	0,00	0,00	0,00	0,00	0,00	0,00	0,00	0,01
Cl FORMULA	0,00	0,00	0,00	0,00	0,00	0,00	0,00	0,00	0,00	0,00	0,00
O FORMULA	24,00	24,00	24,00	24,00	24,00	24,00	24,00	24,00	24,00	24,00	24,00
H FORMULA	3,91	3,99	0,00	0,00	0,00	0,00	4,02	4,02	0,00	4,02	4,02
X-POS	-36,82	-36,90	-36,50	-36,54	-36,58	-36,21	-36,11	-36,26	-35,98	-35,87	-35,78
Y-POS	18,46	18,42	18,90	19,10	19,24	18,59	18,58	18,53	18,78	18,80	18,86

SAMPLE	16_S1-A5_musc	16_S1-A6_grt_rim	16_S1-A6_grt	16_S1-A6_plg_lower	16_S1-A6_plg	16_S1-A6_bt	16_S1-A6_bt_left	16_S1-A6_musc_closest_to_Grt	16_S1-A6_musc	16_S1-A7_grt	16_S1-A7_plg
SiO2 WT%	44,85	38,02	37,48	59,23	59,03	35,96	36,86	45,10	44,78	37,98	59,33
TiO2 WT%	0,18	0,14	0,11	0,02	0,01	1,49	1,36	0,40	0,39	0,07	0,00
Al2O3 WT%	33,42	21,05	21,02	25,94	26,29	18,52	18,56	32,65	32,75	21,48	26,13
FeO WT%	4,03	28,13	27,96	0,18	0,19	16,64	16,03	4,14	4,13	26,79	0,11
MnO WT%	0,02	4,90	4,30	0,02	0,03	0,35	0,39	0,03	0,04	5,97	0,00
MgO WT%	1,06	3,53	3,57	0,00	0,00	12,29	12,51	1,33	1,25	3,62	0,01
CaO WT%	0,00	5,18	5,71	7,25	7,42	0,15	0,23	0,01	0,01	5,09	7,56
Na2O WT%	0,50	0,03	0,04	7,68	7,55	0,10	0,09	0,40	0,44	0,02	7,41
K2O WT%	10,71	0,00	0,00	0,06	0,09	9,66	9,64	10,86	10,89	0,00	0,10
F WT%	0,14	0,00	0,00	0,11	0,11	0,53	0,63	0,14	0,14	0,00	0,09
Cr2O3 WT%	0,03	0,01	0,02	0,01	0,00	0,05	0,04	0,05	0,04	0,02	0,00
Cl WT%	0,00	0,01	0,00	0,00	0,00	0,02	0,01	0,00	0,02	0,00	0,01
O WT%	0,00	0,00	0,00	0,00	0,00	0,00	0,00	0,00	0,00	0,00	0,00
H2O WT%	4,44	0,00	0,00	0,00	0,00	4,00	4,01	4,43	4,43	0,00	0,00
Total	99,38	100,80	100,11	100,50	100,71	99,75	100,36	99,55	99,31	100,77	100,75
O≡Cl,F	0,07					0,28	0,33	0,07	0,08		
TOTAL	99,30					99,46	100,03	99,47	99,23		
FORMULA	24	24	24	24	24	24	24	24	24	24	24
BASIS	O	O	O	O	O	O	O	O	O	O	O
Si FORMULA	6,11	6,00	5,96	7,91	7,87	5,42	5,50	6,14	6,12	5,98	7,90
Ti FORMULA	0,02	0,02	0,01	0,00	0,00	0,17	0,15	0,04	0,04	0,01	0,00
Al FORMULA	5,37	3,92	3,94	4,08	4,13	3,29	3,26	5,24	5,28	3,99	4,10
Fe FORMULA	0,46	3,71	3,72	0,02	0,02	2,10	2,00	0,47	0,47	3,53	0,01
Mn FORMULA	0,00	0,66	0,58	0,00	0,00	0,04	0,05	0,00	0,00	0,80	0,00
Mg FORMULA	0,22	0,83	0,85	0,00	0,00	2,76	2,78	0,27	0,26	0,85	0,00
Ca FORMULA	0,00	0,88	0,97	1,04	1,06	0,02	0,04	0,00	0,00	0,86	1,08
Na FORMULA	0,13	0,01	0,01	1,99	1,95	0,03	0,03	0,10	0,12	0,01	1,91
K FORMULA	1,86	0,00	0,00	0,01	0,01	1,86	1,84	1,89	1,90	0,00	0,02
F FORMULA	0,06	0,00	0,00	0,05	0,05	0,25	0,30	0,06	0,06	0,00	0,04
Cr FORMULA	0,00	0,00	0,00	0,00	0,00	0,01	0,00	0,01	0,00	0,00	0,00
Cl FORMULA	0,00	0,00	0,00	0,00	0,00	0,00	0,00	0,00	0,00	0,00	0,00
O FORMULA	24,00	24,00	24,00	24,00	24,00	24,00	24,00	24,00	24,00	24,00	24,00
H FORMULA	4,03	0,00	0,00	0,00	0,00	4,02	3,99	4,03	4,04	0,00	0,00
X-POS	-35,93	-35,69	-35,72	-35,63	-35,57	-35,69	-35,70	-35,91	-35,95	-35,34	-35,15
Y-POS	18,81	19,82	20,02	19,80	19,78	19,74	19,76	19,78	19,76	20,42	20,50

SAMPLE	16_S1-A7_bt (not bt I think)	16_S1-A7_bt	16_S1- A7_musc	16_S2-A1_grt	16_S2-A1_bt rim-to-core						
SiO2 WT%	57,79	36,70	45,17	37,51	37,11	37,14	36,94	36,88	37,16	37,07	37,02
TiO2 WT%	0,03	2,11	0,07	0,03	1,77	1,85	1,79	1,85	1,88	1,80	1,86
Al2O3 WT%	26,73	17,93	32,82	21,28	17,90	18,18	18,15	18,11	18,09	18,11	18,18
FeO WT%	0,24	15,96	4,12	26,12	15,45	15,29	15,31	15,58	15,51	15,42	15,53
MnO WT%	0,02	0,12	0,31	6,86	0,23	0,20	0,17	0,17	0,17	0,15	0,14
MgO WT%	0,11	12,71	1,56	3,51	13,37	13,25	13,19	13,21	13,14	13,31	13,17
CaO WT%	8,63	0,03	0,06	5,06	0,03	0,01	0,01	0,03	0,01	0,00	0,03
Na2O WT%	6,73	0,05	0,49	0,00	0,07	0,10	0,12	0,13	0,15	0,14	0,12
K2O WT%	0,13	9,90	10,53	0,01	9,57	9,69	9,71	9,70	9,63	9,67	9,74
F WT%	0,11	0,40	0,13	0,00	0,41	0,40	0,39	0,40	0,38	0,43	0,40
Cr2O3 WT%	0,00	0,04	0,04	0,03	0,03	0,04	0,04	0,03	0,03	0,05	0,04
Cl WT%	0,02	0,01	0,00	0,00	0,01	0,01	0,01	0,00	0,01	0,01	0,01
O WT%	0,00	0,00	0,00	0,00	0,00	0,00	0,00	0,00	0,00	0,00	0,00
H2O WT%	4,63	4,02	4,43	0,00	4,04	4,04	4,04	4,03	4,04	4,04	4,03
Total	105,17	99,95	99,74	100,17	99,97	100,21	99,87	100,13	100,20	100,20	100,26
O=Cl,F			0,07		0,21	0,21	0,21	0,21	0,20	0,23	0,21
TOTAL			99,67		99,76	100,00	99,67	99,92	99,99	99,97	100,05
FORMULA	24	24	24	24	24	24	24	24	24	24	24
BASIS	O	O	O	O	O	O	O	O	O	O	O
Si FORMULA	7,13	5,49	6,14	5,96	5,52	5,51	5,50	5,49	5,52	5,51	5,50
Ti FORMULA	0,00	0,24	0,01	0,00	0,20	0,21	0,20	0,21	0,21	0,20	0,21
Al FORMULA	3,89	3,16	5,26	3,99	3,14	3,18	3,19	3,18	3,17	3,17	3,18
Fe FORMULA	0,03	2,00	0,47	3,47	1,92	1,90	1,91	1,94	1,93	1,92	1,93
Mn FORMULA	0,00	0,01	0,04	0,92	0,03	0,03	0,02	0,02	0,02	0,02	0,02
Mg FORMULA	0,02	2,83	0,32	0,83	2,97	2,93	2,93	2,93	2,91	2,95	2,92
Ca FORMULA	1,14	0,01	0,01	0,86	0,00	0,00	0,00	0,00	0,00	0,00	0,00
Na FORMULA	1,61	0,02	0,13	0,00	0,02	0,03	0,04	0,04	0,04	0,04	0,03
K FORMULA	0,02	1,89	1,83	0,00	1,82	1,83	1,85	1,84	1,82	1,83	1,85
F FORMULA	0,04	0,19	0,06	0,00	0,19	0,19	0,18	0,19	0,18	0,20	0,19
Cr FORMULA	0,00	0,00	0,00	0,00	0,00	0,00	0,00	0,00	0,00	0,01	0,00
Cl FORMULA	0,00	0,00	0,00	0,00	0,00	0,00	0,00	0,00	0,00	0,00	0,00
O FORMULA	24,00	24,00	24,00	24,00	24,00	24,00	24,00	24,00	24,00	24,00	24,00
H FORMULA	3,81	4,01	4,02	0,00	4,01	4,00	4,01	4,00	4,00	4,00	4,00
X-POS	-35,07	-35,24	-35,40	-30,73	-30,76	-30,78	-30,81	-30,82	-30,86	-30,89	-30,97
Y-POS	20,32	20,48	20,48	19,74	19,77	19,78	19,79	19,79	19,80	19,80	19,81

SAMPLE	16_S2-A1_bt rim-to-core	16_S2-A2_grt	16_S2-A2_bt upper	16_S2-A2_bt lower	16_S2-A3_grt	16_S2- A3_plg	16_S2- A3_plg	16_S2-A4_grt	16_S2-A4_grt	16_S2-A4_grt	16_S2-A5_grt lower
SiO2 WT%	36,84	37,92	36,71	36,45	37,66	59,23	61,43	37,67	37,48	37,65	37,67
TiO2 WT%	1,81	0,03	1,50	1,68	0,04	0,00	0,01	0,03	0,00	0,03	0,02
Al2O3 WT%	17,74	21,49	18,01	17,89	21,13	25,94	24,46	21,28	21,32	21,15	21,23
FeO WT%	14,04	26,26	15,47	15,45	26,45	0,20	0,17	27,91	28,23	28,44	27,58
MnO WT%	0,14	7,30	0,18	0,19	6,74	0,01	0,02	5,11	5,14	5,01	5,29
MgO WT%	12,92	3,51	13,42	13,41	3,47	0,00	0,01	3,64	3,62	3,56	3,52
CaO WT%	0,00	5,08	0,15	0,10	4,88	7,34	5,60	4,66	4,41	4,63	4,57
Na2O WT%	0,11	0,01	0,17	0,15	0,01	7,68	8,70	0,00	0,02	0,03	0,03
K2O WT%	9,66	0,01	9,25	9,14	0,00	0,09	0,07	0,01	0,00	0,01	0,00
F WT%	0,44	0,00	0,64	0,49	0,00	0,06	0,10	0,00	0,00	0,00	0,00
Cr2O3 WT%	0,05	0,03	0,03	0,03	0,01	0,00	0,01	0,00	0,01	0,00	0,00
Cl WT%	0,01	0,00	0,01	0,01	0,01	0,00	0,01	0,00	0,01	0,00	0,00
O WT%	0,00	0,00	0,00	0,00	0,00	0,00	0,00	0,00	0,00	0,00	0,00
H2O WT%	4,06	0,00	4,03	4,04	0,00	0,00	0,00	0,00	0,00	0,00	0,00
Total	97,82	101,36	99,56	99,01	100,15	100,54	100,60	100,10	100,01	100,32	99,71
O≡Cl,F	0,23		0,34		0,26						
TOTAL	97,58		99,23		98,75						
FORMULA	24	24	24	24	24	24	24	24	24	24	24
BASIS	O	O	O	O	O	O	O	O	O	O	O
Si FORMULA	5,57	5,96	5,50	5,48	5,99	7,90	8,15	5,98	5,97	5,98	6,00
Ti FORMULA	0,21	0,00	0,17	0,19	0,00	0,00	0,00	0,00	0,00	0,00	0,00
Al FORMULA	3,16	3,98	3,18	3,17	3,96	4,08	3,83	3,98	4,00	3,96	3,99
Fe FORMULA	1,78	3,45	1,94	1,94	3,52	0,02	0,02	3,71	3,76	3,78	3,68
Mn FORMULA	0,02	0,97	0,02	0,02	0,91	0,00	0,00	0,69	0,69	0,67	0,71
Mg FORMULA	2,91	0,82	3,00	3,00	0,82	0,00	0,00	0,86	0,86	0,84	0,84
Ca FORMULA	0,00	0,86	0,02	0,02	0,83	1,05	0,80	0,79	0,75	0,79	0,78
Na FORMULA	0,03	0,00	0,05	0,04	0,00	1,99	2,24	0,00	0,01	0,01	0,01
K FORMULA	1,86	0,00	1,77	1,75	0,00	0,02	0,01	0,00	0,00	0,00	0,00
F FORMULA	0,21	0,00	0,30	0,23	0,00	0,02	0,04	0,00	0,00	0,00	0,00
Cr FORMULA	0,01	0,00	0,00	0,00	0,00	0,00	0,00	0,00	0,00	0,00	0,00
Cl FORMULA	0,00	0,00	0,00	0,00	0,00	0,00	0,00	0,00	0,00	0,00	0,00
O FORMULA	24,00	24,00	24,00	24,00	24,00	24,00	24,00	24,00	24,00	24,00	24,00
H FORMULA	4,10	0,00	4,03	4,05	0,00	0,00	0,00	0,00	0,00	0,00	0,00
X-POS	-31,01	-30,40	-30,46	-30,53	-30,21	-30,24	-30,30	-30,21	-30,23	-30,27	-30,08
Y-POS	19,81	19,39	19,41	19,42	20,11	20,13	20,10	19,60	19,59	19,56	20,02

SAMPLE	16_S2-A5_grt upper	16_S2- A5_plg	16_S2- A5_plg	16_S2-A5_bt lower	16_S2-A5_bt	16_S2-A5_bt upper	16_S3-A1_bt amph-incl	16_S3-A1_bt amph-incl	16_S3- A1_cal amph- incl	16_S3- A2_amph	16_S3- A2_amph
SiO2 WT%	37,60	57,09	56,30	36,61	36,58	36,91	36,76	37,40	3,89	42,79	42,46
TiO2 WT%	0,10	0,02	0,03	1,89	1,93	1,86	1,40	1,38	0,00	0,47	0,47
Al2O3 WT%	21,05	27,30	27,65	18,19	18,22	18,43	17,47	17,62	0,02	14,90	15,00
FeO WT%	27,99	0,21	0,28	15,81	16,06	15,82	14,84	14,72	1,51	17,44	17,64
MnO WT%	5,37	0,00	0,07	0,16	0,17	0,15	0,15	0,19	1,48	0,37	0,37
MgO WT%	3,66	0,01	0,00	12,79	12,72	12,86	14,34	14,40	1,31	9,21	9,41
CaO WT%	4,85	8,87	9,36	0,02	0,00	0,03	0,11	0,06	48,97	9,47	9,43
Na2O WT%	0,03	6,66	6,39	0,08	0,08	0,10	0,05	0,04	0,00	1,96	1,85
K2O WT%	0,00	0,05	0,07	9,79	9,71	9,71	9,56	9,53	0,01	0,35	0,34
F WT%	0,00	0,07	0,11	0,36	0,35	0,42	0,44	0,47	0,07	0,23	0,16
Cr2O3 WT%	0,03	0,00	0,00	0,04	0,04	0,03	0,01	0,02	0,00	0,00	0,02
Cl WT%	0,01	0,00	0,00	0,00	0,01	0,01	0,01	0,01	0,01	0,01	0,00
O WT%	0,00	0,00	0,00	0,00	0,00	0,00	0,00	0,00	0,00	0,00	0,00
H2O WT%	0,00	0,00	0,00	4,03	4,02	4,03	4,04	4,05	3,12	2,01	2,01
Total	100,50	100,27	100,25	99,76	99,88	100,35	99,19	99,89	60,35	99,19	99,15
O≡Cl,F				0,19	0,18	0,22	0,23	0,25			
TOTAL				99,57	99,70	100,13	98,96	99,64			
FORMULA	24	24	24	24	24	24	24	24	24	24	24
BASIS	O	O	O	O	O	O	O	O	O	O	O
Si FORMULA	5,97	7,67	7,59	5,48	5,47	5,48	5,51	5,55	1,24	6,41	6,37
Ti FORMULA	0,01	0,00	0,00	0,21	0,22	0,21	0,16	0,15	0,00	0,05	0,05
Al FORMULA	3,94	4,32	4,39	3,21	3,21	3,23	3,08	3,08	0,01	2,63	2,65
Fe FORMULA	3,71	0,02	0,03	1,98	2,01	1,97	1,86	1,83	0,40	2,19	2,21
Mn FORMULA	0,72	0,00	0,01	0,02	0,02	0,02	0,02	0,02	0,40	0,05	0,05
Mg FORMULA	0,87	0,00	0,00	2,85	2,83	2,85	3,20	3,19	0,62	2,06	2,10
Ca FORMULA	0,82	1,28	1,35	0,00	0,00	0,01	0,02	0,01	16,76	1,52	1,52
Na FORMULA	0,01	1,73	1,67	0,02	0,02	0,03	0,02	0,01	0,00	0,57	0,54
K FORMULA	0,00	0,01	0,01	1,87	1,85	1,84	1,83	1,81	0,00	0,07	0,07
F FORMULA	0,00	0,03	0,05	0,17	0,17	0,20	0,21	0,22	0,07	0,11	0,08
Cr FORMULA	0,00	0,00	0,00	0,00	0,00	0,00	0,00	0,00	0,00	0,00	0,00
Cl FORMULA	0,00	0,00	0,00	0,00	0,00	0,00	0,00	0,00	0,00	0,00	0,00
O FORMULA	24,00	24,00	24,00	24,00	24,00	24,00	24,00	24,00	24,00	24,00	24,00
H FORMULA	0,00	0,00	0,00	4,02	4,01	3,99	4,04	4,01	6,64	2,01	2,01
X-POS	-29,96	-29,85	-29,92	-30,03	-29,95	-29,87	-32,41	-32,45	-32,64	-31,23	-31,24
Y-POS	19,82	19,92	19,83	20,01	20,03	19,97	17,34	17,34	17,36	17,42	17,46

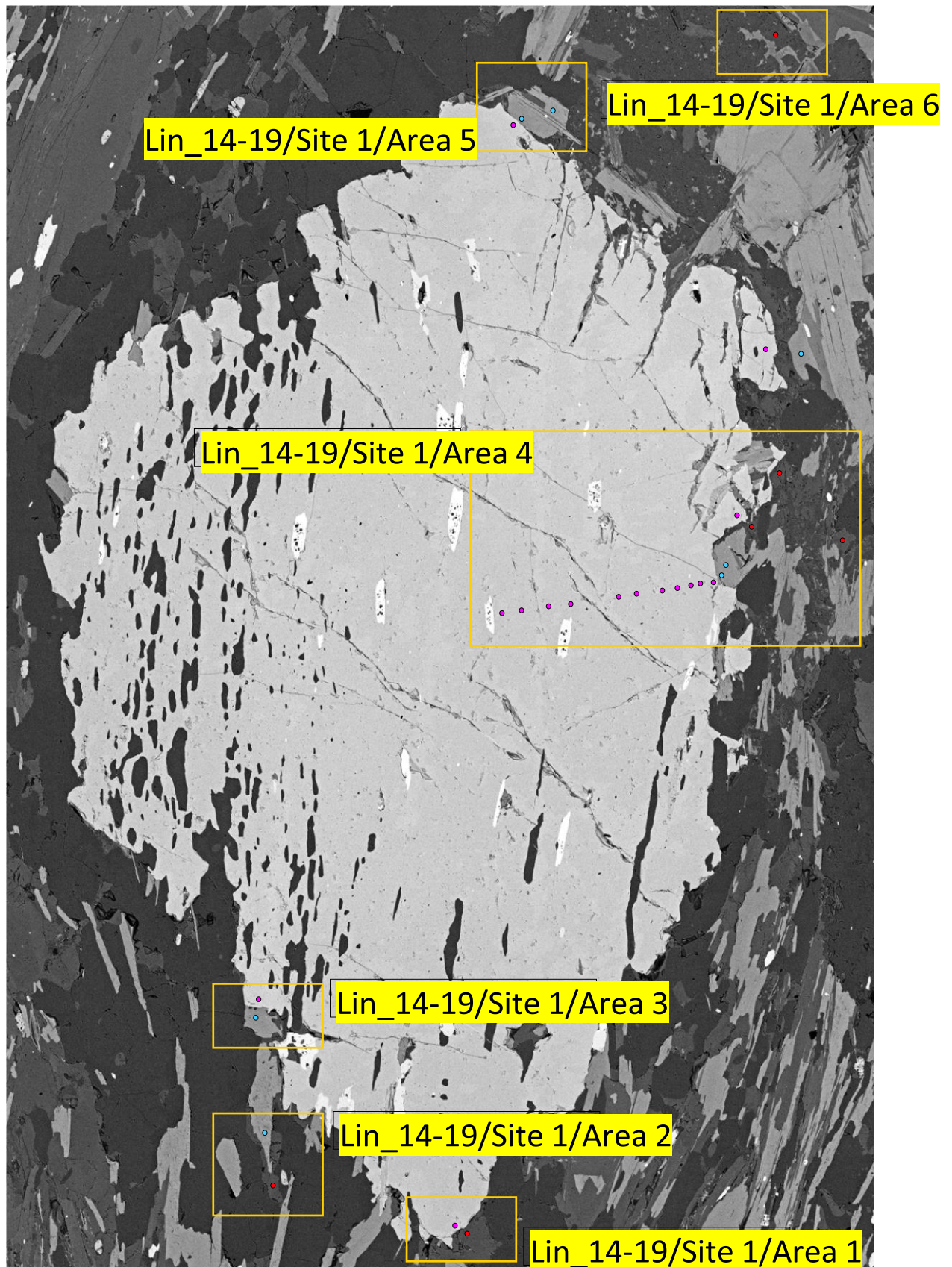
SAMPLE	16_S3-A2_amph							
SiO2 WT%	42,36	42,52	42,58	41,61	42,25	42,54	42,44	42,53
TiO2 WT%	0,43	0,48	0,41	0,37	0,38	0,33	0,44	0,40
Al2O3 WT%	14,88	14,92	14,97	14,47	15,29	14,68	15,51	15,27
FeO WT%	17,58	17,38	17,64	16,43	16,64	16,11	16,35	17,15
MnO WT%	0,37	0,37	0,42	0,39	0,37	0,34	0,40	0,42
MgO WT%	9,38	9,43	9,49	9,30	9,67	10,21	9,58	9,72
CaO WT%	9,48	9,62	9,41	9,32	10,18	10,41	10,22	9,61
Na2O WT%	1,85	1,80	1,84	1,70	1,69	1,70	1,71	1,69
K2O WT%	0,32	0,32	0,31	0,31	0,32	0,35	0,30	0,31
F WT%	0,21	0,15	0,20	0,18	0,20	0,16	0,18	0,19
Cr2O3 WT%	0,01	0,00	0,00	0,04	0,01	0,01	0,02	0,00
Cl WT%	0,00	0,01	0,00	0,04	0,01	0,01	0,00	0,00
O WT%	0,00	0,00	0,00	0,00	0,00	0,00	0,00	0,00
H2O WT%	2,01	2,01	2,01	2,02	2,01	2,02	2,02	2,01
Total	98,88	99,00	99,28	96,16	99,03	98,87	99,16	99,29
O≡Cl,F								
TOTAL								
FORMULA	24	24	24	24	24	24	24	24
BASIS	O	O	O	O	O	O	O	O
Si FORMULA	6,37	6,38	6,38	6,41	6,33	6,37	6,33	6,35
Ti FORMULA	0,05	0,05	0,05	0,04	0,04	0,04	0,05	0,04
Al FORMULA	2,64	2,64	2,64	2,63	2,70	2,59	2,73	2,69
Fe FORMULA	2,21	2,18	2,21	2,12	2,08	2,02	2,04	2,14
Mn FORMULA	0,05	0,05	0,05	0,05	0,05	0,04	0,05	0,05
Mg FORMULA	2,10	2,11	2,12	2,13	2,16	2,28	2,13	2,16
Ca FORMULA	1,53	1,55	1,51	1,54	1,63	1,67	1,63	1,54
Na FORMULA	0,54	0,52	0,53	0,51	0,49	0,49	0,50	0,49
K FORMULA	0,06	0,06	0,06	0,06	0,06	0,07	0,06	0,06
F FORMULA	0,10	0,07	0,09	0,09	0,10	0,08	0,08	0,09
Cr FORMULA	0,00	0,00	0,00	0,01	0,00	0,00	0,00	0,00
Cl FORMULA	0,00	0,00	0,00	0,01	0,00	0,00	0,00	0,00
O FORMULA	24,00	24,00	24,00	24,00	24,00	24,00	24,00	24,00
H FORMULA	2,01	2,01	2,01	2,07	2,01	2,01	2,01	2,01
X-POS	-31,26	-31,27	-31,29	-31,30	-31,32	-31,33	-31,35	-31,36
Y-POS	17,50	17,54	17,58	17,61	17,65	17,69	17,72	17,77

Appendix 5 – EMPA areas

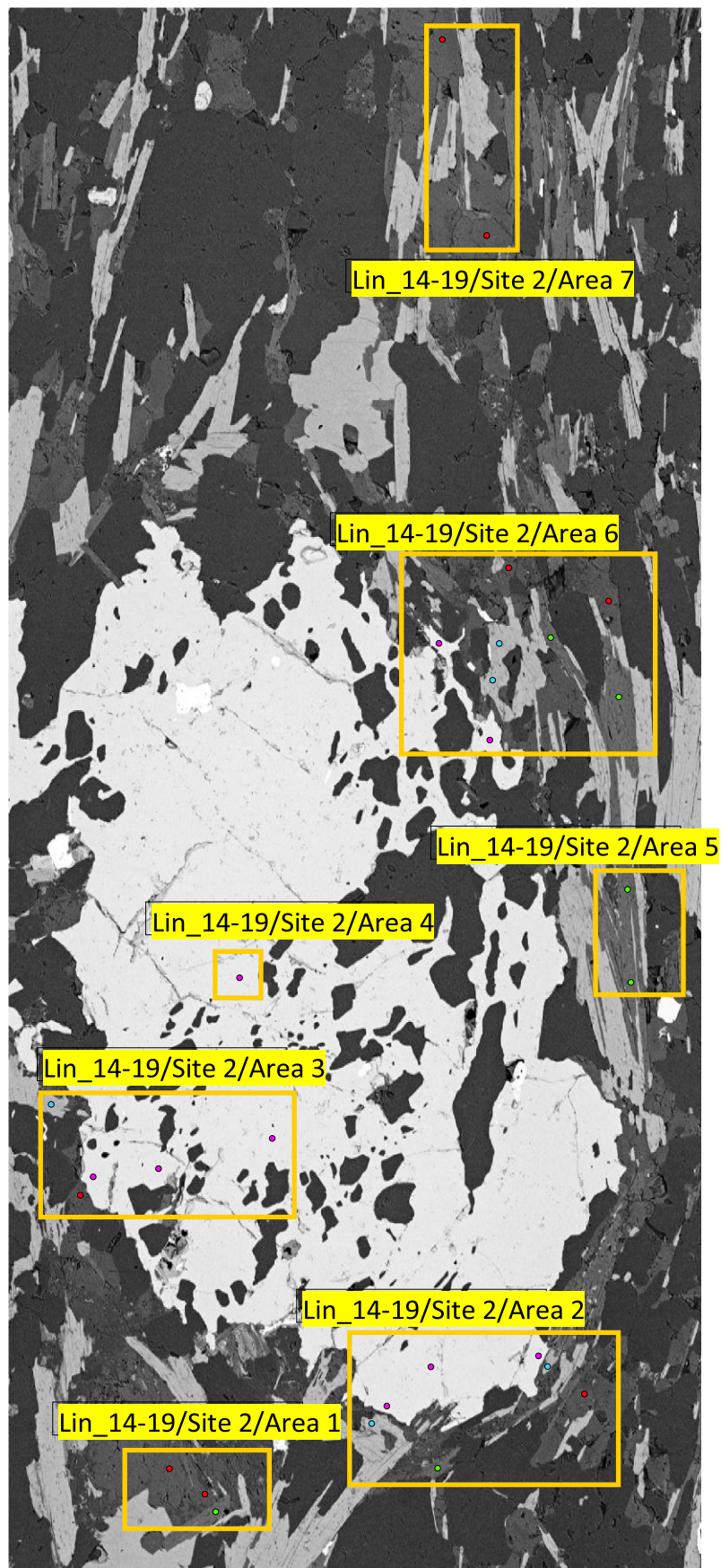
Lin_14-19



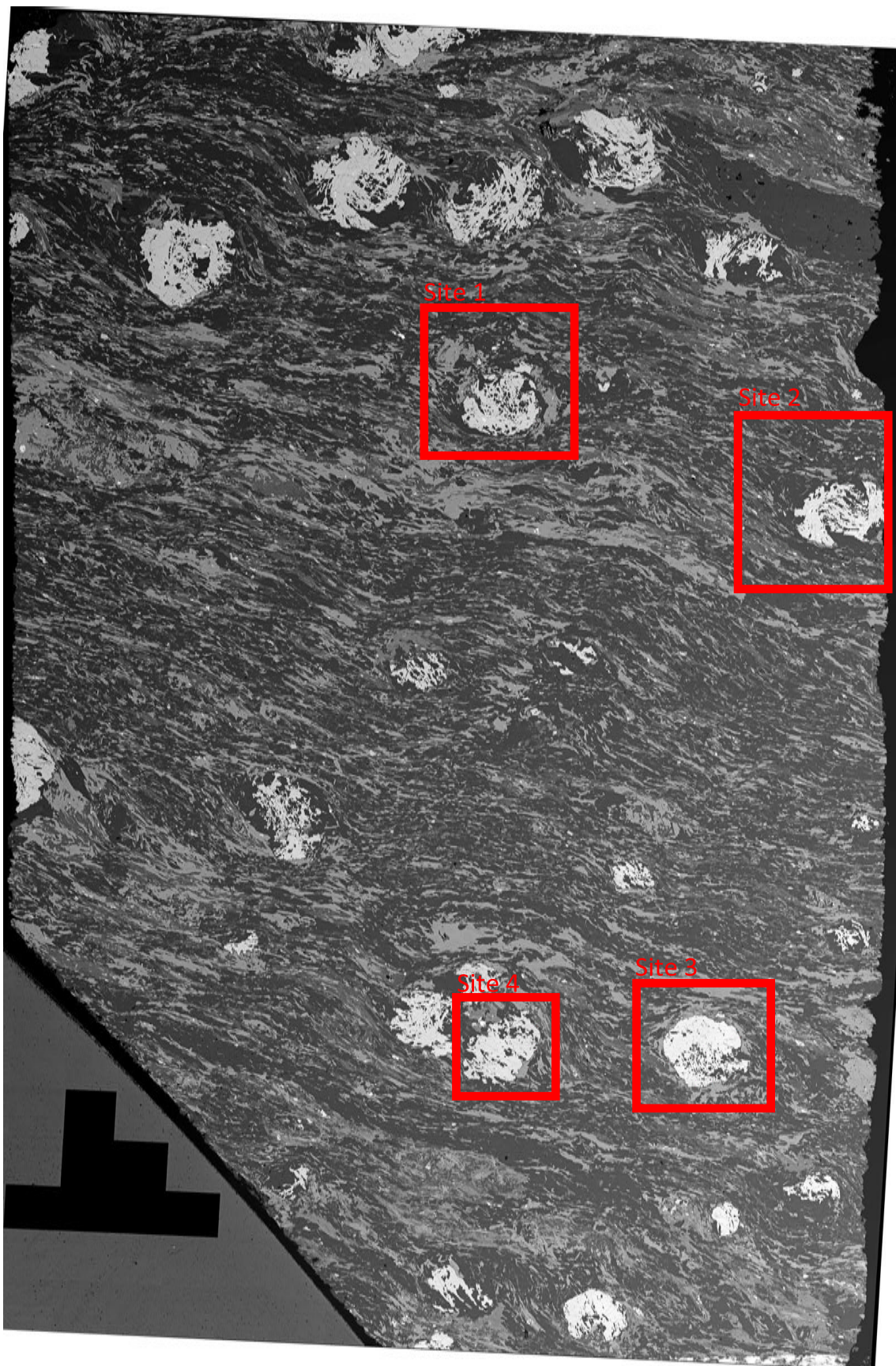
Lin_14-19/Site 1



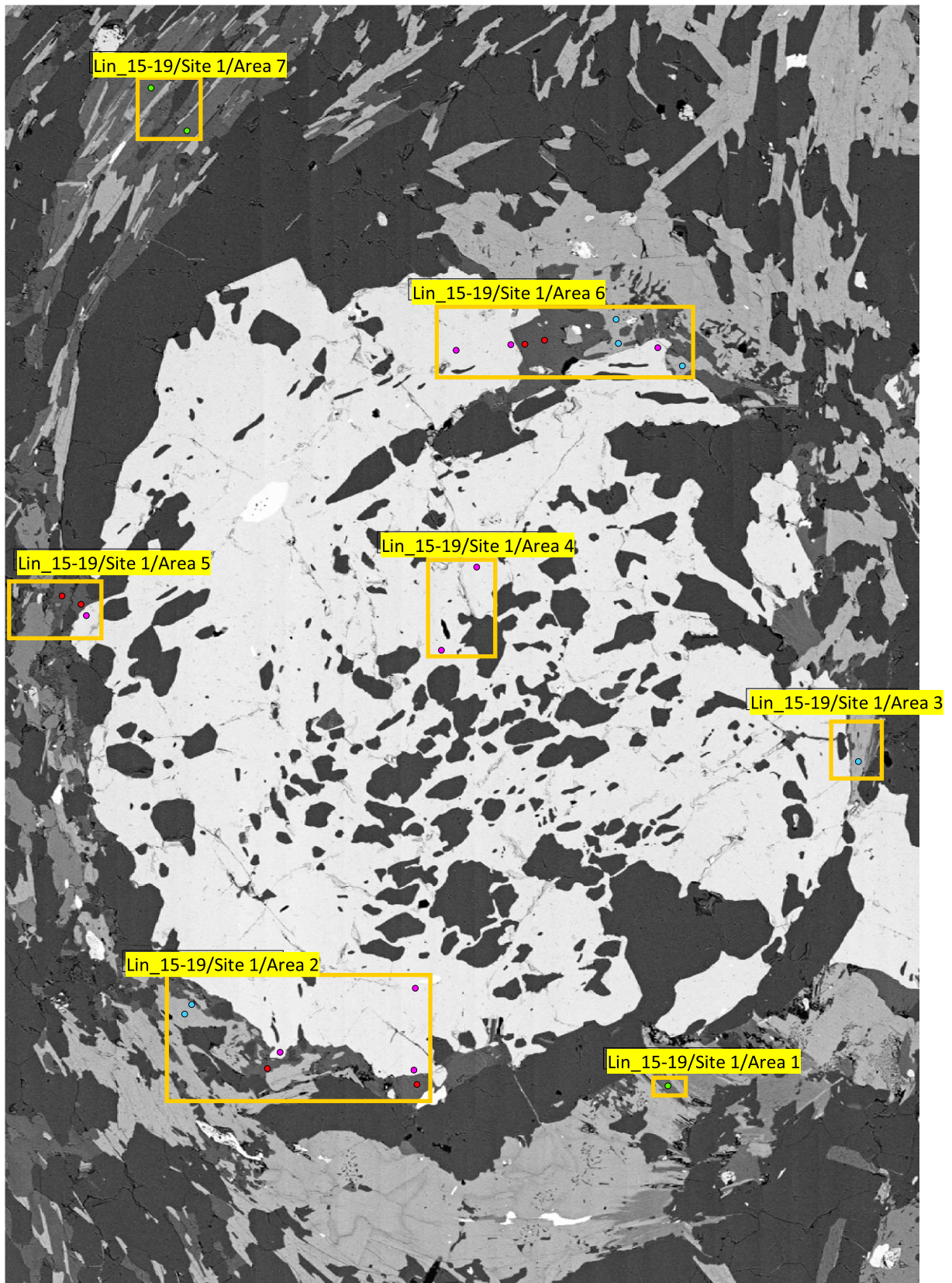
Lin_14-19/Site 2



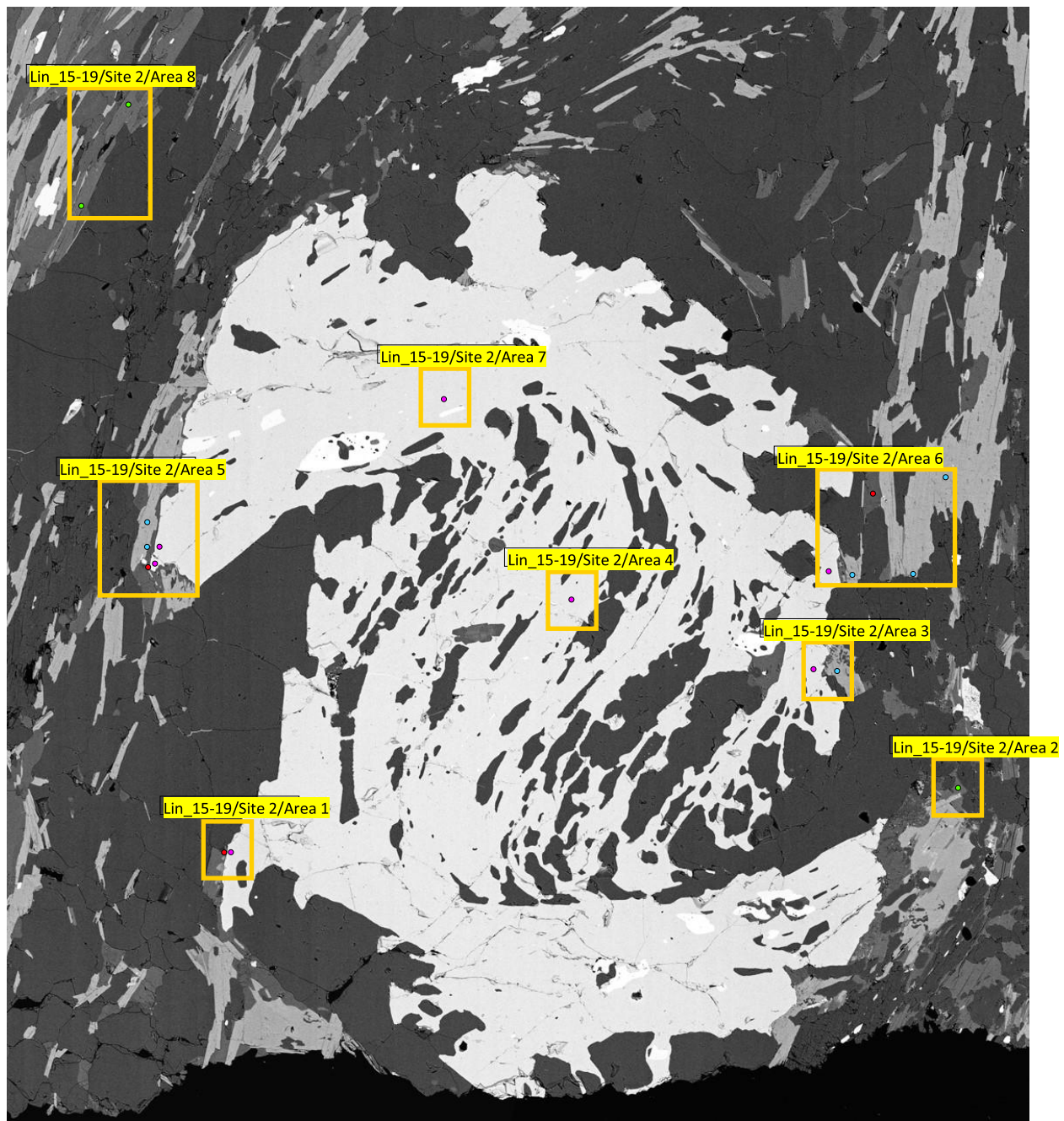
Lin_15-19



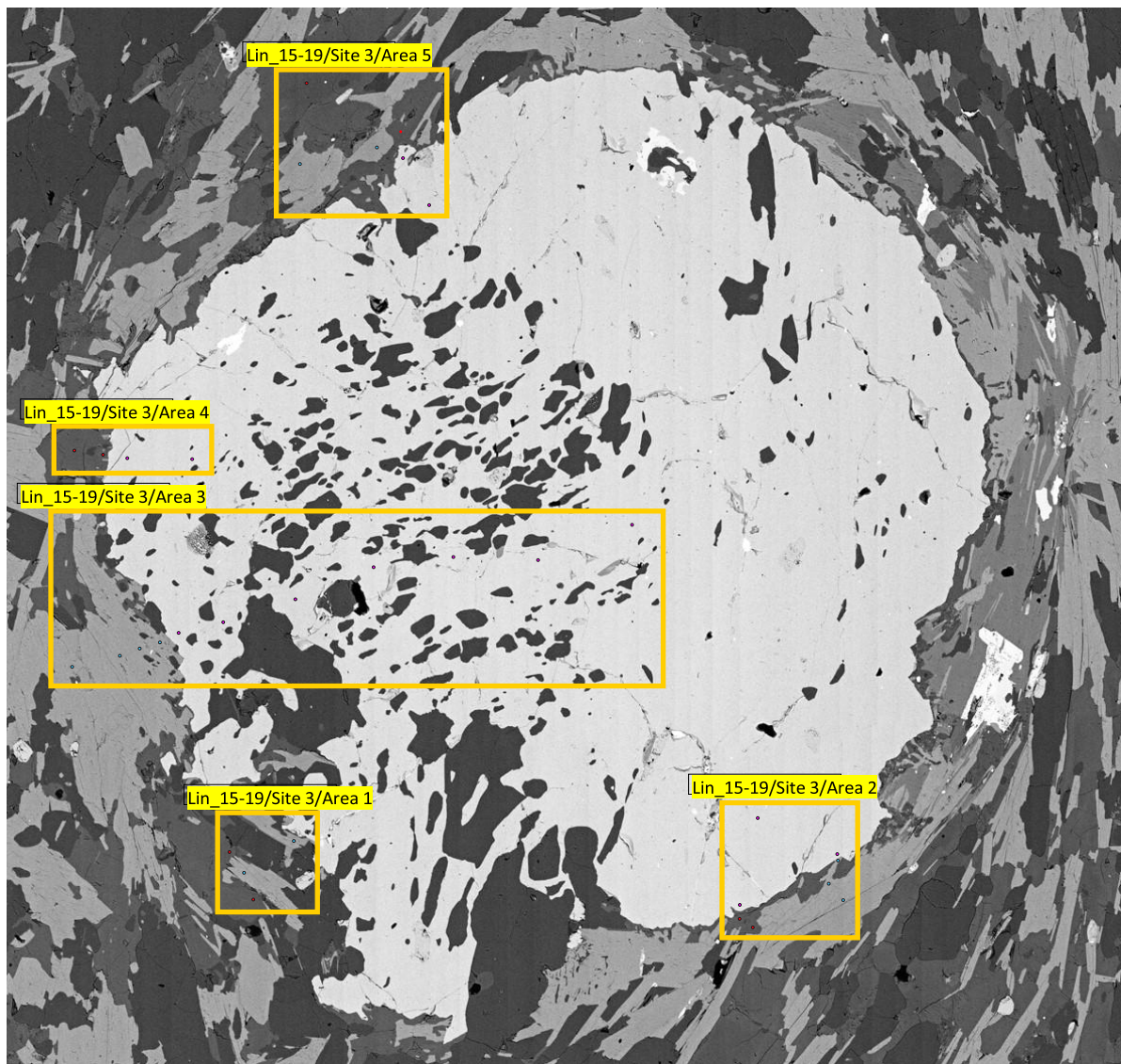
Lin_15-19/Site 1



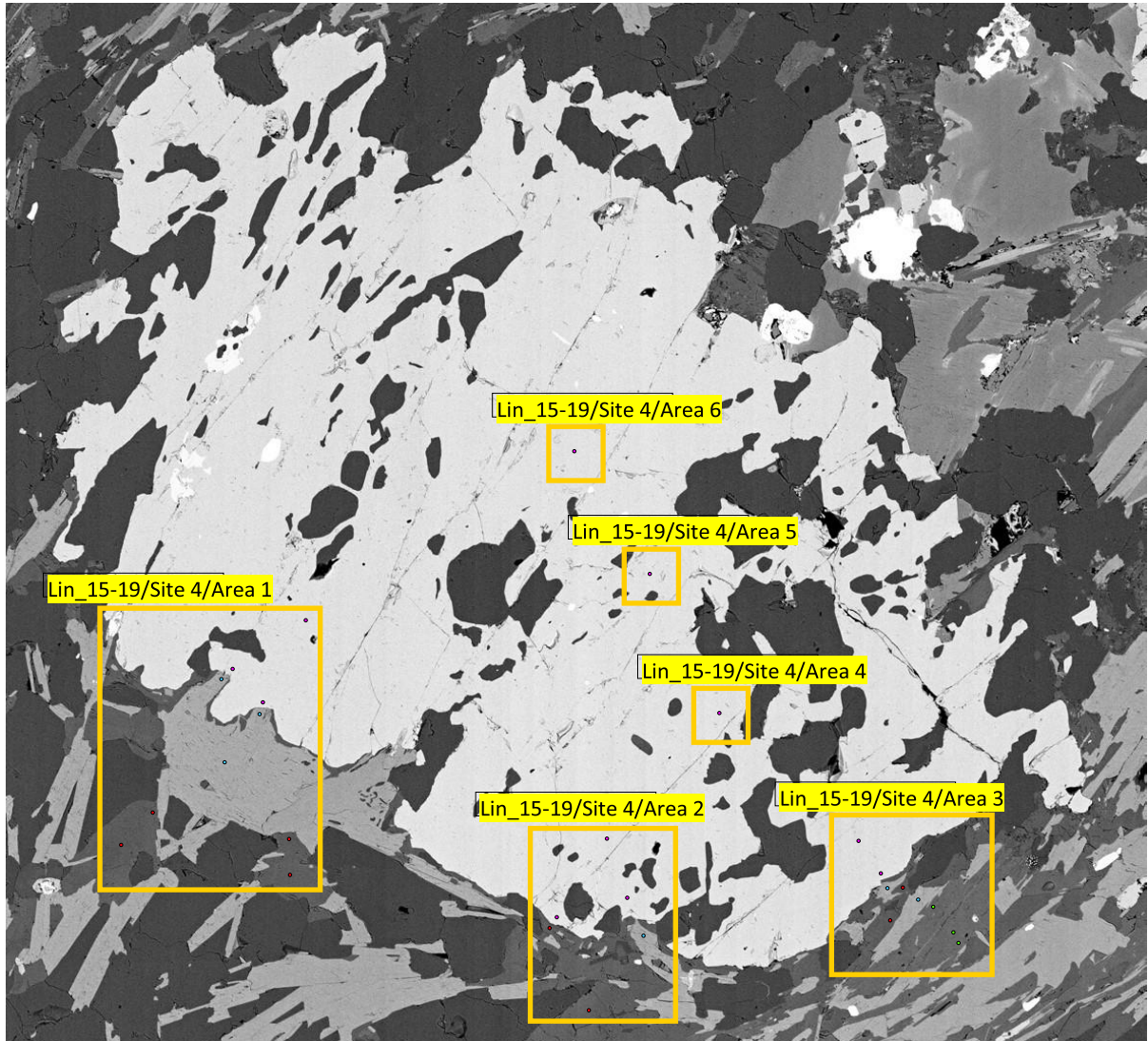
Lin_15-19/Site 2



Lin_15-19/Site 3



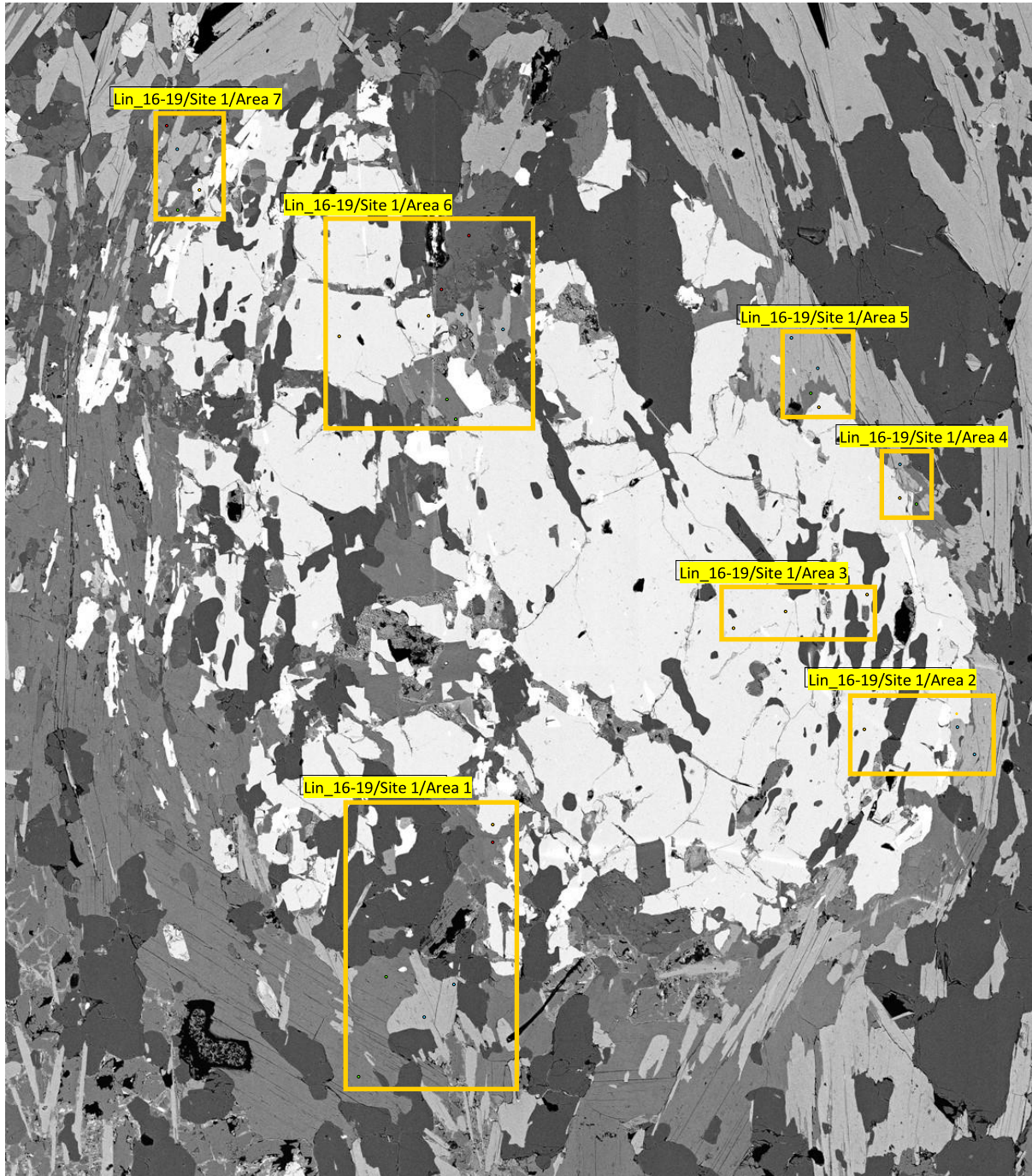
Lin_15-19/Site 4



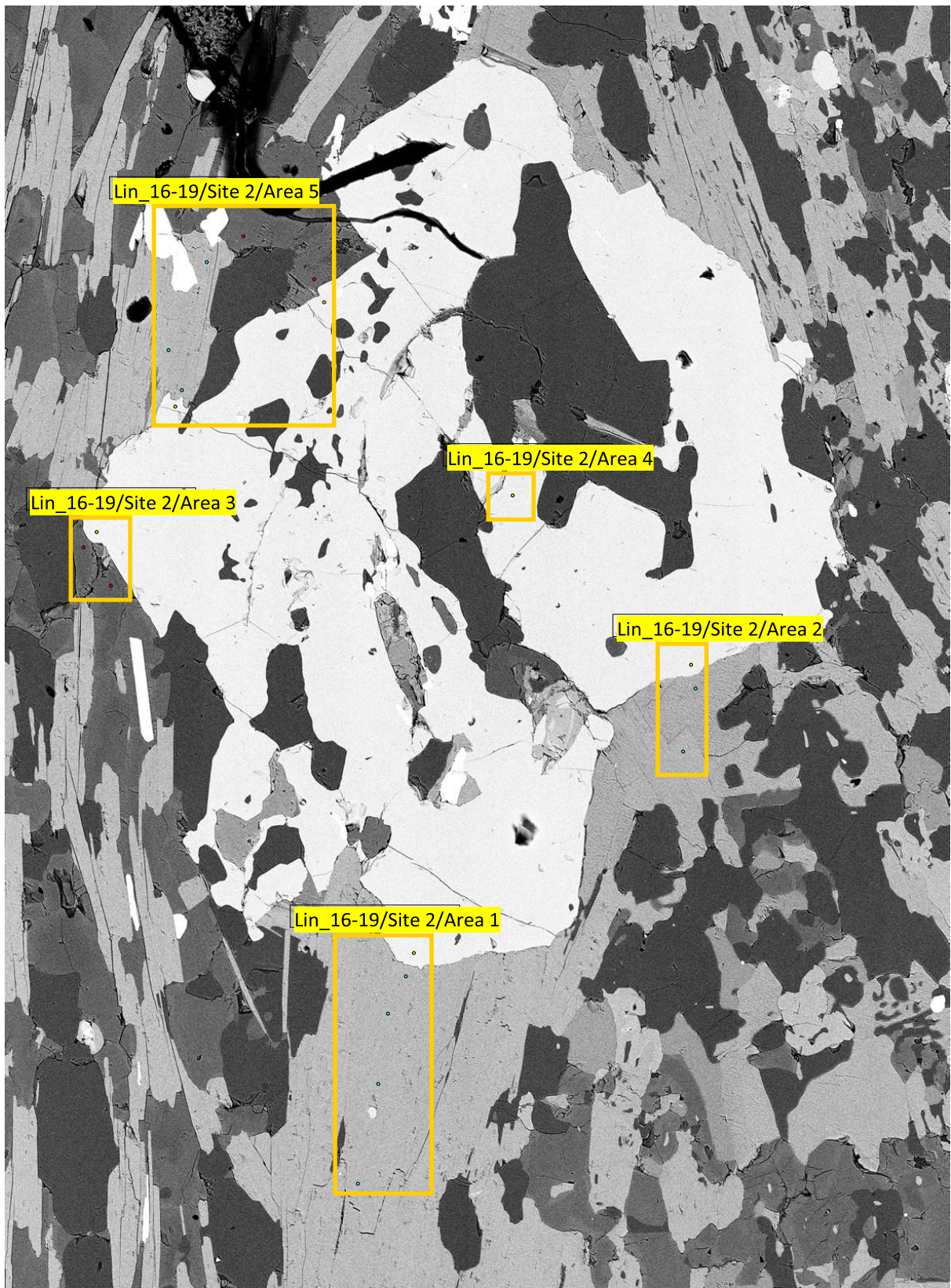
Lin_16-19



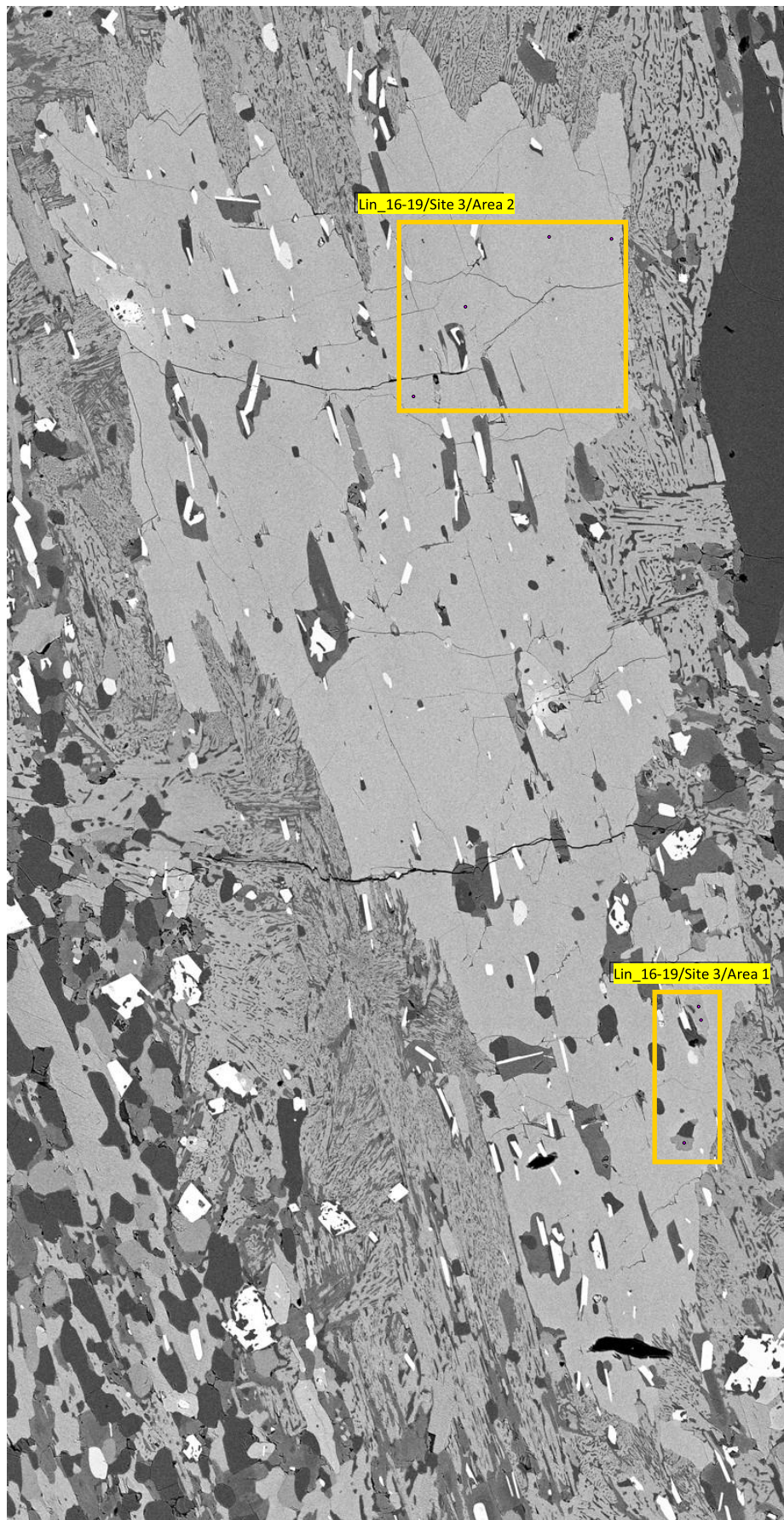
Lin_16-19/Site 1



Lin_16-19/Site 2



Lin_16-19/Site 3



Appendix 6 – LA-ICP-MS analysis

Sample	Si29	Si29 2SE	Ca43	Ca43 2SE	Ti47	Ti47 2SE	Ti49	Ti49 2SE	V51	V51 2SE	Cr52	Cr52 2SE
A1-S1	25398	16043	751	326	600000	0	602145	44650	1423	60	383	13
A1-S2	87546	17578	4719	513	600000	0	727714	43681	1233	43	386	13
A5-S1	585725	88266	18880	6226	600000	0	1870377	161156	2178	124	1063	82
A5-S2	-451	11944	-14,1	212	600000	0	552194	30489	1101	40	526	16
A5-S3	46981	10777	1934	428	600000	0	501410	32938	1151	59	529	32
A5-S4	94902	14068	1566	371	600000	0	528780	25381	1330	62	502	16
A5-S5	-6478	12926	2027	542	600000	0	419557	19539	1182	61	429	14
A6-S1	52969	10861	1863	372	600000	0	426725	20829	1075	43	315	12
A8-S2	272857	21474	5322	478	600000	0	680435	33720	1401	50	415	16
A9-S2	698345	122386	120454	19352	600000	0	1762235	268872	1700	67	262	35
A9-S3	196322	32990	1429	741	600000	0	822161	68821	1683	74	487	25
<i>Group Stats</i>	<i>186738</i>	<i>145545</i>	<i>14448</i>	<i>21436</i>	<i>600000</i>	<i>0</i>	<i>808521</i>	<i>309730</i>	<i>1405</i>	<i>201</i>	<i>482</i>	<i>127</i>
NIST610												
NIST610	325634	11075	82335	2022	452	0	141	10	449	10	256	7
NIST610	339212	12544	82293	1943	452	0	147	11	460	10	259	7
NIST610	317354	10861	81449	1934	452	0	142	11	457	10	257	8
NIST610	327709	12284	82433	1861	452	0	100	11	474	10	266	7
NIST610	328850	10501	82200	1917	452	0	119	9	487	12	263	7
NIST610	326041	11199	82205	1948	452	0	105	8	512	11	290	7
NIST610	330837	10110	82594	1932	452	0	121	10	515	12	287	8
NIST610	325848	9907	81981	1962	452	0	130	9	496	11	284	8
NIST610	325670	9989	81230	1880	452	0	116	8	504	13	282	8
NIST610	324595	10878	82719	1884	452	0	104	10	514	13	282	7
NIST610	341617	12334	83318	2324	452	0	-44,7	12,1	911	25	270	8
NIST610	338841	10997	82073	1873	452	0	78,3	8,5	894	22	263	7
NIST610	312262	9806	80969	1983	452	0	163	11	843	21	240	7
NIST610	329144	11569	82640	2075	452	0	68,1	8,4	850	22	240	7

Sample	Si29	Si29 2SE	Ca43	Ca43 2SE	Ti47	Ti47 2SE	Ti49	Ti49 2SE	V51	V51 2SE	Cr52	Cr52 2SE
NIST610	325561	9364	81904	1765	452	0	109	8	527	11	278	7
NIST610	328533	9521	82280	1966	452	0	124	8	525	13	281	8
NIST610	321138	9827	83101	1938	452	0	130	9	516	12	280	7
NIST610	323952	9243	81383	1713	452	0	106	9	506	11	280	6
NIST610	334569	9944	82274	1663	452	0	127	8	512	10	278	7
NIST610	328130	9722	82393	1730	452	0	116	8	739	17	278	7
NIST610	329499	11184	81511	2045	452	0	116	8	709	17	272	7
NIST610	321520	9890	82487	1868	452	0	115	9	681	15	270	7
NIST610	327020	10183	82033	1715	452	0	127	9	641	13	270	7
NIST610	330473	9466	82178	1855	452	0	113	8	593	13	275	7
<i>Group Stats</i>	327667	2682	82166	229	452	0	111	16	596	61	271	5
<i>Reference</i>	327180	0	82144	0	452	10	452	10	450	9	408	10
NIST612												
NIST612	440720	86817	100969	17821	44,0	0,0	22,0	23,1	46,6	9,3	31,5	5,6
NIST612	407566	73471	92746	17115	44,0	0,0	38,4	20,7	41,2	8,7	29,8	5,8
NIST612	423344	83025	91782	22879	44,0	0,0	52,7	26,0	41,3	10,7	33,1	6,9
NIST612	440885	64474	107088	16632	44,0	0,0	19,1	22,4	50,7	8,3	32,9	4,9
NIST612	460349	58991	110530	13961	44,0	0,0	23,9	23,4	51,9	6,8	34,3	5,2
NIST612	143047	235674	50959	44113	44,0	0,0	11,0	30,5	22,8	21,8	37,4	17,1
NIST612	336149	114071	85263	20528	44,0	0,0	41,1	17,3	46,7	10,9	30,2	6,0
NIST612	420054	66880	105161	17393	44,0	0,0	38,3	19,7	55,1	9,7	31,9	5,7
NIST612	362181	62162	91898	14825	44,0	0,0	28,5	17,2	49,1	8,1	31,5	6,2
NIST612	458813	130081	118968	31787	44,0	0,0	37,4	24,4	63,8	17,4	42,4	21,2
NIST612	681133	342527	147052	78472	44,0	0,0	61,4	57,7	145	79	24,9	16,9
NIST612	465722	165629	97050	34141	44,0	0,0	18,6	29,4	94,9	35,2	26,2	7,3
NIST612	298096	162991	59527	34237	44,0	0,0	10,3	29,2	52,9	36,3	25,3	10,3
NIST612	408696	179301	87174	40023	44,0	0,0	13,5	30,6	86,2	43,8	38,1	12,0
NIST612	386518	185653	89587	38769	44,0	0,0	26,6	30,6	87,0	40,6	28,5	16,3

Sample	Si29	Si29 2SE	Ca43	Ca43 2SE	Ti47	Ti47 2SE	Ti49	Ti49 2SE	V51	V51 2SE	Cr52	Cr52 2SE
NIST612	393298	69893	98381	17157	44,0	0,0	46,4	20,3	56,3	10,0	30,3	5,8
NIST612	306404	81919	81390	33166	44,0	0,0	32,8	27,9	43,7	18,4	29,6	7,8
NIST612	358197	404400	111083	104302	44,0	0,0	-59,8	126	59,3	56,4	19,6	46,3
NIST612	319972	41941	82041	11441	44,0	0,0	52,3	21,9	44,8	6,3	19,9	3,6
NIST612	448389	209425	96356	63227	44,0	0,0	29,2	32,0	67,1	29,1	32,5	15,2
NIST612	416974	142731	99549	33345	44,0	0,0	19,2	19,6	63,0	29,2	34,7	12,4
NIST612	398354	138493	77385	40947	44,0	0,0	53,0	29,3	52,3	34,5	32,1	7,4
NIST612	355318	154060	81469	40882	44,0	0,0	16,6	30,4	70,4	30,1	27,1	7,7
NIST612	309305	183117	82615	45711	44,0	0,0	35,7	23,7	63,1	36,4	35,7	11,0
NIST612	529415	154205	123996	36325	44,0	0,0	37,9	18,5	85,7	23,7	31,3	5,5
<i>Group Stats</i>	398756	38599	94801	7897	44,0	0,0	28,2	9,3	61,6	9,7	30,8	2,1
<i>Reference</i>	336061	0	85002	0	44,0	2,3	44,0	2,3	38,8	1,2	36,4	1,5
RR632												
R632	2671	15765	-85	250	600000	0	599161	23106	1183	46	190	11
R632	-991	15685	-61	286	600000	0	599324	27233	1157	55	185	11
R632	10970	14404	-315	245	600000	0	605231	23726	1198	41	199	10
R632	8993	14401	-132	254	600000	0	594517	25481	1164	42	194	10
R632	17305	14218	-216	226	600000	0	601542	24575	1186	49	181	9
R632	-1369	18544	-19,5	287	600000	0	601675	26363	1181	48	185	12
R632	23332	11670	-242	261	600000	0	594362	27273	1171	44	193	12
R632	-8211	17693	-88,0	309	600000	0	613229	27534	1185	43	190	11
R632	-11382	14947	-74,9	228	600000	0	586045	26115	1183	43	186	11
R632	-15679	15706	-164	265	600000	0	606593	27797	1176	38	193	12
R632	-6265	11967	-151	274	600000	0	597226	25648	1175	42	185	10
R632	16162	12703	34,7	258	600000	0	603610	21981	1185	38	200	9
R632	2765	12008	-10,5	246	600000	0	603616	24751	1189	43	189	9
R632	3219	10721	151	262	600000	0	590515	23623	1161	37	183	9

Sample	Si29	Si29 2SE	Ca43	Ca43 2SE	Ti47	Ti47 2SE	Ti49	Ti49 2SE	V51	V51 2SE	Cr52	Cr52 2SE
R632	6545	11322	-31,6	247	600000	0	604350	22773	1191	43	190	10
R632	5063	11840	159	251	600000	0	595821	26215	1161	53	184	10
R632	26476	11908	166	279	600000	0	610876	26563	1203	47	198	10
R632	4141	11469	215	284	600000	0	592186	23256	1173	43	191	10
R632	-7158	11903	441	267	600000	0	603927	23174	1177	40	192	9
R632	-2717	10571	45,6	267	600000	0	599185	24224	1179	41	183	9
<i>Group Stats</i>	<i>3693</i>	<i>5014</i>	<i>-18,9</i>	<i>80</i>	<i>600000</i>	<i>0</i>	<i>600150</i>	<i>3016</i>	<i>1179</i>	<i>5</i>	<i>190</i>	<i>2</i>
<i>Reference</i>					<i>600000</i>	<i>10000</i>	<i>600000</i>	<i>10000</i>	<i>1179</i>	<i>0</i>	<i>190</i>	<i>32</i>

All values are in ppm

2SE = 2 standard error

Sample	Cr53	Cr53 2SE	Fe56	Fe56 2SE	Fe57	Fe57 2SE	Zr90	Zr90 2SE	Zr91	Zr91 2SE	Nb93	Nb93 2SE
A1-S1	380	12	1909	178	1664	71	145	3	129	4	1525	62,4
A1-S2	389	13	2199	227	1823	83	143	4	126	4	1116	47,4
A5-S1	1091	80	34852	3792	27586	2588	143	10	129	12	2486	204
A5-S2	525	19	4045	478	3016	344	151	4	132	6	1648	69,4
A5-S3	634	23	3176	254	2853	147	146	5	133	6	2349	90,1
A5-S4	498	17	13225	1266	10515	1019	148	5	139	8	1854	93,7
A5-S5	438	15	5516	652	4325	417	144	4	125	4	1294	72,9
A6-S1	318	11	5897	448	2955	113	126	5	114	4	1164	74,6
A8-S2	418	16	10647	1674	10460	1630	148	5	132	5	792	30,7
A9-S2	234	17	371	312	1533	168	137	6	117	8	1706	86,9
A9-S3	463	21	84466	6847	85160	7007	152	5	136	6	1076	51,2
<i>Group Stats</i>	490	136	15118	15043	13808	15002	144	4	128	5	1546	322
NIST610												
NIST610	267	8	352	84	829	46	454	10	401	10	288	7
NIST610	269	8	296	76	678	36	461	10	401	10	293	7
NIST610	265	8	478	81	580	29	454	11	394	10	288	7
NIST610	268	8	208	65	490	27	462	9	398	9	292	6
NIST610	271	8	185	56	451	24	455	10	390	9	292	7
NIST610	287	8	46,2	48,6	352	21	468	12	410	11	307	8
NIST610	284	8	33,3	51,3	363	19	466	13	407	10	305	8
NIST610	287	9	55,3	49,6	352	19	454	11	404	10	298	8
NIST610	277	8	58,5	49,7	349	21	454	12	401	11	291	7
NIST610	278	7	-2,51	51,6	333	20	455	13	406	12	297	7
NIST610	285	9	202	69	-781	49	516	17	438	14	309	9
NIST610	279	8	118	62	-799	46	502	15	426	12	297	8
NIST610	257	7	67,8	55,6	-668	40	479	15	408	12	282	7
NIST610	267	8	200	62	-574	41	512	18	430	14	297	10

Sample	Cr53	Cr53 2SE	Fe56	Fe56 2SE	Fe57	Fe57 2SE	Zr90	Zr90 2SE	Zr91	Zr91 2SE	Nb93	Nb93 2SE
NIST610	282	8	385	65	695	36	449	10	398	9	295	7
NIST610	285	8	289	62	581	30	453	11	404	10	298	7
NIST610	283	8	269	47	514	26	457	11	412	12	295	7
NIST610	283	7	233	42	491	23	452	10	402	9	294	7
NIST610	279	8	181	40	386	21	460	10	405	9	294	7
NIST610	280	8	401	74	821	44	459	10	399	9	301	7
NIST610	271	8	332	60	720	36	451	11	397	10	296	8
NIST610	280	8	275	56	603	31	458	10	400	9	299	7
NIST610	273	7	228	47	533	28	449	9	396	10	292	6
NIST610	277	9	194	37	440	21	463	11	398	9	294	7
<i>Group Stats</i>	276	3	212	52	322	201	464	8	405	5	296	2
<i>Reference</i>	408	10	458	9	458	9	448	9	448	9	465	34
NIST612												
NIST612	30,5	5,6	219	249	767	348	51,3	9,6	43,4	9,4	28,5	5,1
NIST612	26,0	4,7	346	167	365	133	47,2	8,6	40,5	7,4	26,3	5,2
NIST612	29,9	6,9	282	215	309	137	43,9	11,8	41,7	11,9	26,1	6,4
NIST612	28,5	4,5	85,2	124	159	92	52,3	8,7	43,0	5,3	31,3	5,2
NIST612	31,9	4,9	72,5	97,2	173	60	53,9	7,1	47,6	6,3	31,6	3,9
NIST612	15,7	10,0	179	115	88,1	38,1	22,9	22,8	20,2	19,5	15,5	13,4
NIST612	30,1	8,5	-7,89	48,5	43,1	26,6	38,9	14,1	37,3	10,1	25,5	7,0
NIST612	29,6	4,5	32,6	46,0	30,0	25,0	49,0	8,9	44,5	7,7	31,7	5,4
NIST612	25,4	4,7	28,3	44,9	23,2	21,9	43,0	8,2	38,4	7,7	27,0	4,9
NIST612	35,3	8,1	-6,46	55	52,5	61,8	57,3	14,6	49,9	12,3	36,6	10,3
NIST612	28,9	9,1	169	276	-333	419	85,7	46,8	76,2	46,0	50,4	28,3
NIST612	32,8	13,8	-7,86	113	-199	104	51,1	25,6	41,7	20,0	30,8	12,1
NIST612	16,4	12,5	-60,8	117	-172	118	29,5	22,4	23,9	18,1	18,8	12,8
NIST612	28,5	12,8	-66,2	108	-167	117	47,8	25,3	47,8	26,6	28,8	14,1
NIST612	20,9	13,2	-64,3	100	-15,9	135	44,0	25,5	48,6	14,5	26,2	13,7

Sample	Cr53	Cr53 2SE	Fe56	Fe56 2SE	Fe57	Fe57 2SE	Zr90	Zr90 2SE	Zr91	Zr91 2SE	Nb93	Nb93 2SE
NIST612	29,3	5,2	-8007	4840	418	158	48,2	9,3	38,3	6,9	27,0	4,6
NIST612	23,1	9,2	947	795	238	129	36,3	14,4	36,9	10,3	22,5	9,4
NIST612	50,1	31,0	-45,4	651	-158	405	57,6	49,4	92,3	78,1	31,6	30,2
NIST612	22,9	3,7	89,6	103	120	35	35,9	5,5	32,8	4,4	23,6	3,3
NIST612	25,8	15,9	-16,3	178	43,0	112	55,6	24,0	42,5	23,4	26,0	19,1
NIST612	27,1	12,1	107	137	88,0	97,8	49,2	16,7	37,0	18,8	30,8	10,3
NIST612	18,5	16,3	70,9	158	111	130	39,6	20,2	43,7	16,5	24,5	11,7
NIST612	25,4	10,3	97,1	155	170	94	38,0	21,7	41,1	14,8	23,8	13,9
NIST612	32,6	9,0	135	123	161	98	39,6	23,5	36,0	20,2	24,9	14,0
NIST612	37,2	11,7	99,2	106	95,8	64,3	64,6	22,3	55,2	19,1	36,9	11,0
<i>Group Stats</i>	28,1	2,8	-213	655	96,4	90,1	47,3	4,9	44,0	5,8	28,3	2,7
<i>Reference</i>	36,4	1,5	51,0	2,0	51,0	2,0	37,9	1,2	37,9	1,2	38,9	2,1
RR632												
R632	193	10	3005	230	3000	142	4236	223	4301	171	449	16
R632	189	10	3002	211	3022	161	4487	249	4459	184	451	19
R632	199	10	3011	202	2999	134	4358	207	4451	167	449	16
R632	183	8	3012	191	3007	134	4242	191	4237	162	436	16
R632	185	9	3001	201	3005	141	4294	215	4281	158	440	16
R632	189	9	3003	178	3003	146	4440	226	4358	161	447	17
R632	195	10	3039	214	3017	139	4147	225	4274	149	455	17
R632	188	10	2929	214	2982	139	4631	251	4423	139	443	16
R632	187	9	3077	198	3030	144	4396	243	4194	145	434	16
R632	189	9	2979	222	3000	133	4278	210	4332	146	448	16
R632	187	9	2987	197	2992	135	4384	252	4314	169	439	19
R632	195	8	3046	183	3034	116	4431	232	4514	151	467	15
R632	193	9	2983	186	2983	120	4311	217	4358	155	439	15
R632	178	9	3000	185	3011	142	4172	216	4192	143	425	15

Sample	Cr53	Cr53 2SE	Fe56	Fe56 2SE	Fe57	Fe57 2SE	Zr90	Zr90 2SE	Zr91	Zr91 2SE	Nb93	Nb93 2SE
R632	194	9	3011	170	3008	135	4256	202	4319	154	455	16
R632	193	9	2964	186	2987	134	4388	239	4338	176	440	18
R632	190	10	3030	167	3046	140	4451	240	4406	165	452	17
R632	191	8	3031	172	3019	136	4290	229	4355	154	437	16
R632	186	8	2953	181	2968	120	4314	196	4274	123	449	15
R632	190	9	3030	185	3043	132	4311	222	4318	158	446	18
<i>Group Stats</i>	<i>190</i>	<i>2</i>	<i>3005</i>	<i>15</i>	<i>3008</i>	<i>9</i>	<i>4341</i>	<i>51</i>	<i>4335</i>	<i>38</i>	<i>445</i>	<i>4</i>
<i>Reference</i>	<i>190</i>	<i>32</i>	<i>3006</i>	<i>303</i>	<i>3006</i>	<i>303</i>	<i>4330</i>	<i>51</i>	<i>4330</i>	<i>51</i>	<i>445</i>	<i>262</i>

Sample	Mo95	Mo95 2SE	Mo98	Mo98 2SE	Sn117	Sn117 2SE	Sn118	Sn118 2SE	Sb121	Sb121 2SE	Hf178	Hf178 2SE
A1-S1	1,26	0,28	0,973	0,163	196	8	199	8	0,736	0,114	6,93	0,43
A1-S2	1,33	0,34	1,18	0,22	213	9	212	9	0,993	0,133	6,22	0,39
A5-S1	1,62	1,05	2,28	0,82	297	21	312	22	1,21	0,44	5,94	0,99
A5-S2	1,40	0,26	1,11	0,17	177	8	180	8	0,867	0,120	6,84	0,41
A5-S3	1,11	0,30	1,25	0,23	178	7	178	7	0,721	0,109	6,40	0,43
A5-S4	2,03	0,42	1,53	0,26	210	10	208	9	0,755	0,101	7,73	0,64
A5-S5	1,36	0,28	1,25	0,20	155	6	158	6	0,575	0,088	6,31	0,39
A6-S1	1,80	0,34	1,59	0,21	179	7	174	6	0,784	0,110	4,97	0,40
A8-S2	1,48	0,36	1,21	0,25	164	7	168	6	0,682	0,114	6,86	0,49
A9-S2	2,22	1,02	1,52	0,66	232	18	230	17	0,914	0,301	5,96	0,72
A9-S3	0,978	0,379	1,70	0,35	201	10	202	8	0,749	0,149	6,70	0,55
<i>Group Stats</i>	<i>1,51</i>	<i>0,23</i>	<i>1,42</i>	<i>0,22</i>	<i>200</i>	<i>24</i>	<i>202</i>	<i>26</i>	<i>0,817</i>	<i>0,105</i>	<i>6,44</i>	<i>0,43</i>
NIST610												
NIST610	400	10	389	10	298	7	303	8	254	6	402	9
NIST610	398	11	395	11	298	8	307	8	256	7	402	9
NIST610	397	11	384	10	292	7	297	8	252	6	391	10
NIST610	406	11	392	10	297	7	303	7	253	6	400	9
NIST610	399	11	396	11	295	7	299	7	254	6	401	9
NIST610	415	11	416	10	298	7	294	7	255	6	389	10
NIST610	415	10	415	11	298	8	294	7	257	6	393	12
NIST610	410	10	413	10	292	8	292	7	254	6	390	11
NIST610	405	11	401	10	291	8	289	7	253	6	382	11
NIST610	414	11	415	10	299	9	294	7	255	7	392	13
NIST610	436	16	444	14	342	12	329	10	269	8	487	19
NIST610	420	12	426	13	322	11	317	9	254	7	425	15
NIST610	402	12	399	11	298	10	287	7	234	6	382	13
NIST610	414	13	417	13	329	12	307	9	245	7	449	21

Sample	Mo95	Mo95 2SE	Mo98	Mo98 2SE	Sn117	Sn117 2SE	Sn118	Sn118 2SE	Sb121	Sb121 2SE	Hf178	Hf178 2SE
NIST610	413	10	391	9	280	7	291	6	246	5	373	8
NIST610	425	10	400	11	292	8	296	8	250	6	387	10
NIST610	417	10	400	10	287	7	293	7	251	6	381	9
NIST610	413	10	393	10	289	7	290	6	247	6	385	9
NIST610	412	10	398	11	290	7	291	7	248	6	388	9
NIST610	409	10	399	9	290	8	288	6	252	6	390	9
NIST610	399	10	385	9	285	7	283	7	250	6	390	10
NIST610	404	10	398	10	290	7	288	7	252	6	388	10
NIST610	396	9	393	9	282	6	285	7	248	6	389	9
NIST610	406	11	393	10	297	8	287	6	251	6	393	9
<i>Group Stats</i>	409	4	402	6	297	6	296	4	252	2	398	10
<i>Reference</i>	417	21	417	21	430	29	430	29	396	19	435	12
NIST612												
NIST612	43,0	7,4	42,0	8,2	31,5	5,9	33,3	6,0	27,6	5,2	41,8	7,4
NIST612	40,7	7,7	38,4	7,4	27,4	5,9	29,2	6,7	23,3	5,2	39,1	7,9
NIST612	43,5	10,6	38,3	9,4	31,6	8,7	34,5	8,1	24,8	6,2	44,8	13,6
NIST612	47,2	9,3	45,3	8,1	33,8	4,8	36,5	5,6	29,1	5,0	48,2	8,3
NIST612	46,2	6,2	45,8	5,8	37,5	5,3	36,3	4,4	29,2	3,6	45,6	6,3
NIST612	20,5	21,9	21,5	19,6	7,93	19,3	17,8	12,4	13,6	11,8	18,4	17,3
NIST612	34,2	11,6	38,3	7,7	31,7	9,6	24,4	10,0	22,5	6,2	29,8	11,8
NIST612	49,0	8,5	45,5	7,6	31,9	4,7	28,7	4,5	26,2	4,4	39,6	7,0
NIST612	37,9	7,2	40,6	6,8	29,2	5,2	29,6	5,0	23,5	4,4	35,9	7,4
NIST612	51,3	12,5	52,9	15,7	34,5	11,4	38,0	11,6	30,5	7,7	46,6	12,8
NIST612	73,7	44,9	70,8	35,9	44,0	30,0	35,8	17,2	39,0	22,0	75,4	44,8
NIST612	43,0	20,3	42,3	18,5	26,3	10,8	32,9	10,8	25,3	11,4	41,3	21,1
NIST612	29,5	20,7	27,2	17,8	14,9	18,3	20,6	10,4	15,9	10,2	24,0	19,0
NIST612	43,8	21,4	39,9	20,2	32,7	15,5	32,0	14,9	26,4	13,0	42,2	23,8
NIST612	41,2	19,8	40,5	20,5	35,2	11,2	30,9	14,1	24,2	11,9	41,4	20,9

Sample	Mo95	Mo95 2SE	Mo98	Mo98 2SE	Sn117	Sn117 2SE	Sn118	Sn118 2SE	Sb121	Sb121 2SE	Hf178	Hf178 2SE
NIST612	44,3	8,0	39,4	6,5	29,5	5,2	28,8	4,6	25,7	4,5	38,4	7,0
NIST612	32,0	11,7	32,0	11,0	24,8	9,6	26,0	10,1	22,5	6,3	29,2	12,1
NIST612	41,0	52,9	37,9	41,4	25,3	30,6	34,5	27,2	28,2	31,0	40,6	43,3
NIST612	36,3	4,7	33,2	4,9	23,6	3,5	24,0	3,4	20,5	3,0	29,5	5,1
NIST612	42,6	29,5	47,2	23,2	36,1	14,6	29,8	18,3	28,9	13,0	37,8	25,3
NIST612	44,1	14,3	44,2	15,1	31,5	10,1	27,4	11,1	25,8	8,8	37,2	16,6
NIST612	39,9	14,5	36,9	15,6	29,3	13,1	25,1	11,9	19,9	11,3	31,8	17,4
NIST612	48,7	14,7	31,6	19,8	34,3	14,0	28,0	11,2	19,6	12,1	33,0	17,8
NIST612	40,5	17,9	35,6	20,0	28,9	14,1	26,8	10,5	26,0	10,4	37,5	16,3
NIST612	47,6	12,5	56,9	19,0	34,1	11,5	34,6	8,9	27,8	7,0	52,6	16,6
<i>Group Stats</i>	42,5	3,8	41,0	3,9	29,9	2,9	29,8	2,1	25,0	2,0	39,3	4,3
<i>Reference</i>	37,4	1,5	37,4	1,5	38,6	1,3	38,6	1,3	34,7	1,8	36,7	1,2
RR632												
R632	18,7	1,1	18,5	1,0	286	10	283	11	1,26	0,14	107	5
R632	18,3	1,3	17,7	1,1	275	11	283	12	1,25	0,14	110	5
R632	18,6	1,1	19,2	1,0	306	11	306	12	1,42	0,14	111	4
R632	18,4	1,2	17,5	1,0	303	12	302	12	1,28	0,14	105	4
R632	17,0	1,1	17,9	1,0	271	10	275	12	1,31	0,13	106	4
R632	18,9	1,4	19,2	1,1	291	11	282	13	1,19	0,15	108	4
R632	17,4	1,1	17,8	0,9	301	13	305	13	1,40	0,16	109	4
R632	19,4	1,2	18,5	1,1	303	11	306	12	1,26	0,15	109	4
R632	17,7	1,2	17,9	1,0	280	11	271	10	1,27	0,13	105	4
R632	17,9	1,2	18,0	1,0	287	11	291	11	1,36	0,16	111	5
R632	18,4	1,2	17,9	1,1	281	11	276	11	1,21	0,14	107	4
R632	18,4	1,2	19,0	1,0	300	11	302	10	1,38	0,14	110	4
R632	17,7	1,1	18,6	1,0	296	10	295	11	1,31	0,14	108	4
R632	18,1	1,2	17,2	1,0	272	10	274	10	1,22	0,12	104	4

Sample	Mo95	Mo95 2SE	Mo98	Mo98 2SE	Sn117	Sn117 2SE	Sn118	Sn118 2SE	Sb121	Sb121 2SE	Hf178	Hf178 2SE
R632	18,7	1,3	18,4	1,0	300	12	299	11	1,45	0,14	107	4
R632	18,2	1,1	17,9	0,9	283	12	277	10	1,33	0,14	107	4
R632	18,6	1,3	19,5	1,2	303	12	302	11	1,31	0,14	108	5
R632	18,2	1,2	17,2	1,0	286	10	287	11	1,22	0,13	110	4
R632	17,8	1,2	18,1	1,1	293	10	294	9	1,45	0,13	107	4
R632	18,2	1,2	18,7	0,9	279	11	283	11	1,21	0,11	108	4
<i>Group Stats</i>	<i>18,2</i>	<i>0,2</i>	<i>18,2</i>	<i>0,3</i>	<i>290</i>	<i>5</i>	<i>290</i>	<i>5</i>	<i>1,30</i>	<i>0,04</i>	<i>108</i>	<i>1</i>
<i>Reference</i>	<i>18,2</i>	<i>1,2</i>	<i>18,2</i>	<i>1,2</i>	<i>289</i>	<i>0</i>	<i>289</i>	<i>0</i>	<i>1,30</i>	<i>0,11</i>	<i>108</i>	<i>6</i>

Sample	Hf180	Hf180 2SE	Ta181	Ta181 2SE	W182	W182 2SE	W183	W183 2SE
A1-S1	6,98	0,33	141	4	131	4	134	4
A1-S2	6,80	0,38	103	3	98,1	2,7	100	3
A5-S1	7,86	1,09	146	7	205	11	207	14
A5-S2	6,79	0,33	81,8	2,3	71,1	3,0	72,7	3,1
A5-S3	6,75	0,42	111	3	89,0	3,3	86,9	3,7
A5-S4	7,00	0,38	92,9	3,7	139	5	140	6
A5-S5	6,43	0,37	58,6	2,1	57,3	2,0	55,0	2,2
A6-S1	4,94	0,30	66,7	4,1	56,6	2,3	56,6	2,3
A8-S2	7,47	0,46	57,2	2,9	202	9	200	10
A9-S2	5,64	0,61	201	10	141	6	140	7
A9-S3	7,94	0,59	110	4	114	4	114	5
<i>Group Stats</i>	6,78	0,54	106	26	119	31	119	31
NIST610								
NIST610	358	8	472	12	374	10	381	10
NIST610	366	8	471	17	374	9	380	9
NIST610	364	9	441	19	367	10	381	10
NIST610	372	8	486	11	375	9	385	10
NIST610	372	9	479	13	372	9	379	10
NIST610	386	10	444	12	367	9	362	9
NIST610	390	12	470	14	370	10	360	10
NIST610	382	10	463	12	371	9	376	10
NIST610	377	11	468	14	363	10	359	10
NIST610	388	13	482	16	365	11	363	10
NIST610	452	18	556	22	428	14	403	12
NIST610	391	14	462	17	372	11	357	10
NIST610	354	12	390	14	343	10	329	9
NIST610	410	16	533	19	375	12	337	11

Sample	Hf180	Hf180 2SE	Ta181	Ta181 2SE	W182	W182 2SE	W183	W183 2SE
NIST610	355	8	437	11	366	9	363	9
NIST610	366	10	446	13	376	10	373	11
NIST610	367	9	460	11	370	10	369	9
NIST610	368	8	455	11	375	9	374	10
NIST610	374	8	470	11	373	10	369	11
NIST610	359	8	474	11	382	9	375	10
NIST610	358	9	462	12	378	8	379	10
NIST610	361	8	452	11	385	9	380	10
NIST610	359	8	449	12	383	9	376	9
NIST610	365	8	467	12	383	10	378	10
<i>Group Stats</i>	375	9	466	13	375	6	370	6
<i>Reference</i>	435	12	446	33	444	29	444	29
NIST612								
NIST612	37,1	6,1	48,3	8,9	39,6	7,3	40,1	7,8
NIST612	32,8	7,5	44,9	9,0	36,8	7,6	33,5	8,3
NIST612	33,7	8,7	44,1	11,9	34,7	9,5	38,3	9,3
NIST612	40,6	7,0	55,5	10,1	41,5	6,8	43,8	7,6
NIST612	40,8	5,5	54,1	7,2	41,4	5,6	45,8	5,3
NIST612	17,7	17,1	22,5	24,2	15,5	18,6	18,2	16,8
NIST612	29,5	12,0	41,5	11,0	32,3	7,8	31,6	7,8
NIST612	38,7	6,9	50,0	8,9	38,4	6,6	40,4	7,4
NIST612	36,9	6,3	46,1	8,1	34,5	6,0	33,7	5,8
NIST612	46,4	11,5	58,3	15,6	46,1	13,3	43,6	12,2
NIST612	69,4	41,0	91,6	54,4	56,9	28,8	54,3	32,1
NIST612	41,7	20,1	49,8	24,3	37,0	16,7	35,3	13,4
NIST612	21,2	17,6	31,0	22,1	22,8	16,0	20,7	14,1
NIST612	41,1	20,6	49,2	26,6	38,9	18,2	37,6	16,7
NIST612	40,5	16,3	47,1	25,0	40,4	14,6	37,1	16,0

Sample	Hf180	Hf180 2SE	Ta181	Ta181 2SE	W182	W182 2SE	W183	W183 2SE
NIST612	33,3	6,2	41,8	7,4	36,8	7,4	33,9	6,0
NIST612	28,8	11,4	35,7	15,2	32,2	11,7	25,9	11,3
NIST612	44,5	37,2	100	107	43,2	41,8	39,4	42,3
NIST612	28,4	4,0	37,2	5,3	29,9	4,5	28,9	3,9
NIST612	43,1	19,5	52,5	25,3	34,6	26,0	45,1	21,8
NIST612	36,9	13,0	49,0	17,1	37,4	15,7	34,7	15,2
NIST612	29,0	16,7	45,0	18,5	36,7	15,0	34,2	13,3
NIST612	29,8	15,7	37,6	22,9	23,4	21,6	29,9	17,1
NIST612	29,8	17,4	40,1	24,0	31,2	19,0	40,7	14,4
NIST612	41,5	10,9	62,4	19,7	48,4	14,7	47,3	14,5
<i>Group Stats</i>	36,5	4,0	49,4	6,6	36,4	3,4	36,6	3,3
<i>Reference</i>	36,7	1,2	37,6	1,9	38,0	1,1	38,0	1,1
RR632								
R632	107	4	37,5	1,4	1217	47	1203	46
R632	109	4	38,3	1,7	1229	53	1223	47
R632	109	4	39,0	1,4	1303	46	1328	48
R632	106	4	37,2	1,4	1235	41	1242	46
R632	108	4	37,5	1,4	1178	45	1185	45
R632	108	5	38,1	1,5	1205	46	1215	46
R632	109	5	38,6	1,5	1262	44	1290	56
R632	106	4	37,7	1,4	1262	45	1261	43
R632	105	4	36,9	1,4	1199	40	1192	46
R632	111	5	38,3	1,5	1254	46	1232	44
R632	109	5	37,7	1,6	1216	46	1187	49
R632	110	4	39,2	1,4	1290	41	1292	39
R632	105	4	37,6	1,4	1266	49	1240	43
R632	105	4	37,0	1,4	1171	44	1187	43

Sample	Hf180	Hf180 2SE	Ta181	Ta181 2SE	W182	W182 2SE	W183	W183 2SE
R632	110	4	37,9	1,3	1268	44	1245	48
R632	108	4	37,8	1,6	1186	46	1195	51
R632	111	4	38,2	1,3	1288	50	1287	46
R632	107	4	38,2	1,5	1272	41	1263	42
R632	106	3	37,6	1,4	1253	41	1242	41
R632	108	4	37,7	1,3	1164	40	1191	40
<i>Group Stats</i>	<i>108</i>	<i>1</i>	<i>37,9</i>	<i>0,3</i>	<i>1236</i>	<i>19</i>	<i>1235</i>	<i>19</i>
<i>Reference</i>	<i>108</i>	<i>6</i>	<i>37,9</i>	<i>3,2</i>	<i>1235</i>	<i>0</i>	<i>1235</i>	<i>0</i>

